Charles University in Prague

First Faculty of Medicine

Department of Cell Biology and Pathology

Mgr. Martina Huranová

Assembly and recycling of functional splicing complexes *in vivo*.

PhD thesis

Supervisor: **Mgr. David Staněk, Ph.D.**
Department of RNA Biology
Institute of Molecular Genetics
Academy of Sciences of the Czech Republic

Datum obhájení práce.....

Praha 2010

Prohlášení:

Prohlašuji, že jsem závěrečnou práci zpracovala samostatně a že jsem uvedla všechny použité informační zdroje. Současně dávám svolení k tomu, aby tato závěrečná práce byla archivována v Ústavu vědeckých informací 1. Lékařské fakulty Univerzity Karlovy v Praze a zde užívaná ke studijním účelům. Za předpokladu, že každý, kdo tuto práci použije pro svou přednáškovou nebo publikační aktivitu, se zavazuje, že bude tento zdroj informací řádně citovat.

Souhlasím se zpřístupněním elektronické verze mé práce v Digitálním repozitáři Univerzity Karlovy v Praze (http://repozitar.cuni.cz). Práce je zpřístupněna pouze v rámci Univerzity Karlovy v Praze.

V Praze, 14.5.2010 Martina Huranová

Acknowledgements

I would like to thank my supervisor David Staněk for his continuous support, guidance and supply of necessary knowledge to perform my research on very interesting topics.

I am particularly grateful to my labmates and all friends who have made my PhD life a real and exciting experience.

Many thanks belong to my family for constant support and encouragement during my PhD studies.

Content

Abbreviations

BAC	bacterial artificial chromosome
CB	Cajal body
CFP	cyan fluorescent protein
DAPI	4,6-diamino-2-phenylindole dichloride
Df	diffusion coefficient
DRB	5,6-dichlorobenzimidazole riboside
E3	β-globin model gene containing three exons
FCS	fluorescence correlation spectroscopy
FLIM	fluorescence lifetime imaging microscopy
FRAP	fluorescence recovery after photobleaching
FRET	förster/fluorescence resonance energy transfer
GFP	green fluorescent protein
Hela	human cell line derived from adenocarcinoma cervix cells
k_{off}	dissociation constant
mRED	monomeric red florescent protein
mRNA	messenger RNA
MS2	MS2 coat protein derived from MS2 bacteriophage
PA-GFP	photoactivable GFP
pre-mRNA	precursor of mRNA
RAC	RNA affinity chromatography
RB-FRET	RNA-binding FRET
RNA	ribonucleic acid
SDS-PAGE	sodium dodecyl sulphate polyacrylamide gel electrophoresis
siRNA	silencing RNA
snRNP	small nuclear ribonucleoprotein particle
Tet-on	tetracycline inducible system switching the expresion on
U2-OS	human cell line derived from osteosarcoma cells
3`UTR	3` untranslated region
YFP	yellow fluorescent protein

Outline of the PhD thesis

In this thesis we concentrated on assembly and recycling of functional splicing complexes in the cell nucleus. We took an advantage of using fluorescent microscopy as a powerfull tool for live cell imaging and analysis of biological events *in vivo*. First, we focused on spatial and temporal organization of snRNP dynamics within the cell nucleus during transcription and splicing. Next, we assessed the effect of a disease linked mutation in snRNP specific protein on snRNP metabolism. Finally, we introduced a method for studying RNA-protein interactions in living cells.

General Introduction offers an overview of current knowledge in the field of pre-mRNA splicing and provides sufficient theoretical background underlying the projects presented in this thesis.

In chapter 2, we addressed the role of Cajal bodies (CB), non-membrane nuclear structures, in biogenesis and metabolism of spliceosomal snRNPs. We showed that individual snRNPs repeatedly cycle through CBs and proposed a model of snRNP recycling in CBs after accomplishing the pre-mRNA splicing.

In chapter 3, we examined the snRNPs interactions with pre-mRNA and determined their dissociation rates. We showed that these interactions disappeared when transcription was inhibited, which resulted in diffusional movement of snRNP throughout the nucleoplasm. We elucidated how the snRNPs assemble the spliceosome and estimated the splicing kinetics in living cells.

In chapter 4, we focused on the AD29 mutation in *HPRP31* gene, which encodes the hPrp31 protein that specifically associates with snRNPs. The AD29 mutation belongs to a series of mutations that were initially linked with the autosomal dominant disorder retinitis pigmentosa type 11. We showed that association between the AD29 mutant and snRNPs in the cell nucleus was significantly reduced. In addition, we reported that expression of this mutant protein affected cell proliferation and altered the structure of Cajal bodies.

In chapter 5, we established a new method for detecting RNA-protein interactions *in situ* based on fluorescence resonance energy transfer (FRET). We tested this approach by analyzing binding of hnRNP H protein to its cognate RNA. We

showed that this method provides a powerful tool to study spatial and temporal localization of specific RNA–protein complexes.

In a General Discussion (chapter 6) the dynamic behaviour of splicing factors is discussed in the context of the pre-mRNA processing events and nuclear architecture.

CHAPTER 1

General introduction

The cell nucleus is the hallmark of eukaryotic cells, where genetic information - DNA is accommodated and replicated prior to cell division and where the initial steps of gene expression take place. In higher eukaryotes protein coding genes consists of coding sequences – exons and non – coding sequences – introns. Transcription of these genes results in precursors (pre-mRNAs) that must be processed before translation of the message into protein. During pre-mRNA splicing introns are excised and exons joined together to generate mature messenger RNA (mRNA). One pre-mRNA can be spliced in alternative ways and several different mRNAs and proteins can be produced from one DNA sequence. As it is currently estimated that over two-thirds of human genes produce alternatively spliced mRNAs, pre-mRNA splicing is the major source of protein diversity (Blencowe 2006). Pre-mRNA splicing is regulated both on a global level and in a gene-specific manner, for example during cell cycle and in response to cellular stress (Shin, Feng et al. 2004). Mutations of several splicing factors and abberant splicing have been linked to a broad spectrum of human diseases (Faustino and Cooper 2003; Licatalosi and Darnell 2006), underscoring the importance to understand the mechanisms that underline the process of pre-mRNA splicing.

Spliceosome - the executor of pre-mRNA splicing.

Splicing of pre-mRNA is carried out in a two-step phosphodiester transesterification reaction. Although there is a broad variety of introns, they are very well defined by several features that are in higher eukaryotes highly conserved: the 5’ and 3’ splice site (ss) sequences GU and AG respectively, the branchpoint adenosine and the polypyrimidine track located between branchpoint and 3’ss. The splicing reaction starts with a nucleophilic attack on the 5’ splice site by the 2’ hydroxyl of the branchpoint adenosine resulting in a 2’-5’ phosphodiester branch in the intron and a free 3’ hydroxyl group on the 5’ exon. Attack of the 3’ hydroxyl group on the phosphodiester bond at the 3’ss by the 3’OH nucleophile of the 5’ exon during the second transesterification reaction results in the joining of the two exons via a 3’-5’ phosphodiesterbond and the displacement of the intron lariat. Intron removal is a

complex process and requires dynamic splicing machinery capable to recognize the intronic features and accomplish the transesterification reactions with high precision and fidelity. This machinery is called the spliceosome and it is a huge ribosome-size ribonucleoprotein complex composed of five major spliceosomal small ribonucleoprotein particles (snRNPs) U1, U2, U4, U5, and U6, plus additional splicing factors (Jurica and Moore 2003). Each snRNP consists of a unique snRNA that is associated with a specific set of proteins (Will and Luhrmann 2001).

During splicing several rearrangements must occur, which require the association, displacement and switching of snRNPs within the spliceosome (Staley and Guthrie 1998). The prevailing model of spliceosome assembly is derived from *in vitro* splicing experiments, which indicate a step-wise addition and displacement of individual snRNPs to the pre-mRNA (Fig. 1.1.A). U1 snRNP binds to 5‘ ss of the intron followed by U2 snRNP interaction with the 3‘ss forming the A complex. U4, U5 and U6 snRNPs, pre-assembled into the U4/U6.U5 tri-snRNP, subsequently enter the A complex to form the pre-catalytic B complex. U1 snRNP dissociates from the 5‘ss and is substituted by U6 snRNP from the tri-snRNP. Prior to catalytic steps, U6 snRNP switches partners by dissociating from U4 snRNP and binding to U2 snRNP forming the activated B* complex. The activated spliceosome performs two transesterification reactions, the intron is excised, the exons are ligated together and mRNA is released. Finally, U2.U6.U5 snRNPs disassemble from the intron lariat to be recycled in new rounds of splicing and the intron is degraded.

While the ordered assembly model of the spliceosome is conserved from yeast to humans, other models have been proposed, suggesting that the association of the spliceosome can occur in a pre-assembled complex also called the `holospliceosome` or the `penta-snRNP` (Fig. 1.1.B). The penta-snRNP was isolated from yeast extract under law salt conditions (Stevens, Ryan et al. 2002) and was shown to bind pre-mRNA directly via interaction of U1 snRNP with 5’ss (Malca, Shomron et al. 2003). However, how the spliceosome assembles *in vivo* still remains an open question. In this thesis I analyzed *in vivo* formation of the spliceosome using fluorescent live-cell imaging techniques FRAP and FCS.

Spatial organization and compartmentalization of the splicing machinery.

The biogenesis and maturation of the U1, U2, U4, U5, and U6 snRNPs is a complex process that occurs both in the nucleus and in the cytosol (Fig. 1.2.). U1, U2,

U4 and U5 snRNAs are synthetized by RNA polymerase II, capped at their 5' ends and transported to the cytoplasm. In the cytoplasm a ring of seven Sm proteins is assembled on snRNAs by the sequential action of pCl1 and SMN complex (Paushkin, Gubitz et al. 2002). The 5' end is hypermethylated by TGS1 methyltransferase and core snRNPs are imported back to the nucleus to participate in the splicing process. The U6 snRNA is synthetized by RNA polymerase III and its maturation occurs solely in the nucleoplasm. In the cell nucleus, prior entering splicing pathway, snRNPs first accumulate in CBs (Sleeman and Lamond 1999), where snRNAs are posttranscriptionally modified by 2′-O-ribose methylation and pseudouridylation (Jady, Darzacq et al. 2003; Kiss 2004) and likely associate with snRNP-specific proteins.

Mature snRNPs are exclusively localized to the cell nucleus. Besides their presence in the nucleoplasm, where the splicing occurs, they accumulate also to dynamic subnuclear structures: splicing factor compartments or `speckles` and aforementioned CBs. Speckles are enriched in splicing factors 5-10 folds compared to nucleoplasm and are located in the interchromatin regions of the nucleus, often observed close to highly active transcription sites (Huang and Spector 1991; Xing, Johnson et al. 1995). Several lines of evidence point to speckles functioning as storage compartments that can supply splicing factors to sites of transcription (Misteli, Caceres et al. 1997).

In contrast to common localization of all snRNPs in speckles, accumulation in CBs is predominantly specific for U2 and U4/U6 di-snRNP. Besides snRNAs posttranscriptional modifications, CBs serve as the sites of complex assembly steps that involve RNA-RNA annealing and the sequential addition of snRNP-specific proteins. Assembly of both 12S and mature 17S U2 snRNP, U4/U6 di-snRNP and U4/U6.U5 tri-snRNP takes place in CBs (Nesic, Tanackovic et al. 2004; Schaffert, Hossbach et al. 2004; Stanek and Neugebauer 2004). Mathematical modeling of U4/U6 snRNP formation in the cell nucleus revealed that accumulation of U4 and U6 snRNPs in CBs increases the efficiency of U4/U6 di-snRNP assembly (Klingauf, Stanek et al. 2006). In addition, recent observations showed that depletion of coilin, a protein required for snRNP concentration in CB, impairs cell proliferation (Lemm, Girard et al. 2006) and that coilin-dependent snRNP assembly is essential for zebrafish embryogenesis (Strzelecka, Trowitzsch et al. 2010), which underscores the role of CBs in snRNPs assembly.

Inhibition of tri-snRNP formation by knockdown of hPrp6 (U5 snRNP) or hPrp31 (U4/U6 di-snRNP) leads to accumulation of the U4/U6 snRNPs in CBs, while levels of the U5 snRNA and U5-specific proteins remain unchanged (Schaffert, Hossbach et al. 2004). These data show that U4/U6 di-snRNP is retained in CB until the U5 snRNP joins; only when the mature tri-snRNP is formed it is released from the CB. To avoid lack of U5 snRNP that might be partially entrapped in many post-spliceosomes, there are specific proteins that release snRNPs from the intron-lariat (Arenas and Abelson 1997; Tanaka, Aronova et al. 2007). In this thesis I addressed the role of CBs in snRNP recycling after splicing.

Splicing and diseases.

Pre-mRNA splicing is a tightly regulated process. A splicing error that adds or removes even 1nt will disrupt the open reading frame of an RNA and result in production of a non-functional or even a harmfull protein. The spliceosome must act very precisely, when recognizing the correct splice sites prior to the cut-and-paste reactions. The diseases caused by defects in pre-mRNA splicing can be caused either by *cis*-acting mutations affecting the splice sites, or by *trans*-acting mutations affecting the splicing machinery.

The most common mutations causing human diseases disrupt classical splicing signals of constitutive exons. The result is expression of proteins containing internal deletions, a shift in the reading frame or C-terminal truncations. In most cases, use of unnatural splice sites or intron retention introduces premature termination stop codons into the mRNA, which results in degradation by nonsence-mediated decay (Hentze and Kulozik 1999). Pre-mRNA mutations that affect the use of alternative splice sites mostly shift the ratio of natural protein isoforms (Caceres and Kornblihtt 2002).

There are several genetic diseases in which a mutation disrupts the splicing machinery, either the core spliceosomal components or the auxiliary factors that regulate alternative splicing. In humans regulation of alternative splicing is impaired in several forms of cancer and myotonic dystrophy. Mutations that disrupt the assembly or function of spliceosomal snRNPs are responsible for two human diseases: retinitis pigmentosa (RP) and spinal muscular atrophy (SMA), in which two different subsets of cells are affected.

RP is a heterogeneous disease characterized by progressive retinal degeneration, night blindness, loss of peripheral vision, and ultimately total blindness. RP is caused by

loss of rod photoreceptor cells and it can be inherited as autosomal dominant, autosomal recessive, or X-linked disorder. More then 30 RP-linked genes were identified, most of which have retina specific functions, like opsin. Interestingly, four genes, namely *HPRP31*, *HPRP3*, *HPRP8* and *SNRNP200*, involved in RP development encode U4/U6.U5 tri-snRNP specific proteins (McKie, McHale et al. 2001; Vithana, Abu-Safieh et al. 2001; Chakarova, Hims et al. 2002; Zhao, Bellur et al. 2009). hPrp31 and hPrp3 are U4/U6 di-snRNP associated proteins and hPrp8 and SNRNP200 are the core components of the U5 snRNP. hPrp31 promotes association between U4/U6 di-snRNP and U5 snRNP by direct interaction with hPrp6, U5-specific protein, which results in tri-snRNP formation (Schaffert, Hossbach et al. 2004). Tri-snRNP is an essential component of the spliceosome assembly pathway. It is recruited to the prespliceosomal pre-mRNA-U1-U2 snRNP complex to form the catalytically competent spliceosome. Mutations in HPRP31 gene causing RP include insertions, deletions, missence mutations, and splice site mutations. One of these mutations is AD29, a missence mutation Ala216Pro, which is not contained within the U4 or U5 snRNP interacting domains. It was shown that the mutant protein is not fully translocated to the nucleus and interacts stronger with hPrp6, suggesting a mechanism for negative regulation. However, the splicing efficiency was not impaired in cells expressing the mutant form (Deery, Vithana et al. 2002; Wilkie, Vaclavik et al. 2008), so it is still unclear how this mutation initiates development of RP. In this thesis I examined the effect of the AD29 mutation in HPRP31 gene on snRNP metabolism and cell behaviour.

Tools for studying biological processes.

A central challenge to cell biologists is to understand the extensive networks of protein-protein, DNA-protein and RNA-protein interactions that regulate cellular processes. Traditionally, binding reactions between molecules have been studied using *in vitro* techniques. However, recent advances in microscopy methods have made it possible to visualize the molecules and analyze their binding properties directly in living cells. By far the most used fluorescent protein label is the green fluorescent protein (GFP) from the jellyfish *Aequorea victoria*. GFP can be fused to any protein and, because several spectrally distinct derivatives are available, multicolour observations of more proteins are possible. The most applied *in vivo* tools, with which we can probe cellular binding interactions are fluorescence resonance energy transfer (FRET), fluorescence recovery after photobleaching (FRAP) and fluorescence correlation

spectroscopy (FCS) (Figure 3.). FRET is non-radiative transfer of energy between two fluorophores (donor and acceptor), which can occur if they are very close to each other (< 10 nm) (Fig. 1.3.A). As a protein-protein interaction usually occurs within 10nm distance, it is possible to measure FRET between two fluorescently tagged molecules, which interact with each other, for example a ligand and a receptor. For FRET to happen the fluorescence emission spectrum of the donor has to overlap with the absorption spectrum of the acceptor. In addition, the transition dipole orientations of the fluorophores must be approximately parallel for FRET to occur. The most used FRET pair is the combination of CFP and YFP (cyan and yellow fluorescent protein). FRET can be measured by the acceptor photobleaching approach or by fluorescence lifetime imaging approach, where we examine quenching of the donor fluorescence in presence and absence of the acceptor. Another approach is sensitized emission, where we look at the fluorescence of the acceptor after excitation of the donor. In this thesis I introduced a new method for studying RNA-protein interactions in living cells based on FRET approch.

The most commonly used technique to determine the dynamic properties of proteins *in vivo* is FRAP (Fig. 1.3.B). This approach involves photo-bleaching of a small area within the cell and monitoring the recovery of fluorescence intensity over time. Fluorescence recovery results from the movement of unbleached molecules from the surroundings into the bleached area. This method is minimally invasive and the dynamics of the observed protein closely reflects its behaviour *in vivo*. FRAP recovery provides not only a qualitative impression of the protein mobility, but more importantly, it contains quantitative information about the diffusion and binding characteristics of analyzed molecules (Sprague and McNally 2005). We can directly determine the apparent diffusion coefficient and the size of the mobile fraction of a protein from the primary data (Lippincott-Schwartz, Snapp et al. 2001). However, computational approaches, particularly kinetic modeling methods allow us to analyze more complicated biological events. Differential equations are often used here, because they can on principle describe basic cellular processs, such as biochemical kinetics, membrane transport and binding events.

FCS provides an alternative approach to measure protein dynamics *in vivo* with microsecond time resolution (Kim, Heinze et al. 2007). In this technique, a laser beam is focused on a spot of interest in the cell and fluctuations of the fluorescence intensity are measured over time (Fig. 1.3.C). The recorded signal reflects the movement of labelled

proteins through the sample volume. The time it takes molecules to move through the sample volume depends on their diffusional properties. The intensity record is transformed into an autocorrelation function that assesses the diffusion correlation time of the detected molecules.

Combination of all these methods provides high temporal and spatial resolution for analysing the binding properties of the proteins and biological processes of our interest in living cells.

Figures to chapter 1:

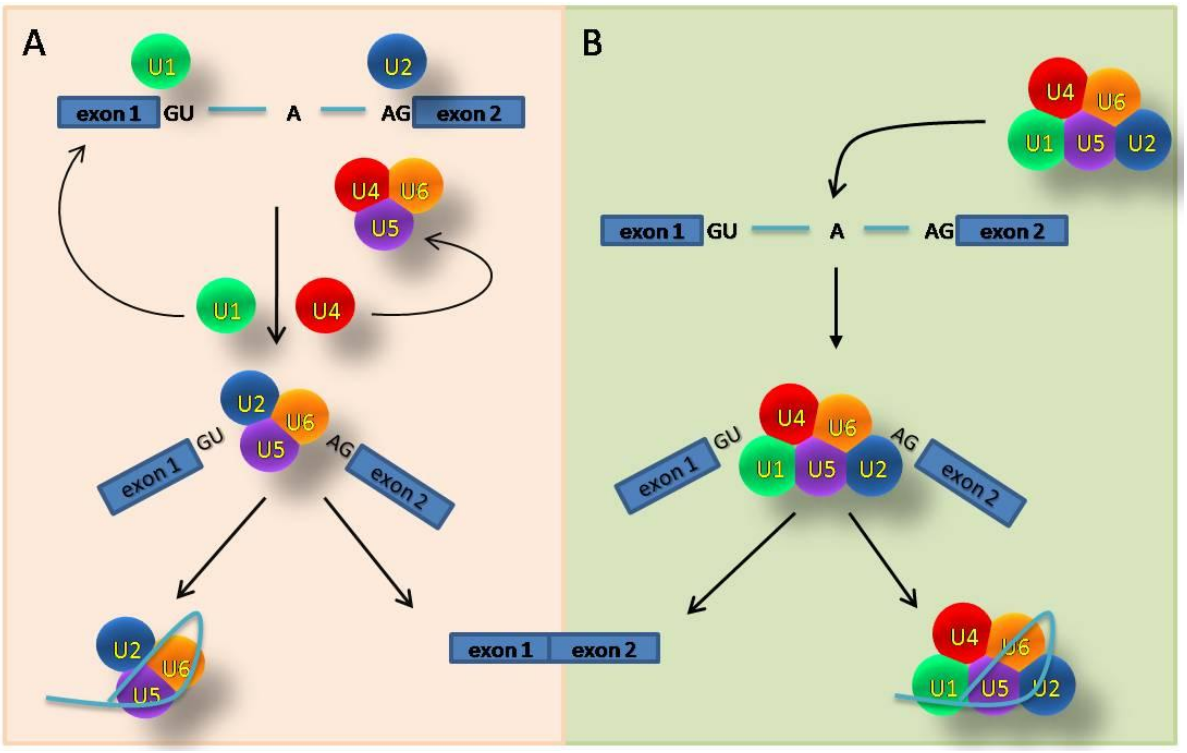

Figure 1.1. Two models of spliceosome assembly. A/ Step-wise assembly of the spliceosome proposes sequential association and dissociation of individual snRNPs with pre-mRNA. B/ Pre-assembled model of the spliceosome proposes direct association of the penta-snRNP with pre-mRNA.

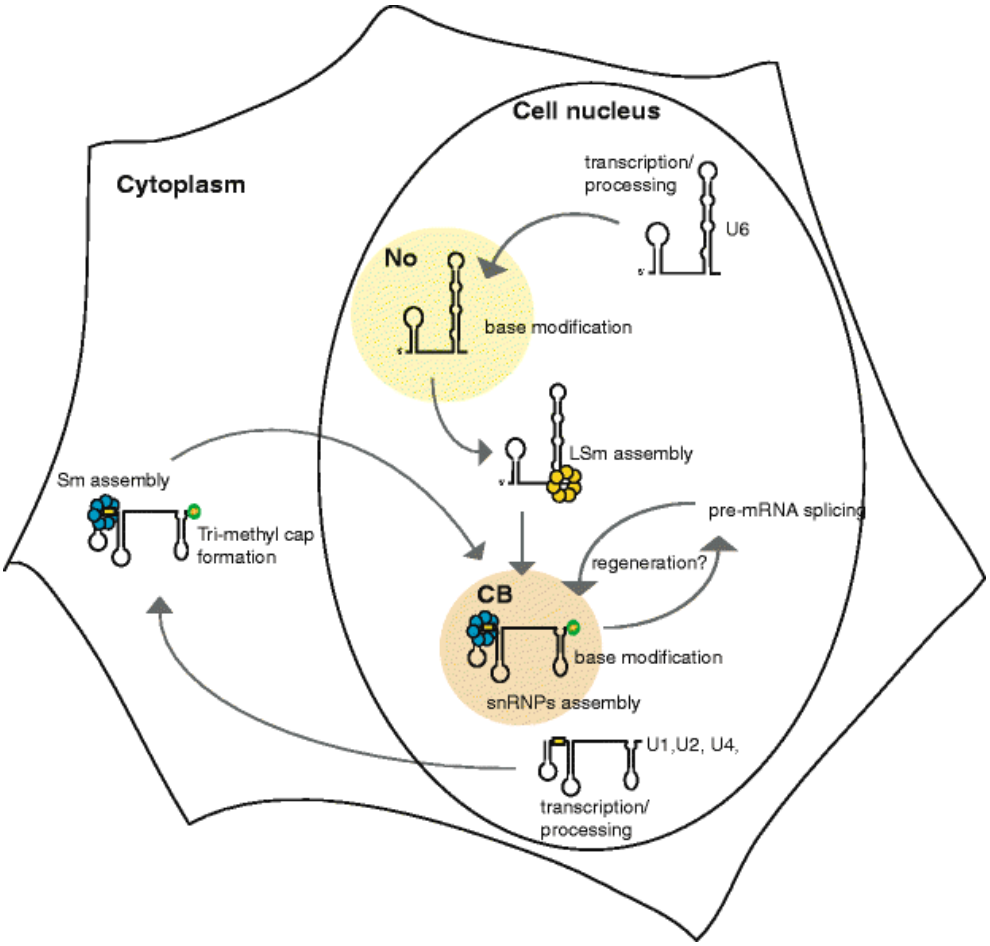

Figure 1.2. Biogenesis of the spliceosomal snRNPs. U1, U2, U4, and U5 snRNAs are transcribed in the cell nucleus by RNA polymerase II. They are then exported to the cytoplasm where the Sm ring (blue balls) is assembled and hypermethylation of the 5′ end occurs. The Sm ring and the trimethyl cap (green ball) act as signals for nuclear reimport. Back in the nucleus, U snRNAs first visit Cajal bodies (CB, beige compartment) where specific nucleotides are modified by base methylation and pseudouridylation and where assembly of the U2, U4/U6, and U4/U6•U5 snRNPs occurs. The U6 snRNA is transcribed by RNA polymerase III, receives a γ monomethyl cap and is thought to remain in the nucleus. The U6 snRNA is base modified in the nucleolus (No, yellow compartment) and then targeted to Cajal bodies where it is incorporated into U4/U6 and U4/U6•U5 snRNPs. Assembly of the LSm ring (yellow balls) on U6 is likely nucleoplasmic. Assembled U4/U6•U5 snRNPs leave the Cajal body and function in splicing in the nucleoplasm; individual snRNPs disassembled by the splicing process potentially return to Cajal bodies for regeneration of active complexes. Adopted from (Staněk and Neugebauer, 2006).

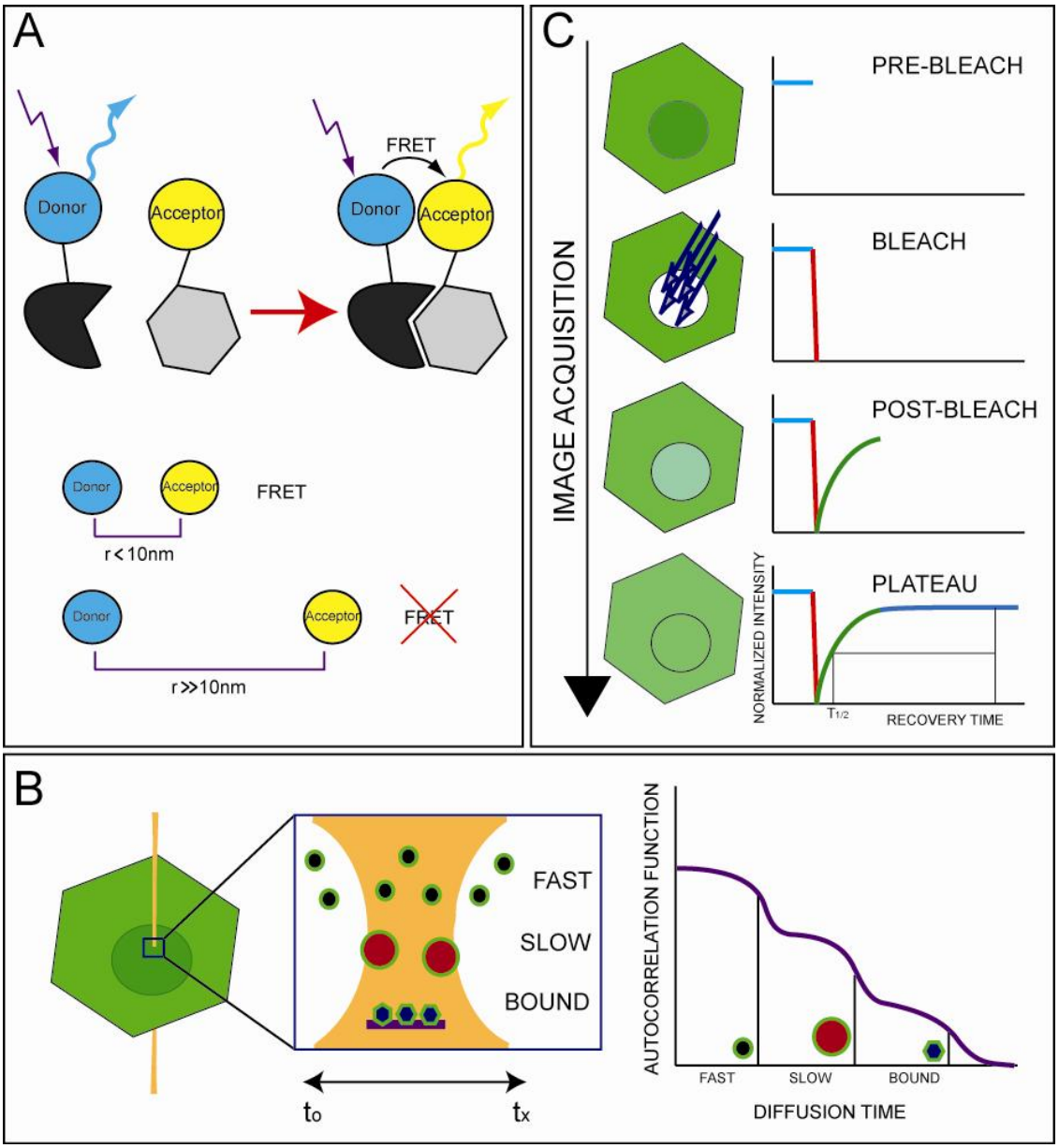

Figure 1.3. Schematic principles of FRET, FCS and FRAP techniques. A/ FRET occurs between two fluorescently labeled molecules (cyan-CFP, yeallow-YFP), when their distance is less then 10nm and spectra of the fluorophores overlap. B/ In FCS the beam (orange) is parked in the sample. The GFP-tagged molecules (black, red, violet) move differently in the focal volume and their movement causes fluctuations of the intensity signal. The readout of these fluctuations is the autocorrelation function that describes diffusional properties of the analysed molecules. C/ In FRAP a region of interest is rapidly bleached and the recovery of the fluorescence is monitored over time. The halftime $T_{1/2}$ of the recovery curve is used to describe the diffusional properties of the analysed molecules.

CHAPTER 2

Spliceosomal small nuclear ribonucleoprotein particles (snRNPs) repeatedly cycle through Cajal bodies

This chapter was reproduced from:
Staněk D., Přidalová J., Novotný I., Huranová M., Blažíková M., Wen X., Sapra A.K., Neugebauer K.M. : Spliceosomal snRNPs Repeatedly Cycle through Cajal Bodies. Mol Biol Cell. 2008 Jun;19:2534–2543.

2.1 Abstract

The Cajal body (CB) is a nuclear structure closely associated with import and biogenesis of small nuclear ribonucleoprotein particles (snRNPs). Here we tested whether CBs also contain mature snRNPs and whether CB integrity depends on the ongoing snRNP splicing cycle. Sm proteins tagged with photo-activatable and color-maturing variants of fluorescent proteins were used to monitor snRNP behavior in living cells over time; mature snRNPs accumulated in CBs, traveled from one CB to another, and were not preferentially replaced by newly imported snRNPs. To test whether CB integrity depends on the snRNP splicing cycle, two human orthologs of yeast proteins involved in distinct steps in spliceosome disassembly after splicing, hPrp22 and hNtr1, were depleted by siRNA treatment. Surprisingly, depletion of either protein led to the accumulation of U4/U6 snRNPs in CBs, suggesting that reassembly of the U4/U6•U5 tri-snRNP was delayed. Accordingly, a relative decrease in U5 snRNPs compared to U4/U6 snRNPs was observed in CBs, as well as in nuclear extracts of treated cells. Taken together, the data show that particular phases of the spliceosome cycle are compartmentalized in living cells, with reassembly of the tri-snRNP occurring in CBs.

2.2 Introduction

Pre-mRNA splicing is a two-step trans-esterification reaction catalyzed by the spliceosome, a large complex assembled from pre-formed subcomplexes, called spliceosomal small nuclear ribonucleoprotein particles (snRNPs) and hundreds of additional proteins (Jurica and Moore 2003). In turn, the five major spliceosomal snRNPs, U1, U2, U4, U5 and U6, each consist of a single small nuclear RNA (snRNA) and specific set of proteins. Among the shared protein components of snRNPs are the seven Sm proteins, which are assembled as a stable, hetero-heptameric ring on the RNA polymerase II-transcribed snRNAs: U1, U2, U4, and U5. After transcription, these snRNAs are transported to the cytoplasm, where the Sm ring is assembled on snRNAs by the SMN complex. Subsequently, the 5'-ends of the snRNAs are hypermethylated to generate the trimethyl-guanosine (TMG) cap, which together with SMN, promotes snRNP nuclear import (reviewed in (Will and Luhrmann 2001; Matera and Shpargel 2006; Tycowski, Kolev et al. 2006). Because snRNPs do not shuttle between the nucleus and cytoplasm (M. Änkö and K. Neugebauer, unpublished data), Sm ring assembly seems to occur early and only once in the lifetime of each snRNP. A related hetero-heptameric ring, consisting of seven "like-Sm" (LSm) proteins, is assembled on U6, an RNA polymerase III transcript, which is thought to remain in the nucleus for all assembly steps (Achsel, Brahms et al. 1999; Mayes, Verdone et al. 1999; Kiss 2004; Listerman, Bledau et al. 2007).

Once back in the cell nucleus, snRNPs first accumulate in CBs before distributing throughout the nucleoplasm, where splicing occurs (Sleeman and Lamond 1999; Sleeman, Ajuh et al. 2001; Neugebauer 2002). This suggests a role for CBs in nuclear steps of snRNP maturation, a prediction borne out by the following set of observations. First, post-transcriptional modifications of the snRNAs themselves occur in CBs after snRNP re-import from the cytoplasm (Darzacq, Jady et al. 2002; Kiss 2002; Jady, Darzacq et al. 2003). These modifications, including pseudouridinylation and 2'-*O*-methylation, are guided by small Cajal body specific RNAs. Second, CBs are the site of complex assembly steps that involve RNA-RNA annealing and the sequential addition of proteins. For example, the U4/U6 snRNP is formed when the U4 and U6 snRNAs anneal, a step catalyzed by U6-specific LSm proteins and SART3 (also named hPrp24 or p110) (Ghetti, Company et al. 1995; Raghunathan and Guthrie 1998; Achsel, Brahms et al. 1999; Bell, Schreiner et al. 2002). Subsequently, the U4/U6•U5 tri-snRNP

assembles when U5 snRNP associates by protein-protein interactions with the U4/U6 snRNP (Makarova, Makarov et al. 2002; Schaffert, Hossbach et al. 2004). Both U4/U6 and U4/U6•U5 tri-snRNP assembly occur in CBs (Schaffert, Hossbach et al. 2004; Stanek and Neugebauer 2004). Recently, mathematical modeling of U4/U6 snRNP formation in the cell nucleus revealed that accumulation of U4 and U6 snRNPs in CBs should greatly increase efficiency of U4/U6 assembly (Klingauf, Stanek et al. 2006). An additional role of CBs in U2 snRNP formation (Nesic, Tanackovic et al. 2004) further points to CBs as the key site of nuclear steps in snRNP assembly. The observation that depletion of coilin, a protein required for snRNP concentration in CBs, impairs cell proliferation (Lemm, Girard et al. 2006) is consistent with the proposal that snRNP assembly is inefficient in the absence of CBs.

SnRNPs must not only assemble *de novo* but may also regenerate after splicing to complete the so-called spliceosome cycle. During spliceosome assembly and activation, snRNPs undergo structural rearrangements, including U4/U6 snRNA unwinding and release of the U4 snRNP from the spliceosome (Staley and Guthrie 1998). After splicing, mRNA is released from the spliceosome by the DEAH-box helicase hPrp22/HRH1 and snRNPs remain associated with the excised intron lariat (Company, Arenas et al. 1991; Ohno and Shimura 1996). In *Saccharomyces cerevisiae*, a complex of three proteins (Prp43/Ntr1/Ntr2) was shown to be essential for release of individual snRNPs from the lariat (Arenas and Abelson 1997; Martin, Schneider et al. 2002; Tsai, Fu et al. 2005; Boon, Auchynnikava et al. 2006; Tanaka, Aronova et al. 2007; Tsai, Tseng et al. 2007). If these released snRNPs are to participate in subsequent rounds of splicing, they have to be reassembled into the active U4/U6•U5 tri-snRNP. Several studies provide genetic and biochemical evidence for snRNP reassembly (Raghunathan and Guthrie 1998; Bell, Schreiner et al. 2002; Verdone, Galardi et al. 2004; Chen, Kao et al. 2006). Although snRNPs are highly expressed, the long half-lives of snRNAs suggests that they likely recycle and function again (Yu, Sharl et al. 1999).

In the present study, we address the hypothesis that snRNPs cycle more than once through CBs. We show in living cells that CBs contain mostly mature snRNPs, which are capable of exchanging with nucleoplasm and visiting multiple CBs. Targeted knockdown of proteins involved in spliceosome recycling, hPrp22 and the human homologue of the recently identified yeast Ntr1, led to a dramatic accumulation of the

U4/U6 snRNP in CBs. These data demonstrate that the CB is a vital way station in the spliceosomal cycle.

2.3 Material and Methods

Cells and antibodies

HeLa cells were cultured in Dulbecco's modified Eagle medium supplemented with 10% fetal calf serum, penicillin and streptomycin (Gibco BRL). To create a stable HeLa cell line expressing human Prp8 tagged with GFP at the C-terminus and expressed under the control of its own promoter, a BAC harboring the human Prp8 gene was obtained from the BACPAC Resources Center (http://bacpac.chori.org). Neo/Kanr-dsRed and EGFP-IRES-Neo cassettes were PCR amplified with primers carrying 50 nucleotides of homology to the targeting sequence. Recombineering of the BACs was performed as described (Zhang, Muyrers et al. 2000)(Gene Bridges, Dresden, Germany), and following transduction, neo-resistant cells were sorted by FACS to obtain single colonies. Immunoprecipitation using anti-GFP antibodies showed that hPrp8-GFP is properly incorporated into the U5 snRNP and the tri-snRNP (data not shown).

The following antibodies were used: rabbit anti-SART3/p110 antibodies (Stanek, Rader et al. 2003), mAb anti-coilin (5P10) (Almeida, Saffrich et al. 1998) kindly provided by M. Carmo-Fonseca, rabbit antibodies against LSm4 (Achsel, Brahms et al. 1999), hPrp31 (U4/U6-61K) (Makarova, Makarov et al. 2002), hPrp4 (U4/U6-60K) (Lauber, Plessel et al. 1997), hSnu114 (U5-116K) (Fabrizio, Laggerbauer et al. 1997) kindly provided by R. Lührmann. Monoclonal antibodies against U2B" and U1-70K were purchased from Progen. Rabbit anti-mouse Ntr1 was raised against a peptide, LQNEFNPNRQRHWQ (aa 32-45; Zymed Laboratories Inc., South San Fransisco, CA) and was provided by Michael Paine (University of Southern California, Los Angeles, CA 90033).

Protein tagging

SART3-CFP, coilin-CFP and hPrp31-CFP were described previously (Stanek and Neugebauer 2004). SMN-YFP was kindly provided by M. Dundr (Dundr, Hebert et al. 2004), SmB-YFP and SmD1-GFP by A. Lamond (Sleeman and Lamond 1999). SmB was subcloned into ECFP-C1 (Clontech), PA-GFP-C1 (Patterson and Lippincott-

Schwartz 2004) and E5-RFP-C1 using HindIII/KpnI sites. SmD1 was recloned into ECFP-C1, PA-GFP-C1 and E5-RFP-C1 using BamHI/PstI sites. E5-RFP-C1 vector was created by replacing GFP sequence in GFP-C1 plasmid (Clontech) with E5-RFP sequence from pTimer-1 plasmid (Clontech) using AgeI/BglII restriction sites. SART3-HcDiRed construct was created by cloning SART3 sequence into the HcDiRed-N1 vector, which originated from the H2B-HcDiRed-N1 plasmid obtained from J. Ellenberg (Gerlich, Beaudouin et al. 2003).

Live cell imaging

Cells were plated on glass bottomed Petri dishes (MatTek) and after 20-24h transfected with appropriate DNA constructs using FuGene 6 (Roche). The cells were imaged 22-24h after transfection using either Zeiss510 equipped with water immersion objective 63x 1.2NA or Leica SP2 confocal microscopes equipped with water immersion objective 63x 1.2NA and an environmental chamber controlling CO_2 level and temperature. PA-GFP was activated by short pulses of 405nm laser line and images of activated PA-GFP (excitation with 488nm laser line) and either CFP (excitation with 458nm laser line) or HcDiRed (excitation with 594nm laser line) were acquired in 15s intervals in the case of activation of one CB or every 2 minutes in the case of activation of the whole nucleus. The raw images were analyzed using ImageJ software. For publication, fluorescent levels were linearly adjusted using Adobe Photoshop.

For E5-RFP experiments, cells were transfected with SmB-E5-RFP or SmD1-E5-RFP, fixed at different times after transfection with 4% paraformaldehyde/PIPES and embedded in glycerol containing 4',6-diamidino-2-phenylindole (DAPI) and 2.5% 1,4-Diazabicyclo [2.2.2]octane (DABCO; Sigma) as an anti-fade reagent. Alternatively, cells were treated for two hours before fixation with 30ng/ml Leptomycin B (LC Laboratories). Images were collected using the DeltaVision microscope system (Applied Precision) coupled with Olympus IX70 microscope equipped with oil immersion objective 60x 1.4NA using the same settings for each sample. Stacks of 25 z-sections with 200nm z-step were collected per sample and subjected to mathematical deconvolution using measured point spread function (SoftWorx, Applied Precision). Mean intensities in green and red channel were quantified using SoftWorx.

FRET measurement

Cells were transfected with fluorescent protein-tagged constructs using Fugene 6, grown for 24-26h and fixed in 4% paraformaldehyde/PIPES (Sigma) for 10 min at room temperature. After rinsing with Mg-PBS (PBS supplemented with 10mM Mg^{2+}) and water, cells were embedded in glycerol containing DABCO. FRET was measured by acceptor photobleaching method as previously described (Stanek and Neugebauer 2004) using the Leica SP2 confocal microscope. Intensities of CFP (excited by 405nm laser set to 5-10% of maximum power) and YFP (excited by 514nm laser line set to 2% of maximum power) were measured. Then, YFP was bleached in a region of interest by 3-5 intensive (30% maximum power) pulses of 514 nm laser line and CFP and YFP fluorescence measured again. Apparent FRET efficiency calculated according to the equation $FRET_{efficiency}[\%]= (CFP_{after} - CFP_{before})x100/ CFP_{after}$. Unbleached regions of the same cell were used as a negative control. Ten cells were measured per each FRET pair and average and standard error calculated.

siRNA transfection

Pre-annealed siRNA duplexes were obtained either from Ambion or Qiagen. Three independent siRNA duplexes were used against hNtr1 and five duplexes were used to target hPrp22. The sequences of sense siRNAs were as follows:

Ambion –

hNtr1-27 - 5'-CCUGUUAAGCAGGACGACUtt;

hNtr1-28 - 5'-GCAGGACGACUUUCCUAAGtt;

hNtr1-29 - 5'-GGAUUAGCAAGAAGCUCACtt;

hPrp22-55 - 5'-GCUUUAAUGCCCAGCGCAGtt;

hPrp22-56 - 5'-GGAAUAAAGUGAAGUCUAGtt;

hPrp22-57 - 5'-CCCAAAUAGACGGCGAAAUtt;

Qiagen –

hPrp22-3 - 5'-GGGACAGGACAAAGAAGAAtt;

hPrp22-4 - 5'-CAGAGAAGUGGGAGAUCAAtt.

The negative control 1 siRNA from Ambion was used as a negative control. Oligofectamine (Invitrogen) was used for siRNA transfection. Cells were incubated 48h prior to further treatment. Within this incubation period we did not observe any extensive cell death with respect to the treatment with the negative control siRNA.

RT-PCR

Total RNA was isolated 48h after siRNA transfection using TRIZOL® reagent (Invitrogen). cDNA was synthesized using a gene-specific reverse primer and SuperScriptIII (Invitrogen). Taq polymerase was used to amplify cDNA (25 cycles). Controls without RT reaction were performed to verify that there was no residual DNA contamination. The following primers were used for RT-PCR and quantitative PCR:

hPrp22-For: CAAGAGGTGGGCTACACCAT;

hPrp22-Rev:5'-TGATCGCGTACTGAGTGAGG;

hNtr1-For: 5'-TGTCTTCACTCCTGGCTCCT;

hNtr1-Rev: 5'-AAGCCACTTGGGGAAGAAGT;

18S-For: 5'-TTGTTGGTTTTCGGAACTGAG;

18S-Rev: 5'-GCAAATGCTTCGGCTCTGGTC;

c-myc-mRNA-For: 5'-GCGACTCTGAGGAGGAACAAGAAG;

c-myc-mRNA-Rev: 5'-ACTCTGACCTTTTGCCAGGAGC;

c-myc-pre-mRNA-For: 5'-TGCTCCCTTTATTCCCCCAC;

c-myc-pre-mRNA-Rev: 5'-GGTCATAGTTCCTGTTGGTGAAGC;

LDHA mRNA-For: 5'-AGAACACCAAAGATTGTCTCTGGC;

LDHA mRNA-Rev: 5'-TTTCCCCCATCAGGTAACGG;

LDHA pre-mRNA-For: 5'-CCTTTCAACTCTCTTTTGGCAACC;

LDHA pre-mRNA-Rev: 5'-AATCTTATTCTGGGGGGTCTGTTC;

Tubulin mRNA-For: 5'-GCTGCTTTGTGGAGTGGATTCC;

Tubulin mRNA-Rev: 5'- CCGTGTTGTTGCCAATGAAGG;

Tubulin pre-mRNA-For: 5'- GACCTTCCTCCTGCTTTCAGTTC;

Tubulin pre-mRNA-Rev: 5'- TCTGCTTGTGTTCCCAGTTGC.

Quantitative PCR was done as described previously (Listerman, Sapra et al. 2006) and ratio of pre-mRNA to mRNA calculated for each siRNA treatment according to $R_{siRNA} = 2^{(Ctpre\text{-}mRNA\text{-}CtmRNA)}$, normalized to NC siRNA treated cells: $R_n = R_{siRNA}/R_{ncsiRNA}$ and plotted.

Glycerol gradient ultracentrifugation

Nuclear extracts were prepared according to (Dignam, Lebovitz et al. 1983), diluted in gradient buffer (20 mM HEPES/KOH pH 8, 150 mM NaCl, 1.5 mM MgCl2, 0.5mM dithiothreitol) and fractionated in a linear 10-30% glycerol gradient by centrifugation 32,000rpm, 17h using the SW-41 rotor (Beckman). Individual fraction (700ml) were

collected and RNA was extracted from each fraction with phenol:chloroform:isoamylalcohol, separated on 10% UREA-PAGE and silver stained. In parallel, proteins were precipitated from the phenol phase by acetone, dissolved in SDS-PAGE sample buffer and analyzed by immunoblotting.

Indirect immunofluorescence

48h after the siRNA transfection the cells were fixed in 4% paraformaldehyde/PIPES for 10 minutes, permeabilized for 5 minutes with 0.2% Triton X-100 (Sigma) and incubated with appropriate primary antibodies. Secondary anti-rabbit antibodies conjugated with FITC and anti-mouse antibodies conjugated with TRITC (Jackson ImmunoResearch Laboratories) were used. Images were collected using the DeltaVision microscope system and subjected to mathematical deconvolution as described above. Mean fluorescence intensities in CBs and the nucleoplasm were determined in individual optical sections using ImageJ as described previously (Stanek and Neugebauer 2004).

In situ hybridization

Digoxigenin-labeled DNA probes directed against human U2, U4 and U5 snRNAs were obtained by PCR as previously described (Bell, Schreiner et al. 2002) using pSP65U2H, pSPU4b, pSP64U5 (Black and Pinto 1989) as templates. 48h after siRNA transfection cells were fixed in 4% paraformaldehyde/PIPES for 10 minutes, permeabilized with 0.5% Triton X-100 for 5 minutes and incubated with anti-SART3 antibodies as a marker of CBs followed by incubation with secondary antibody conjugated with FITC (Jackson ImmunoResearch Laboratories). Cells were again fixed in 4% paraformaldehyde/PIPES for 5 minutes, quenched for 5 minutes in 0.1M glycine/0.2M TRIS pH 7.4 and incubated with digoxigenin-labeled probe in 2xSSC/50% formamide/10% dextran sulphate/1% BSA for 60 minutes at 37ºC. After washing in 2xSSC/50% formamide, 2xSSC and 1xSSC, the probe was detected by mouse anti-digoxigenin antibody (Roche) followed by incubation with goat anti-mouse antibody coupled with TRITC (Jackson ImmunoResearch Laboratories). Images were collected using DeltaVision microscope system and fluorescence intensities in CBs and the nucleoplasm determined as describe above.

2.4 Results

Accumulation of mature snRNPs in Cajal bodies

It is not known whether the pool of snRNPs in CBs consists of only newly imported and incompletely assembled snRNPs, or whether mature snRNPs that have already participated in splicing accumulate in CBs as well. We probed the relative "age" of snRNPs in CBs, by tagging SmB and SmD1 proteins with a "fluorescent timer", a mutant of red fluorescent protein drFP583 (E5-RFP) that changes its fluorescence emission properties during maturation, converting from green to red emission within the course of 3 hours (Terskikh, Fradkov et al. 2000). Changes in the red to green ratio over time are therefore indicative of relative shifts in the age of the molecules present in a given subcellular location. Because there is no evidence of Sm protein exchange once the Sm ring has been assembled on snRNA (Wang and Meier 2004; Shpargel and Matera 2005), we assume that Sm proteins remain stably associated with nuclear snRNPs after assembly and import; thus, Sm protein dynamics likely reflect those of mature snRNPs. In addition, fluorescently tagged Sm proteins efficiently incorporate into snRNP particles and their expression is comparable with endogenous Sm proteins (Supplementary fig. 2.1.). HeLa cells expressing SmB- or SmD1-E5-RFP were fixed at different times after transfection and E5-RFP fluorescence intensities in the green and red spectra were measured (Fig. 2.1.A). Note that both Sm-E5-RFP constructs localized properly in CBs. Surprisingly, both green and red forms of E5-RFP were clearly present in CBs at the earliest time point (11h) that CBs were detectable, indicating that a portion of E5-RFP had already matured to the red form before fluorescence reached the detection threshold. Absolute intensities of green fluorescence did not change over the time, indicating a constant influx of new snRNPs that must reside for a consistent period in the CB. An increase in red fluorescence and the red:green fluorescence ratio was observed and over the period of 22h increased ~2 times in the nucleoplasm and 3 times in CBs. If CBs selectively recruited only newly imported snRNPs, we would have expected the red:green ratio to remain the same or even decrease in CBs, despite the fact that more of the red variant accumulates in the nucleus.

To test whether Sm-E5-RFP proteins are imported to the cell nucleus within snRNP particles, cells were treated for two hours before fixation with Leptomycin B that efficiently inhibits export of newly synthesized snRNAs to the cytoplasm and consequently also import of newly formed snRNPs. A 45% increase in the red:green

ratio observed 38h after transfection (Fig. 2.1.B) indicates impairment of green SmB-E5-RFP import, indicating that SmB-E5-RFP is indeed imported together with snRNAs beginning the biogenesis pathway in the cytoplasm. The finding that CBs accumulate more old snRNPs in CBs compared to the nucleoplasm indicates that the pool of snRNPs concentrated in CB contains not only fresh snRNPs, but also relatively older, presumably mature snRNPs.

A complementary experiment was suggested by the fact that, although they are highly concentrated in CBs, snRNPs exchange rapidly with the surrounding nucleoplasm and only reside in CBs for few seconds on average (Dundr, Hebert et al. 2004; Sleeman 2007). We tagged Sm proteins with photo-activatable GFP (PA-GFP) in order to determine whether the snRNPs that exit CBs at any given moment are replaced by new or old snRNPs. SmB- or SmD1-PA-GFP was expressed and the entire nucleus was photoactivated (Fig. 2.2.). If CBs contain exclusively new (non-activated) snRNPs imported from the cytoplasm, fluorescence would be lost from these CBs over time. On the contrary, SmB-GFP fluorescence CBs remained high 20 minutes after photoactivation (Fig 2.2.), 100 times longer than the residence time of snRNPs in CBs. Measurement of fluorescence intensities in CBs and nucleoplasm revealed a 0-25% decrease (average 6%) in fluorescence intensity in CBs relative to nucleoplasm. These data show that the exchanging population of snRNPs in CBs consists largely of "older" nuclear snRNPs.

To further examine the assembly status of snRNPs in CBs and in the cytoplasm, we probed snRNP interactions with the SMN protein, which is localized both in the cytoplasm and in CBs. The SMN protein is a part of the SMN complex, which ensures proper assembly of Sm rings on snRNPs in the cytoplasm (Terns and Terns 2001; Meister, Eggert et al. 2002; Paushkin, Gubitz et al. 2002; Matera and Shpargel 2006). The significance of SMN accumulation in CBs is not known. Because SMN is required for the import of newly assembled snRNPs (Narayanan, Ospina et al. 2002; Narayanan, Achsel et al. 2004), it is hypothesized that SMN is co-imported into CBs with new snRNPs (Matera and Shpargel 2006). Interactions between snRNPs and the SMN protein were measured by fluorescence (Förster) resonance energy transfer (FRET). Because Sm proteins and SMN are present in the cytoplasm and in CBs, a FRET signal could indicate the presence of snRNP-SMN complexes and/or changes in their structure and composition in the different cellular compartments. SmD1-CFP or SmB-CFP were co-expressed with SMN-YFP in HeLa cells and FRET measured by the acceptor

photobleaching method in the cytoplasm and CBs of the same cell (Fig. 2.3.). As a negative control, SMN-YFP was co-expressed with CFP only. As expected, FRET between SMN and the Sm proteins was detected in the cytoplasm, but no FRET signal above the negative control was observed in CBs. Overall higher FRET values in CBs are likely caused by local accumulation of SMN. In some cells, Sm proteins and SMN accumulated in cytoplasmic bodies, presumably due to co-expression of exogenous SMN and Sm proteins (Shpargel, Ospina et al. 2003); these aggregates resembled recently identified U bodies (Liu and Gall 2007) and contained similar amounts of fluorescent proteins as nuclear CBs. High FRET signals detected in these cytoplasmic inclusions indicate accumulation of SmB-SMN complexes. In addition, FRET between SmB-YFP and SmD1-CFP were robust in the cytoplasm as well as in CBs. Pre-assembled Sm subcomplexes are utilized during assembly of the Sm-ring; SmB and SmD1 proteins are not part of the same Sm subcomplexes but lay next to each other in the ring (Raker, Plessel et al. 1996; Kambach, Walke et al. 1999). Thus, detection of FRET between these two components represents a good marker for Sm-ring assembly and further indicates that fluorescently tagged Sm proteins are correctly incorporated into mature snRNPs. These results show that snRNPs in CBs differ from snRNPs localized in the cytoplasm; snRNPs in CBs either do not interact with SMN or snRNP-SMN complexes in CBs have an altered structure that does not support FRET detection.

Cycling of snRNPs between CBs

Because Sm proteins exchange rapidly between CBs and the nucleoplasm (Dundr, Hebert et al. 2004; Sleeman 2007), our finding that CBs contain predominantly mature snRNPs implies that snRNPs cycle constantly between CBs and the nucleoplasm, visiting CBs repeatedly. To test this directly, SmD1 or SmB proteins tagged with PA-GFP were co-expressed with CFP-tagged markers of CBs (SART3, coilin). The Sm-PA-GFP proteins were activated by a short pulse of 405nm laser in one CB and the movement of activated molecules monitored every fifteen seconds over a five minute time period (Fig. 2.4., Supplementary videos 2.1. and 2.2.). Activated SmB- and SmD1-PA-GFP proteins moved from the activated CB, diffused throughout the nucleoplasm and accumulated in another (non-activated) CB within the time course of the experiment. This behavior was not affected by co-expression of any of the CB markers used and no movement of activated molecules was observed in fixed cells (Supplementary fig. 2.2.). These data show directly that snRNPs repeatedly visit CBs.

Accumulation of U4/U6 snRNPs in CBs after inhibition of spliceosome disassembly

Previous reports showed that ongoing snRNP biogenesis is necessary for structural integrity of CBs (Shpargel and Matera 2005; Lemm, Girard et al. 2006). However, our data show that the CB contains mainly mature snRNPs. We therefore aimed to test whether ongoing supply of mature snRNPs is important for maintaining the CB structure as well. Two proteins implicated in spliceosome disassembly were depleted, with the expectation that inhibition of snRNP recycling after splicing would reduce the supply of mature snRNPs. Three different siRNA duplexes were used to target the human homologue of Ntr1 (also named TFIP11; (Wen, Lei et al. 2005) and five duplexes for hPrp22. After two days, total RNA and proteins were isolated and mRNA and protein levels tested (Fig. 2.5.).

To address effect of hNtr1 and hPrp22 knockdown on CB structure, CBs were immunodetected after the siRNA treatment with anti-coilin and anti-SART3 antibodies. Coilin is a universal marker of CBs and SART3 is a marker of snRNPs that interacts with the U4/U6 snRNP and its presence in the CB is sensitive to transcription/splicing inhibition (Stanek, Rader et al. 2003). Surprisingly, CBs remained intact and accumulated SART3 after either treatment (Fig. 2.6.A and data not shown). In fact, the detection of SART3 fluorescent signal in CBs was enhanced by treatment, and an elevated accumulation in CBs of other U4/U6 snRNP components was also observed upon depletion of hPrp22 or hNtr1 (Fig. 2.6.B). The CB accumulation of U4/U6 specific markers was not solely due to a decrease in nucleoplasmic fluorescence, which remained mostly unaffected by the siRNA treatment. Partial effects on the U2-specific U2B" protein were observed after hPrp22 but not hNtr1 knock-down, and no significant changes in CB localization of the U2 snRNA or the U1-specific U1-70K protein were detected. In contrast, CB localization of the three tested U5 snRNP components - hSnu114, hPrp8-GFP and the U5 snRNA - decreased after siRNA treatment. The hPrp8-GFP protein was expressed from a human BAC under the control of the endogenous promoter and was properly incorporated into the U5 and tri-snRNPs (data not shown).

Depletion of hPrp22 or hNtr1 caused the dramatic and specific accumulation of U4/U6 snRNP components in CBs. To determine whether bona fide U4/U6 snRNP particles had formed in CBs, we used FRET to measure interactions that are specific for the SART3•U4/U6 complex, a transient intermediate *en route* to tri-snRNP formation

that was previously localized to CBs (Stanek and Neugebauer 2004). Cells were incubated for 24h with the indicated siRNA, co-transfected with hPrp31-CFP and SART3-YFP, incubated additional 24h and fixed. SART3-hPrp31 FRET interaction is a marker of the U4/U6•SART3 particle (Stanek and Neugebauer 2004). FRET was measured as described previously in the nucleoplasm and CBs by acceptor photobleaching (Stanek and Neugebauer 2004). No significant changes were observed in CBs after treatment with anti-hPrp22 or anti-hNtr1 siRNAs (Fig. 2.7.), showing that U4/U6 components accumulating in CBs are assembled into the U4/U6 snRNP. These data indicate that inhibition of spliceosome recycling leads to specific accumulation of the U4/U6 snRNPs in CBs. To test whether U4/U6 snRNP accumulation in CBs resulted from an inhibition of splicing, three different genes (c-myc, LDHA and tubulin) were tested for splicing efficiency by RT-qPCR. Partial increases in pre-mRNA:mRNA ratios were detected after treatment with anti-hPrp22 siRNAs, but no substantial inhibition of splicing was observed after hNtr1 depletion (Supplementary fig. 2.3.) indicating that U4/U6 snRNPs concentration in CBs is not likely a general result of splicing inhibition and a lack of expression of necessary snRNP components.

Enhanced accumulation of the U4/U6 snRNPs in CBs had been previously observed after inhibition of U4/U6•U5 snRNP assembly (Schaffert, Hossbach et al. 2004). If depletion of hNtr1 and hPrp22 inhibits spliceosome recycling and thus reduces the amount of the free U5 snRNP, assembly of the functional tri-snRNP might be delayed. To assess the influence of hPrp22 or hNtr1 knock-down on snRNP assembly and recycling, nuclear extract was prepared from cells treated for 48h with anti-hPrp22-3 or anti-hNtr1-27 siRNAs and snRNPs analyzed by glycerol gradient ultracentrifugation. RNA and proteins were isolated from individual fractions and U5-specific hSnu114 and U4/U6-associated hPrp4 proteins detected by immunoblotting (Fig. 2.8.). To determine position of individual snRNP complexes in the gradient snRNAs from each fraction were resolved on denaturing gels and silver stained (data not shown). hPrp4 sedimented in two distinct peaks that reflect U4/U6 snRNPs (fractions 6-8) and U4/U6•U5 tri-snRNPs (fractions 11-13). The U5 marker hSnu114 fractionated with the tri-snRNP and with the mono-U5 snRNP (fractions 8-10). In addition to the mono-U5 and the tri-snRNP, hSnu114 accumulated in complexes with higher sedimentation constant (fractions 15 and 16) in anti-hPrp22 siRNA treated cells, which might correspond to post-spliceosomal complexes (Makarov, Makarova et al. 2002) that were not recycled properly after hPrp22 knock down. Importantly, decreases

in the mono-U5 snRNP relative to the U5 in the tri-snRNP fractions were observed in both hPrp22 and hNtr1 siRNA treated cells, consistent with the reduced U5 snRNP concentration in CBs after both knockdowns (Fig. 2.6.).

2.5 Discussion

It was previously shown that U2, U4/U6, and U4/U6•U5 tri-snRNP assembly steps occur in CBs (Nesic, Tanackovic et al. 2004; Schaffert, Hossbach et al. 2004; Stanek and Neugebauer 2004); however, it was not known whether the assembly events reflected *de novo* snRNP assembly or re-assembly after splicing. In this study, we present data showing that in addition to *de novo* snRNP assembly, CBs could serve as the snRNP recycling center. These conclusions are based on three independent lines of evidence. First, we show by several experimental means, that the snRNPs concentrated in CBs include a substantial "mature" snRNP pool. Second, we show directly that snRNPs visit multiple CBs within the same nucleus and do so frequently; thus, there is no reason to suspect that CBs preferentially contain newly imported snRNPs. Third, targeted depletion of two factors required for spliceosome disassembly and snRNP release, hPrp22 and hNtr1, leads to an accumulation of U4/U6 snRNPs in CBs. We argue below that this accumulation likely reflects a failure of U5 snRNP recovery from spliceosomes; in the absence of sufficient U5 snRNP flux through CBs, tri-snRNP formation is blocked. These observations provide novel insights into how phases of the spliceosome cycle are compartmentalized in living cells.

Experiments establishing the relative maturity of snRNPs in CBs relied on three different fluorescence microscopy techniques. The E5-RFP fluorescent protein tag, which changes emission spectra from green to red as it matures, and photoactivatable GFP (PA-GFP) were both used to tag Sm proteins (B and D1; see Figures 2.1. and 2.2.) and monitor snRNP movements. Both approaches proved that the snRNP pool in CBs largely consists of mature snRNPs that have visited CBs already multiple times. In agreement with these data, snRNP movements between CBs were observed, in which snRNPs photoactivated in one CB reappeared within a time course of minutes in another distant CB. A similar movement of snRNPs between CBs was recently described (Sleeman 2007).

In the third approach, we sought to compare snRNPs in CBs and in the cytoplasm by measuring FRET signals between Sm proteins and SMN, which plays a role in the cytoplasmic phase of snRNP biogenesis. SMN is co-imported with new snRNPs to the nucleus and is highly concentrated in CBs; because SMN binds coilin, it has been proposed that SMN delivers the newly imported snRNPs to CBs (Stanek and Neugebauer 2006). However, although we detected SMN-snRNP interactions in the cytoplasm, we did not observe any significant interaction in CBs. This indicates that either 1) the SMN-snRNP complex falls apart immediately after the import of snRNPs, 2) that a conformational change occurs within the CB that is unfavorable for FRET, or 3) newly imported snRNP-SMN complexes form only a small fraction of snRNPs and SMN in CBs, and these are below the detection limit of the FRET assay. At present, we cannot distinguish among these possibilities; if snRNP-SMN complexes are present in CBs, they must differ at least conformationally from the complexes found in the cytoplasm. Perhaps SMN protein accumulates in the CB as a result of binding coilin after snRNP import and dissociation in the CB. Presumably, SMN eventually returns to the cytoplasm for further rounds of Sm ring assembly.

The conclusion that CBs contain not only new snRNPs imported from the cytoplasm, but also mature snRNPs, agrees with findings that the concentration of snRNPs in CBs is transcription-dependent (Carmo-Fonseca, Pepperkok et al. 1992; Blencowe, Carmo-Fonseca et al. 1993; Stanek, Rader et al. 2003); in the absence of new intron-containing transcripts (i.e. under conditions of transcriptional blockade), the splicing process provides fewer “used” snRNPs for recycling. This highlights a paradox emerging in the field, since it has been proposed that snRNP biogenesis and import from the cytoplasm is required for snRNP accumulation in CBs and for integrity of CBs themselves (Carvalho, Almeida et al. 1999; Shpargel and Matera 2005; Girard, Neel et al. 2006; Lemm, Girard et al. 2006). If only a small proportion of snRNPs in CBs are newly imported, how can this fraction be required for CB integrity? The simplest explanation is that experimental reduction of snRNP biogenesis at various stages has long-term effects on the overall concentration of snRNPs in the nucleus, not just an acute effect on import. A reasonable proposal stemming from our present study and consistent with prior work of others is that CB integrity depends on the cellular level of splicing activity and the absolute concentration of nuclear snRNPs (Carmo-Fonseca, Pepperkok et al. 1992; Blencowe, Carmo-Fonseca et al. 1993; Sleeman, Ajuh et al. 2001; Stanek, Rader et al. 2003).

Our data shows that mature snRNPs repeatedly visit CBs. To test whether this cycling through CBs correlates with snRNP regeneration after splicing, proteins involved in spliceosome disassembly were depleted, and localization of distinct snRNPs in CBs was examined. Surprisingly, depletion of two tested proteins involved in spliceosome disassembly resulted in accumulation of U4/U6 snRNPs in CBs. Because transcription/splicing inhibition by α-amanitin leads to opposite effects - the snRNPs and SART3 leave CBs (Carmo-Fonseca, Pepperkok et al. 1992; Blencowe, Carmo-Fonseca et al. 1993; Sleeman, Ajuh et al. 2001; Stanek, Rader et al. 2003) - it seems unlikely that U4/U6 snRNP accumulates in CBs as a result of splicing inhibition. In addition, splicing of c-fos and c-myc pre-mRNAs was only slightly reduced following siRNA treatment (Supp. Fig. 2.3.). Instead, the phenotype more closely resembles the situation after inhibition of U4/U6•U5 snRNP formation, when accumulation of U4/U6 snRNPs in CBs was also observed (Schaffert, Hossbach et al. 2004). Why does inhibition of spliceosome disassembly and inhibition of tri-snRNP assembly have the same phenotype? According to current models of spliceosome recycling, inhibition of this process should trap U5 and U6 snRNPs in the late spliceosome (Will and Luhrmann 2006) and thus decrease levels of free U5 and U6 snRNPs in the nucleoplasm. In contrast, the U4 snRNP leaves the spliceosome at an earlier step, just as the tri-snRNP joins the assembling spliceosome (Makarov, Makarova et al. 2002; Chan, Kao et al. 2003). Thus, the level of free U4 mono-snRNP in the nucleoplasm should be unaffected by Prp22 or Ntr1 depletion. Early studies showed that there is 2-3 fold excess of the U6 snRNP over the U5 and U4 snRNPs (Tycowski, Kolev et al. 2006), making it unlikely that U6 snRNP levels are limiting. In contrast to U4 and U6, however, levels of free U5 snRNP are likely decreased and formation of the U4/U6•U5 tri-snRNP inhibited, as was shown after Ntr1 depletion in yeast (Boon, Auchynnikava et al. 2006). Consistent with this, we observed a decrease in U5 snRNP levels both in CBs and nuclear extracts after knockdown. Thus, inhibition of spliceosome disassembly leads to a similar situation as inhibition of tri-snRNP assembly - accumulation of the U4/U6 snRNPs in CBs. Apparently, the supply of new U5 snRNPs from the cytoplasm is not sufficient to keep up with tri-snRNP assembly, underscoring the importance of the recycled U5 snRNP for assembly and regeneration of tri-snRNPs.

Taken together, these observations suggest that snRNP reassembly after splicing may obey similar rules to *de novo* snRNP assembly, even though the assembly of new snRNPs includes additional steps that need not be repeated (e.g. post-transcriptional

RNA modification). This implies that snRNP assembly in CBs at any stage of their life cycle must be independent of snRNA posttranscriptional modifications or any other steps in snRNP biogenesis. Finally, it has been shown by mathematical modeling that CBs increase the rate of U4/U6 snRNP assembly, by providing a local environment with elevated snRNP concentrations (Klingauf, Stanek et al. 2006). Thus, the localization of snRNPs to CBs likely promotes the assembly of new as well as regenerating snRNPs by the same mechanism, since snRNPs from either source will meet elevated concentrations of their potential partners in the CB.

Figures and videos to chapter 2:

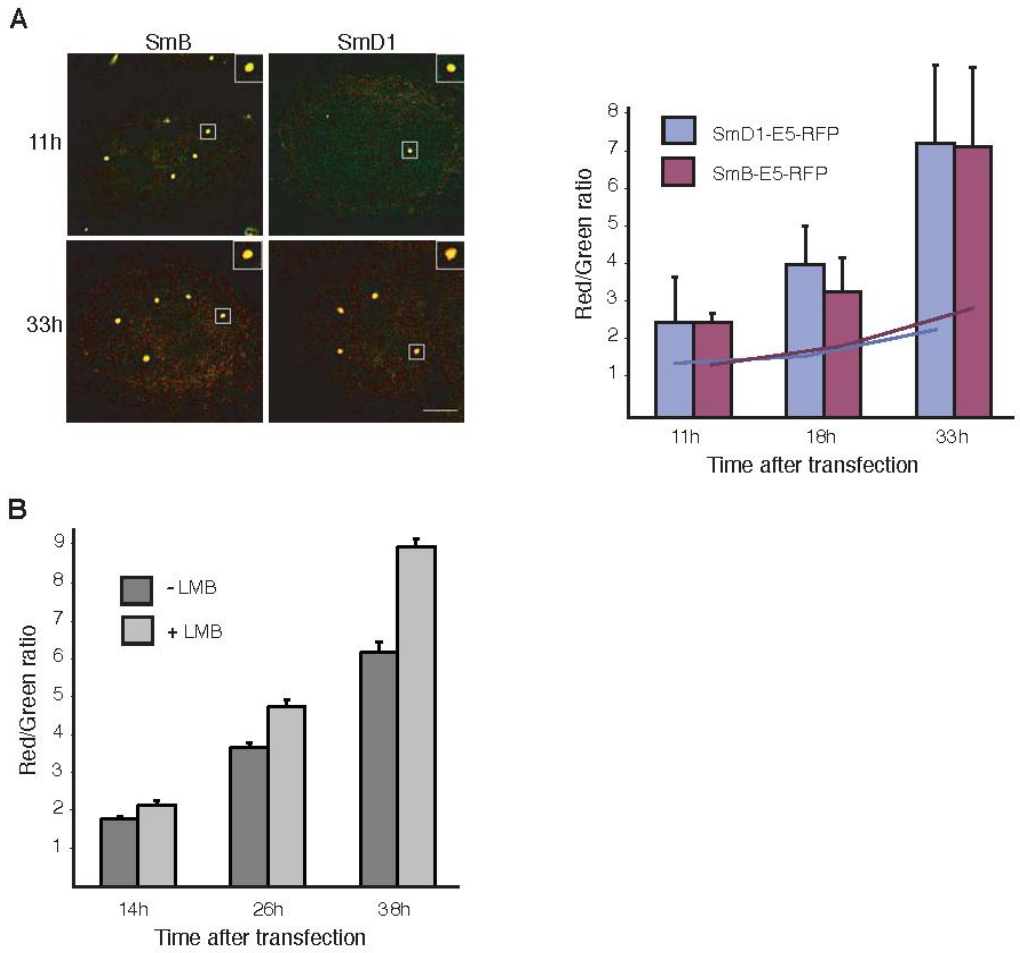

Figure 2.1. Mature snRNPs accumulate in Cajal bodies. To determine the age of snRNPs in CBs, SmB and SmD1 proteins that are stable components of snRNPs were tagged with E5-RFP. During maturation E5-RFP changes its fluorescence from green to red in a time course of a couple hours. A/ HeLa cells were transfected with SmB-E5-RFP or SmD1-E5-RFP and fixed at different times after transfection. Ratio of red to green was measured in CBs (bars - standard deviation indicated) and in the nucleoplasm (lines). Red fluorescence in CBs increased ~3 times over 22h indicating that mature snRNPs accumulate in CBs. B/ Cells were transiently transfected with SmB-E5-RFP and 2 hours before fixation treated with Leptomycin B (LMB) that inhibits biogenesis of new snRNPs by blocking export of new snRNA from the nucleus. 45% increase of red:green ratio after 38h indicates import inhibition of the green (new) variant of SmB-E5-RFP. Standard error bars shown.

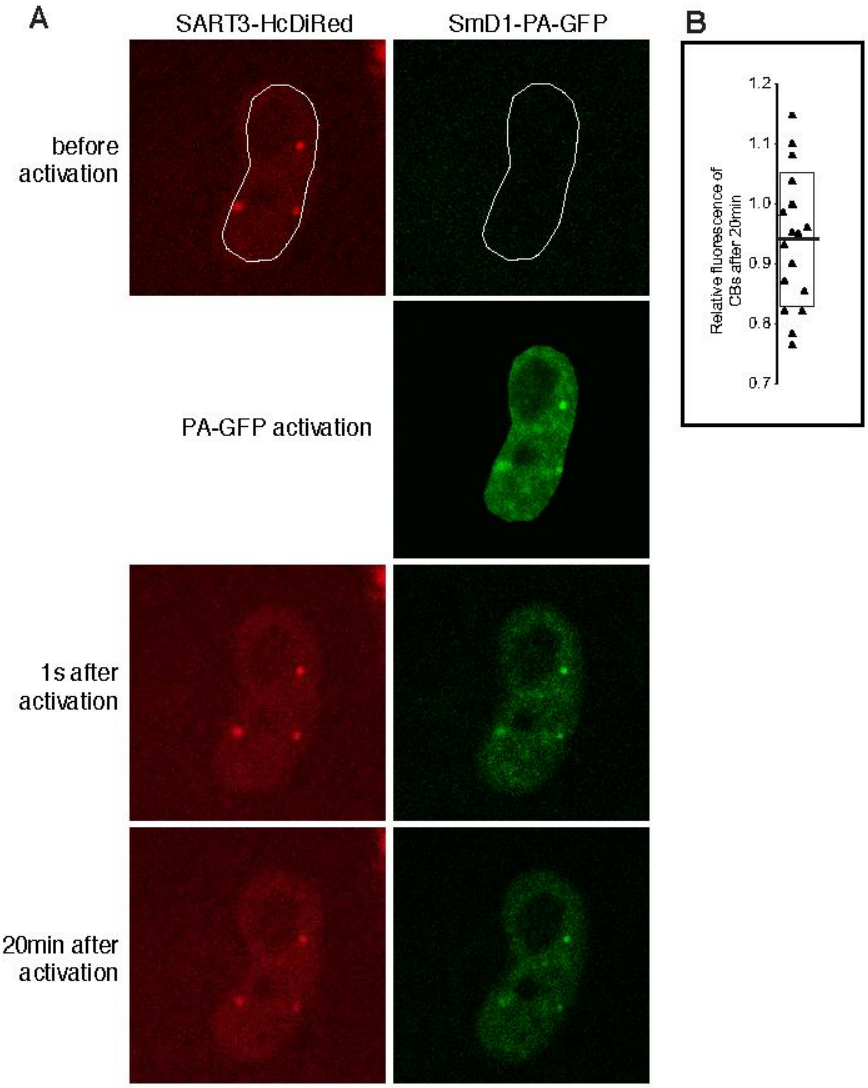

Figure 2.2. snRNPs newly imported from the cytoplasm represent only a minor fraction in CBs. A/ The SmD1 protein was tagged with photoactivatable GFP (PA-GFP) and co-expressed in HeLa cells with SART3-HcDiRed as a marker of CBs. To distinguish between nuclear and cytoplasmic pool of snRNPs, nuclear snRNPs were specifically activated by short pulse of 405nm laser line. Images were taken every two minutes for total 20 minutes. B/ Quantification of CB fluorescence. To avoid photobleaching effects ratio of fluorescent signals CB:nucleoplasm were determined immediately after activation and 20min later and values for individual CBs plotted. Mean value is indicated by a solid line standard deviation by a box. Only small decrease in CB fluorescence indicates that within 20min snRNPs imported from the cytoplasm represent only small fraction of snRNPs in CBs.

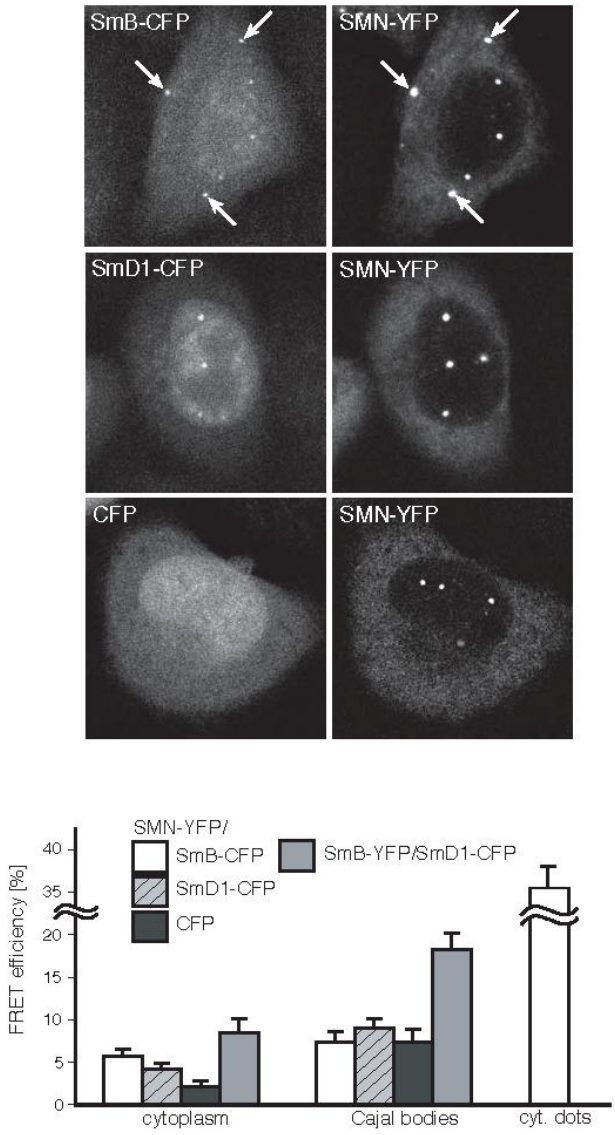

Figure 2.3. The SMN protein interacts with Sm proteins in the cytoplasm. To compare SMN-snRNP complexes in CBs and the cytoplasm, SMN-YFP was co-expressed with SmD1- CFP, SmB-CFP or CFP alone as a negative control and FRET was measured in the cytoplasm and in CBs by acceptor photobleaching method. The SMN-Sm FRET signal was 2-3 fold higher over negative control in the cytoplasm but not in CBs. The SmB - SmD1 pair used as a positive control exhibited high FRET signal both in the cytoplasm and in CBs. In some cells, we observed cytoplasmic accumulation of SmB and SMN proteins (*arrows*) and high FRET signal was measured in these cytoplasmic inclusions. Ten measurements for each pair are averaged and shown in the graph with standard error bars.

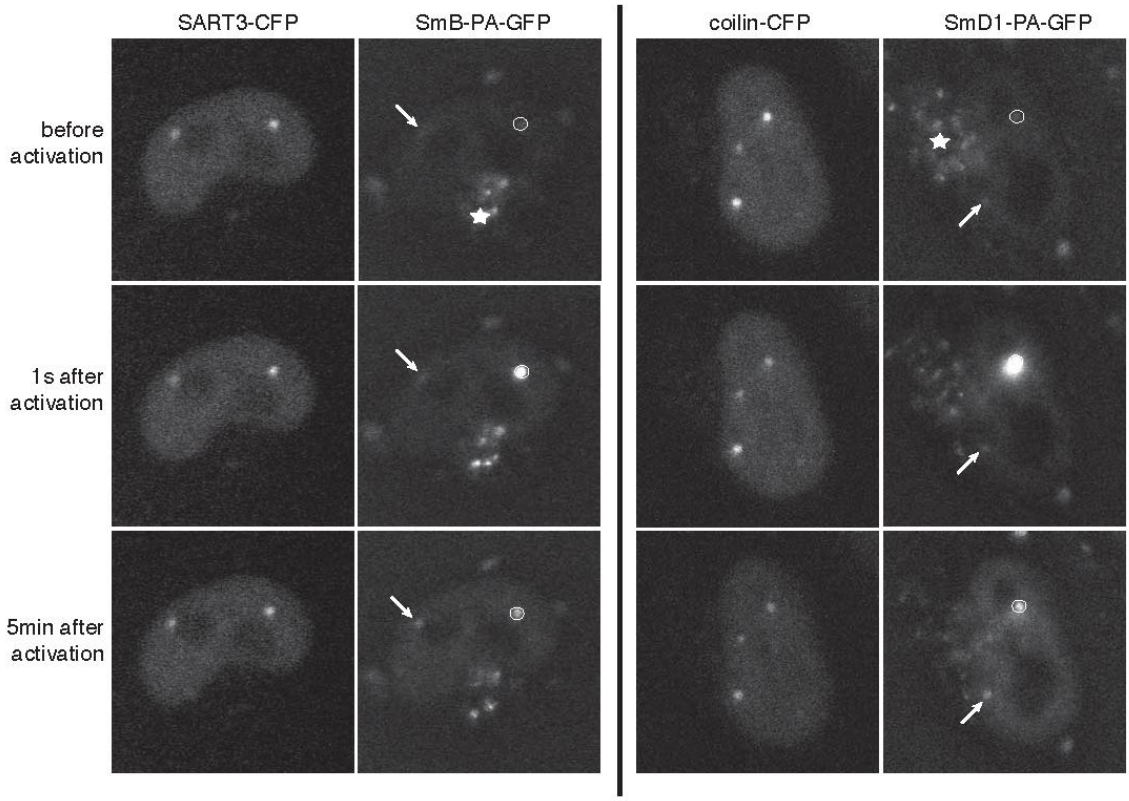

Figure 2.4. snRNPs cycle between CBs. To observe movement of snRNPs between CBs and the nucleoplasm, SmB-PA-GFP was co-expressed with SART3-CFP and SmD1-PA-GFP with coilin- CFP. Sm-PA-GFPs were specifically activated in one CB (*circle*) by short pulse of 405nm laser and movement of activated molecules observed for 5 minutes (see also supplementary videos). Activated molecules moved throughout the whole nucleoplasm and accumulated in other CBs in the same nucleus (*arrows*). The detection system was adjusted to detect very low signals of PA-GFP but using this set up we also detected cell autofluorescence in the cytoplasm (*stars*).

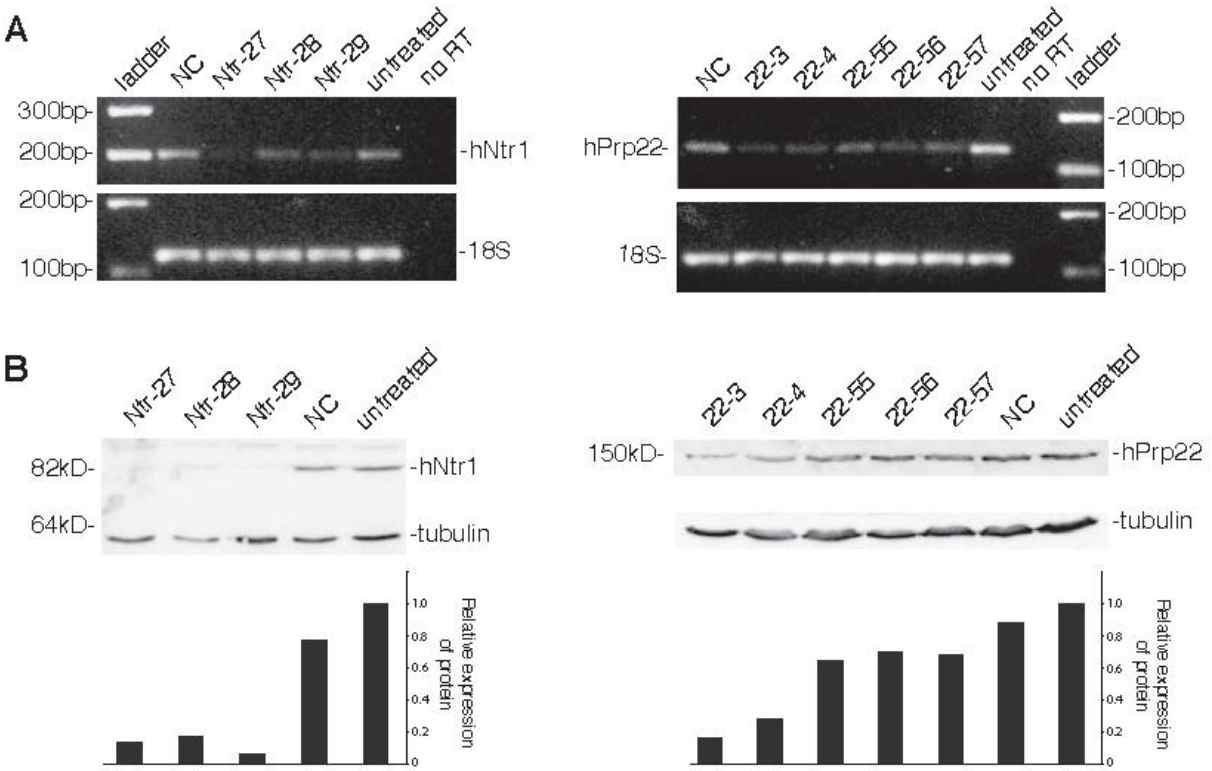

Figure 2.5. siRNA targeted depletion of hPrp22 and hNtr1. A/ Five different siRNAs against hPrp22 and three against hNtr1 protein were used. Cells were treated with siRNAs for 48h and mRNA level of hPrp22 and hNtr1 determined by RT-PCR. RT-PCR of 18S rRNA served as a loading control. B/ Extract from cells treated for 48h with siRNAs was loaded on gel and hNtr1 and hPrp22 protein level determined. Anti-tubulin antibody used as a loading control.

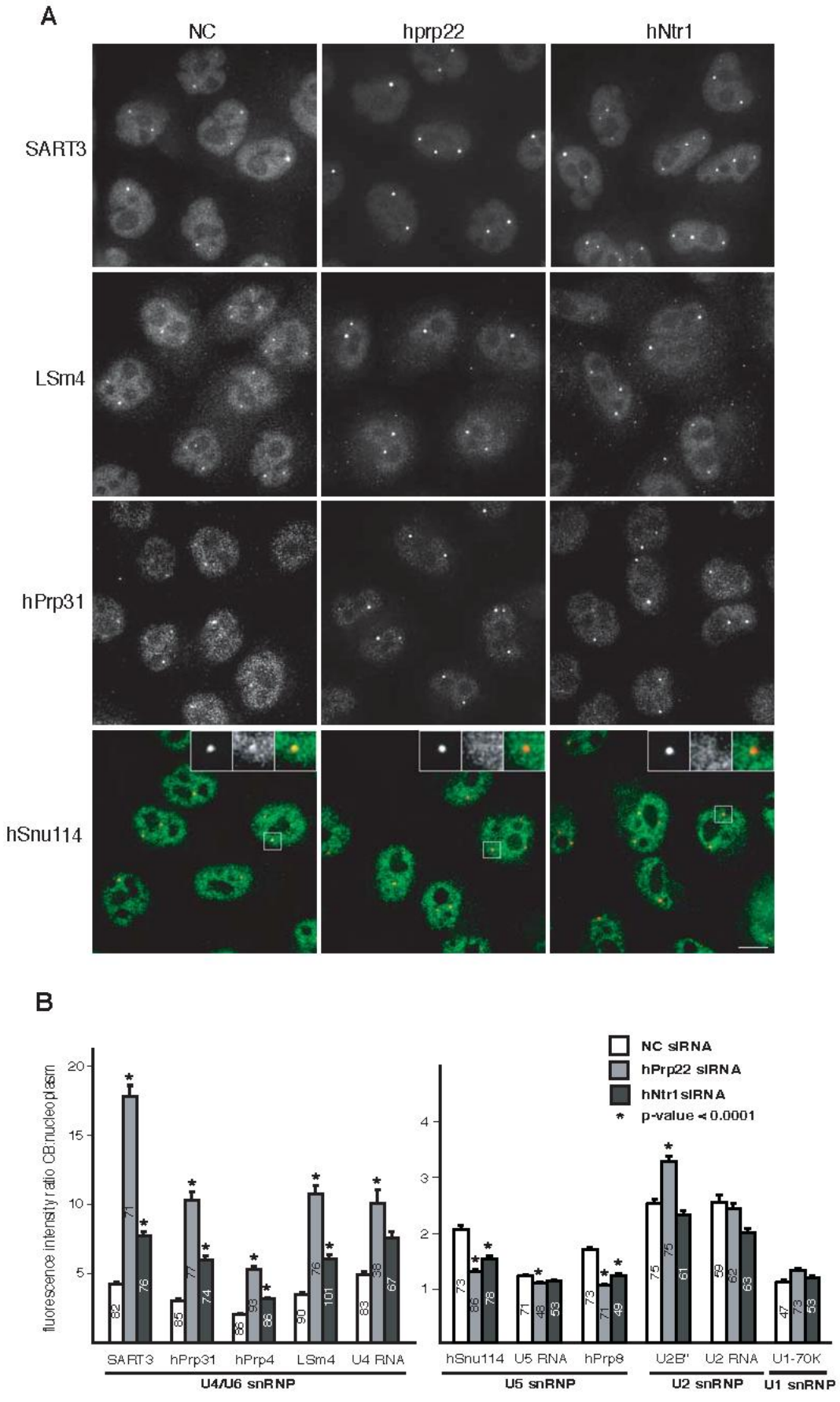
A
NC
hprp22
hNtr1
SART3
LSm4
hPrp31
hSnu114
B
fluorescence intensity ratio CB:nucleoplasm
NC siRNA
hPrp22 siRNA
hNtr1 siRNA
* p-value < 0.0001
SART3
hPrp31
hPrp4
LSm4
U4 RNA
hSnu114
U5 RNA
hPrp8
U2B''
U2 RNA
U1-70K
U4/U6 snRNP
U5 snRNP
U2 snRNP
U1 snRNP

Figure 2.6. U4/U6 specific markers accumulate in CBs after hPrp22 and hNtr1 knockdown. A/ Cell treated with siRNA against hPrp22 (22-3) and hNtr1 (Ntr-27) for 48 hours were fixed and localization of snRNP-specific proteins determined by antibody staining. In order to avoid distortion of CB morphology due to changes in intensity, the intensities of the images shown were adjusted to an equal maximum. This results in apparent fluorescent reduction in the nucleoplasm after siRNA treatments, which was not observed at raw images. NC - negative control siRNA. hSnu114 - green, coilin - red. B/ Quantification of fluorescence is shown in the graph. Fluorescence ratio CB:nucleoplasm was calculated for each CB and average with standard error bars shown (number of measured CBs indicated inside bars). * - p-value < 0.0001 as determined by student test with respect to cells treated with control siRNA.

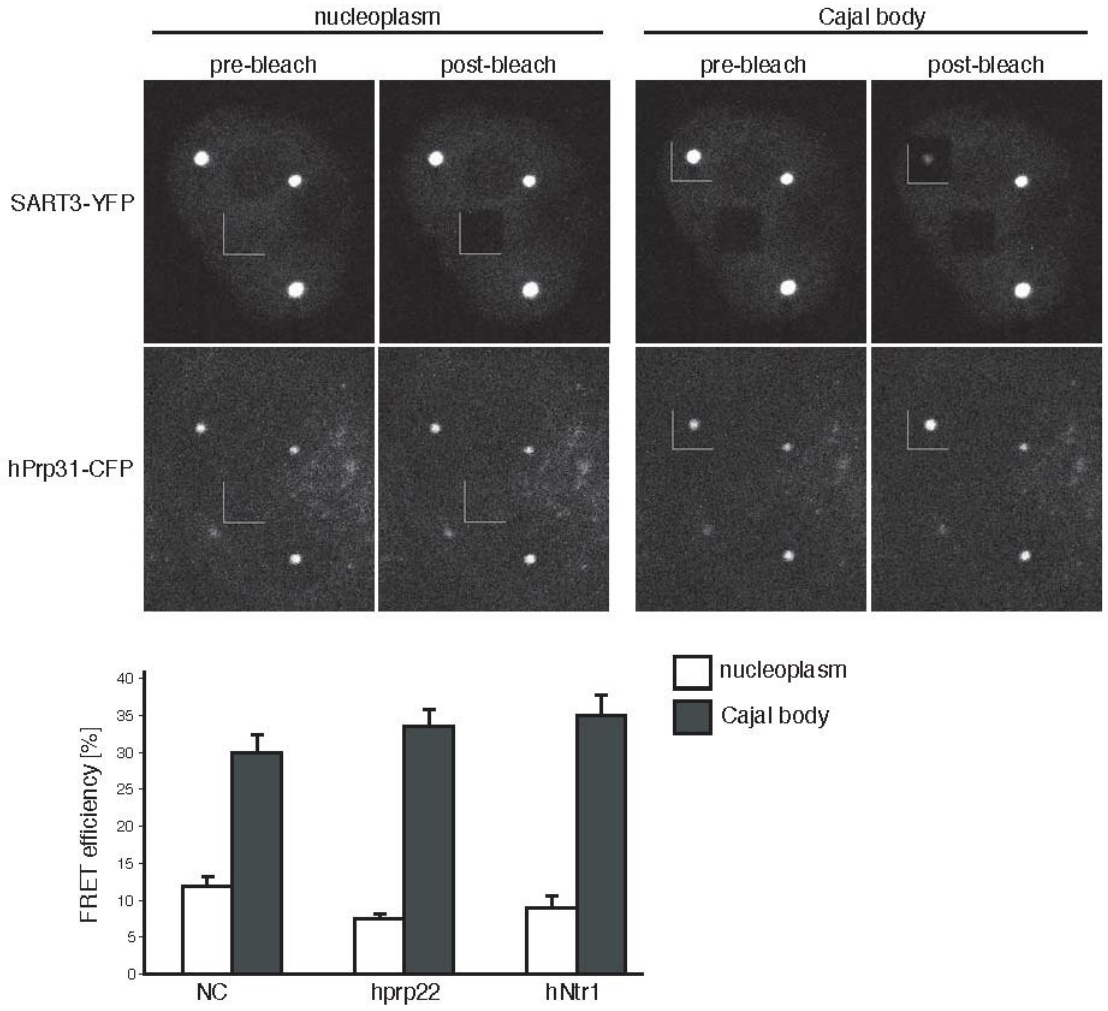

Figure 2.7. Assembled U4/U6 snRNP accumulates in Cajal bodies after hPrp22 and hNtr1 knock-down. Cells treated with siRNA against hPrp22 (22-3) were transfected with SART3-YFP and hPrp31-CFP and FRET was measured by acceptor photobleaching in the nucleoplasm and CBs. Quantification of SART3-YFP / hPrp31-CFP FRET measurements in cells treated with control (NC), hPrp22-3 or hNtr1-27 siRNAs. Average values of ten measurements with standard error bars are shown.

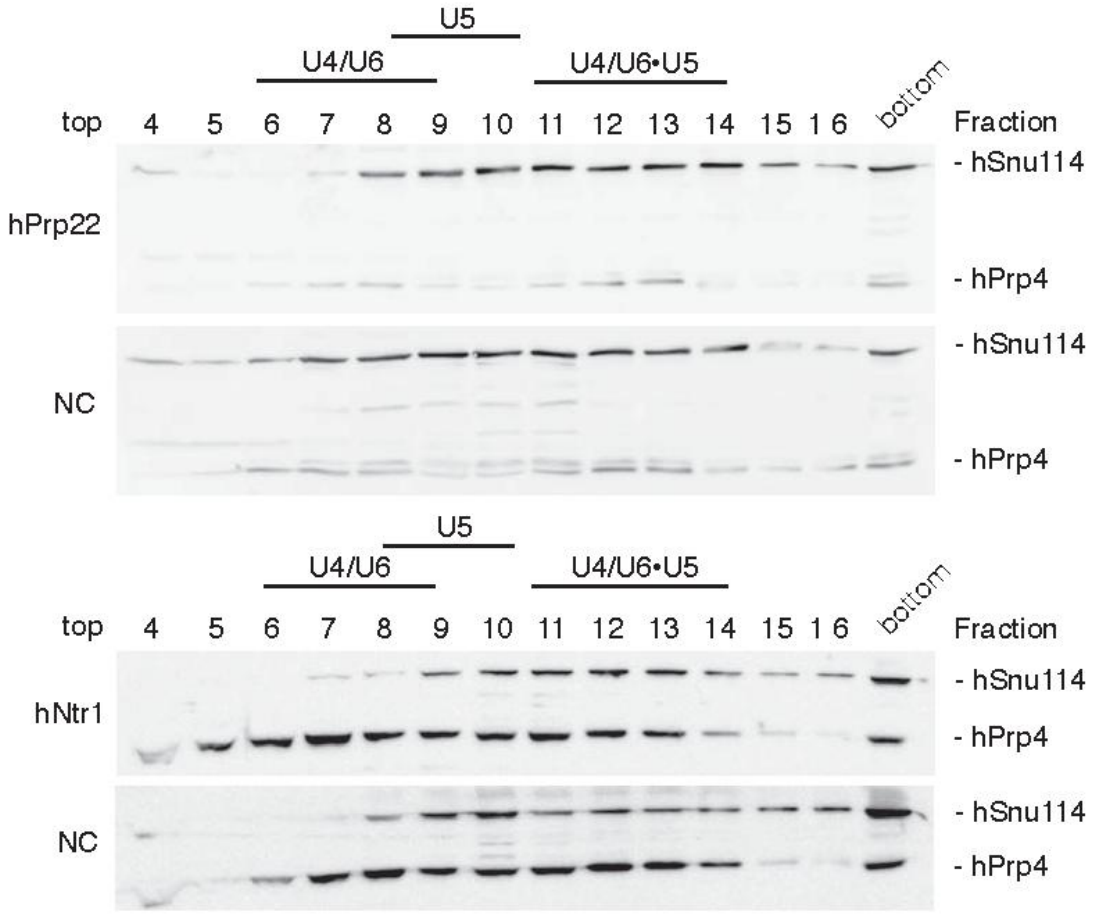

Figure 2.8. Mono-U5 snRNP is reduced after hPrp22 knock-down. HeLa cells were treated with 22-3 or Ntr-27 siRNA for 48h and nuclear extracts were centrifuged on 10-30% glycerol gradients. Parallel RNA gels were used for determination of snRNP complexes position in gradients. Proteins from individual fractions were isolated and hSnu114 (marker of the U5 snRNP) and hPrp4 (marker of the U4/U6 snRNP) were detected. In siRNA treated cells level of the free U5 snRNP decreased (fractions 8-10).

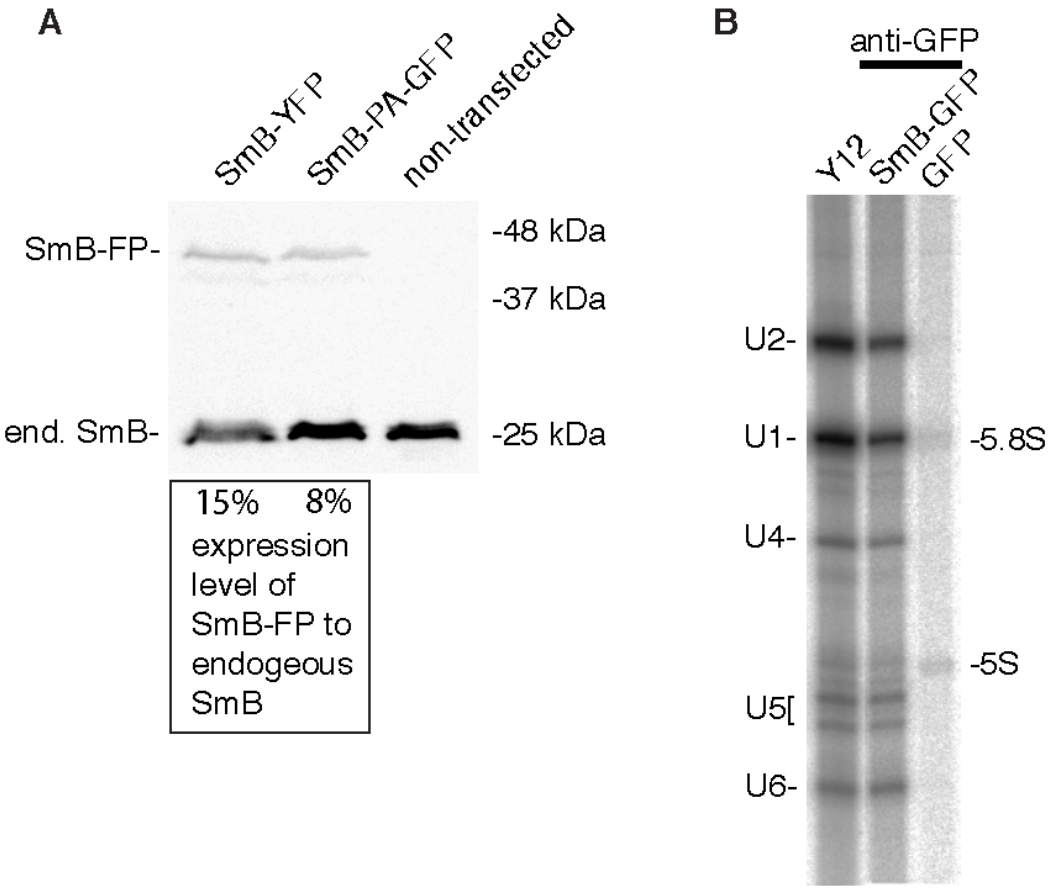

Supplementary figure 2.1. Fluorescently tagged SmB proteins are expressed at levels similar to endogenous and are properly incorporated into snRNPs. A/ HeLa cells were transiently transfected with SmB-YFP or SmB-PA-GFP, cultivated for 24h, total proteins isolated and SmB proteins detected by immunoblotting, using the Y12 monoclonal antibody. Because SmB-YFP signal was 15% of the endogenous SmB signal and transfection efficiency was ~ 15% we conclude that expression of SmB-YFP was similar to expression the endogenous SmB protein. B/ HeLa cells were stably transformed with SmB-GFP tagged on a BAC (a gift of Ralf Kittler and Frank Buchholz). These cells were labeled overnight with P^{32}-orthophosphate, total cell extracts prepared and subjected to immunoprecipitation using anti-GFP or the Y12 antibodies as a positive control. RNA was isolated from pellets and resolved on a denaturing UREA gel, and exposed to a phosphorimager plate. Note that the pattern and intensity of the snRNA signals co-immunoprecipitated with anti-GFP and Y12 were nearly identical.

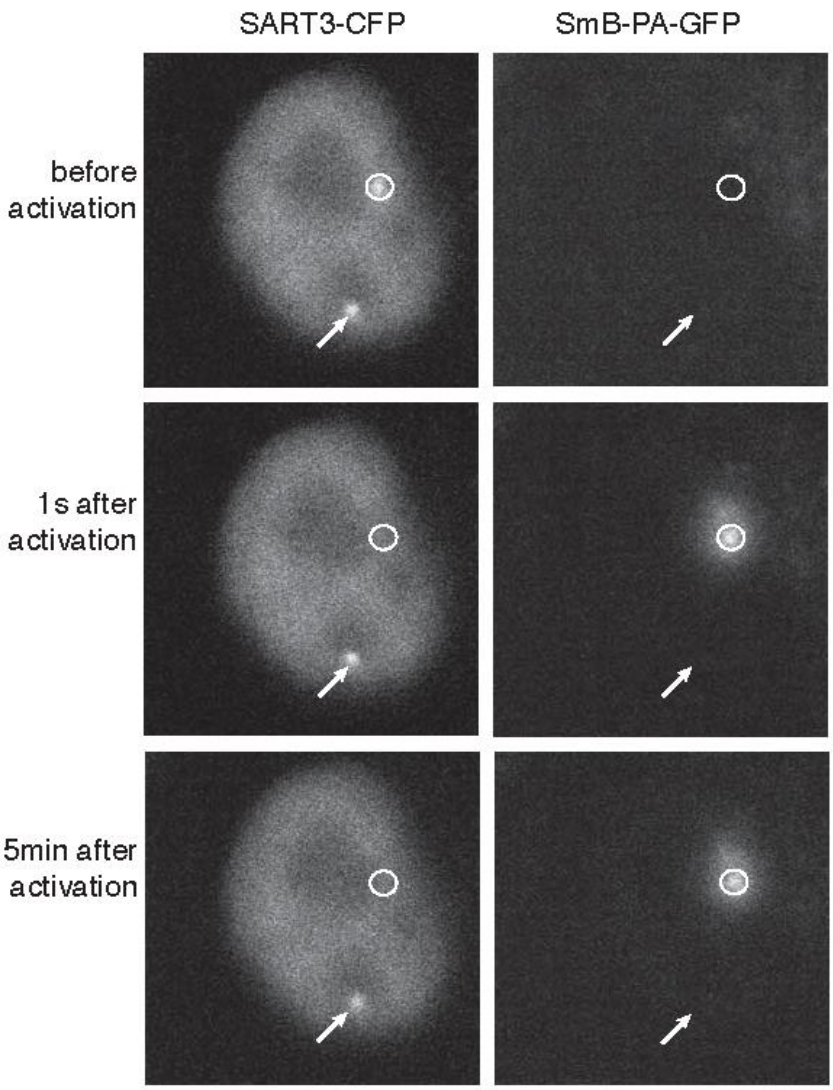

Supplementary figure 2.2. snRNPs do not move after cell fixation. To provide a control for snRNP cycling between CBs, SmB-PA-GFP was co-expressed with SART3-CFP to mark CBs. 24h after transfection cells were fixed for 10min in 4% paraformaldehyde/PIPES and kept in Mg-PBS. SmB-PA-GFP was specifically activated in one CB (*circle*) by short pulse of 405nm laser and images taken every fifteen seconds for 5 minutes. No movement of activated molecules to other CB (*arrow*) was observed.

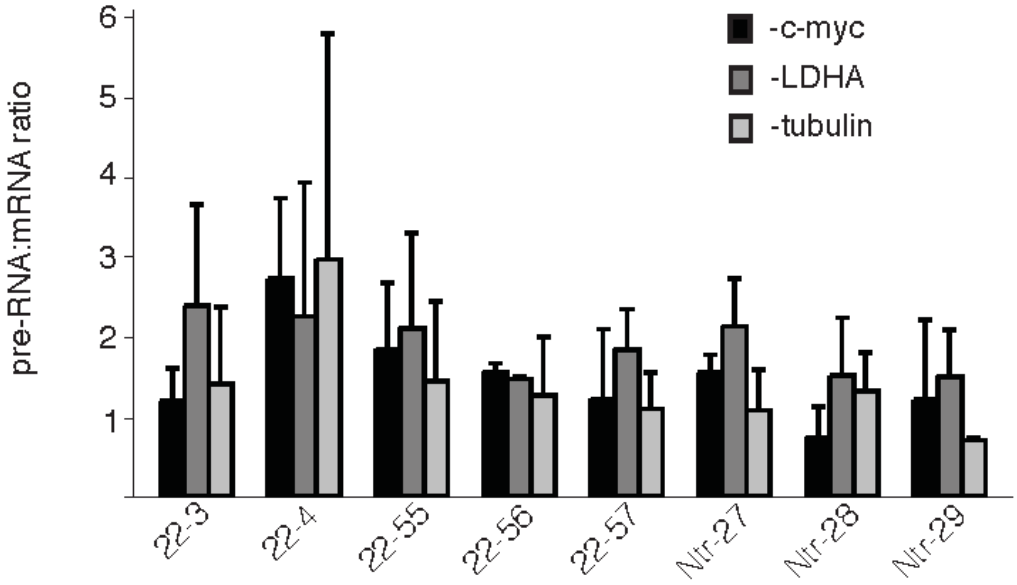

Supplementary figure 2.3. To determine effects of hPrp22 and hNtr1 knock-down on splicing, cells were treated with siRNAs for 48h, total RNA isolated and level of c-myc, LDHA and tubulin pre-mRNAs and mRNAs determined by RT-qPCR. For each siRNA pre-mRNA to mRNA ratio was determined and normalized to cell treated with neg. control siRNA. Averages of two independent experiments with standard deviation are plotted. For majority of tested siRNAs we observed only a partial increase of pre:mRNA ratio indicating that splicing was not totally blocked.

Supplementary videos can be found at:
http://www.molbiolcell.org/cgi/content/full/E07-12-1259/DC1

Video 2.1. snRNPs cycle between CBs. To observe movement of snRNPs in the cell nucleus, SmB-PA-GFP was co-expressed with SART3-CFP (not shown - see also fig. 4) in HeLa cells and activated by short pulse of 405nm laser specifically in one CB. Images were taken every 15s for 5min. Activated molecules moved throughout the whole nucleoplasm and accumulated in other CBs in the same nucleus. The detection system was adjusted to detect very low signals of PA-GFP but using this set up we also detected cell autofluorescence in the cytoplasm. Rate: 4 f/s.

Video 2.2. snRNPs cycle between CBs. To observe movement of snRNPs in the cell nucleus, SmD1-PA-GFP was co-expressed with coilin-CFP (not shown - see also fig. 4) in HeLa cells and activated by short pulse of 405nm laser specifically in one CB. Images were taken every 15s for 5min. Activated molecules moved throughout the whole nucleoplasm and accumulated in other CBs in the same nucleus. The detection system was adjusted to detect very low signals of PA-GFP but using this set up we also detected cell autofluorescence in the cytoplasm. Rate: 4 f/s.

CHAPTER 3

Differential interaction of snRNPs with pre-mRNA reveals splicing kinetics in living cells.

This chapter was reproduced from submitted manuscript:
Huranová M., Ivani I., Benda A., Poser I., Brody Y., Hof M., Shav-Tal Y., Neugebauer K.M., Staněk D. : The differential interaction of snRNPs with pre-mRNA reveals splicing kinetics in living cells. J Cell Biol. *submitted*

3.1 Abstract

Pre-mRNA splicing is catalyzed by the spliceosome, a large ribonucleoprotein complex composed of five small nuclear ribonucleoprotein particles (snRNPs) and additional proteins. Using live cell imaging of GFP-tagged snRNP components expressed at endogenous levels, we examined how the spliceosome assembles *in vivo*. A comprehensive analysis of snRNP dynamics in the cell nucleus enabled us to determine snRNPs diffusion throughout the nucleoplasm as well as the interaction rates of individual snRNPs with pre-mRNA. Core components of the spliceosome, U2 and U5 snRNPs, associated with pre-mRNA for 12-30 s, indicating that splicing is accomplished within this time period. Additionally, binding of U1 and U4/U6 snRNPs with pre-mRNA occurred within seconds indicating that the interaction of individual snRNPs with pre-mRNA is distinct. These results are consistent with the predictions of the step-wise model of spliceosome assembly and provide an estimate on the rate of splicing in human cells.

3.2 Introduction

In eukaryotic cells, protein encoding transcripts contain intronic sequences that must be spliced out prior to translation. This crucial step in gene expression is catalyzed by the spliceosome, a multi-component ribonucleoprotein complex that consists of five major U1, U2, U4, U5 and U6 small nuclear ribonucleoprotein particles (snRNPs) in addition to other proteins (Will and Luhrmann 2001; Jurica and Moore 2003; Wahl, Will et al. 2009). Each snRNP consists of a unique snRNA associated with a specific set of proteins and a ring of seven Sm or Lsm proteins (Urlaub, Raker et al. 2001). During splicing, the spliceosome has to accomplish several functions that involve correct intron recognition, a two-step transesterification reaction to cleave out introns and join together exons, and finally the release of mature mRNA (Staley and Guthrie 1998; Wahl, Will et al. 2009).

Although the process of spliceosome assembly has been intensively studied, the precise mechanism of its *in vivo* formation is still not fully understood. Two models of spliceosome assembly during pre-mRNA splicing have been proposed: 1) The step-wise assembly model that proposes individual snRNPs sequentially assembly on pre-mRNA, and 2) the penta-snRNP or supraspliceosome model, which predicts that a pre-formed spliceosome containing all snRNPs is recruited to pre-mRNA (reviewed in (Rino and Carmo-Fonseca 2009).

According to the step-wise model, snRNPs sequentially interact with the pre-mRNA transcript. Initially, intron boundaries are recognized when the U1 snRNP interacts with the 5' splice site and the U2 snRNP and associated factors interact with the branch point. Once the intron is defined, U4, U5 and U6 snRNPs are recruited as a preassembled U4/U6•U5 tri-snRNP. The spliceosome then undergoes extensive conformational and compositional rearrangements that result in the release of U1 and U4 snRNA, together with their corresponding U1 and U4/U6 snRNP specific proteins and the formation of the catalytic core that is essential for the transesterification reactions. When splicing is accomplished, mature mRNA is released and the U2, U5, and U6 snRNPs dissociate from the intron lariat to be recycled for subsequent rounds of splicing. This model is based on numerous *in vitro* observations that demonstrated the sequential association of individual snRNPs with pre-mRNA (Reed 2000). Further, in both yeast and mammalian *in vitro* systems, distinct intermediates of spliceosome assembly were detected and characterized (Brody and Abelson 1985; Konarska and

Sharp 1986; Bindereif and Green 1987; Jurica, Licklider et al. 2002; Jurica and Moore 2003). Finally, in yeast cells chromatin immunoprecipitation (ChIP) data showed the sequential association of snRNPs with nascent transcripts (Kotovic, Lockshon et al. 2003; Gornemann, Kotovic et al. 2005; Lacadie and Rosbash 2005; Tardiff, Lacadie et al. 2006; Tardiff and Rosbash 2006). However, in mammalian cells ChIP lacks the necessary resolution to analyze the dynamic aspects of spliceosome assembly (Listerman, Sapra et al. 2006).

The second model proposes the existence of a pre-assembled spliceosome that is splicing competent. Several studies performed in yeast and mammalian systems have demonstrated the association of U1 and U2 snRNPs with U4/U6 and U4/U6•U5 snRNPs in the absence of pre-mRNA (Konarska and Sharp 1988; Wassarman and Steitz 1992). This alternative view was supported when the 45S complex was isolated from a yeast extract and was found to contain all five snRNPs. Subsequently, this complex was referred to as the "penta snRNP" (Stevens, Ryan et al. 2002). Additionally, in human cells a large 200S RNP particle named the "supraspliceosome" that contained four penta-snRNP-like subunits was isolated and shown to catalyze RNA splicing (Azubel, Habib et al. 2006; Sperling, Azubel et al. 2008). However, it was also reported in a human *in vitro* system that the penta-snRNP is not essential for early spliceosome assembly steps (Behzadnia, Hartmuth et al. 2006). Fluorescence resonance energy transfer (FRET) studies performed in live cells showed that the interaction between several splicing factors persist after transcriptional inhibition, indicating that the larger splicing complexes are formed *in vivo* in the absence of pre-mRNA (Chusainow, Ajuh et al. 2005; Ellis, Lleres et al. 2008; Rino, Desterro et al. 2008).

To elucidate the dynamic properties of snRNPs and their interactions with pre-mRNA *in vivo* we employed fluorescence correlation spectroscopy (FCS) and fluorescence recovery after photobleaching (FRAP). Live cell imaging techniques have previously been used to investigate the dynamic properties of several macromolecular complexes, including splicing factors and RNA polymerases (Dundr, Hoffmann-Rohrer et al. 2002; Darzacq, Shav-Tal et al. 2007; Rino, Carvalho et al. 2007; Gorski, Snyder et al. 2008) as well as the assembly of the exon junction complex (Schmidt, Im et al. 2009). We took advantage of stable cell lines that contained integrated bacterial artificial chromosomes (BACs) that encoded recombinant GFP-tagged snRNP proteins expressed under endogenous regulatory elements. The expression of GFP-tagged snRNP proteins thus mimics the expression of their endogenous counterparts (Poser,

Sarov et al. 2008; Sapra, Anko et al. 2009). Analysis of the dynamic behavior of snRNP-specific proteins in the cell nucleus revealed the intricate details of spliceosomal complex formation. In addition, we were able to estimate the rate of splicing in living human cells by analyzing the interaction between the core spliceosomal snRNPs with pre-mRNA.

3.3 Material and methods

Protein cloning and tagging

EST clones of human U1-70K and U2B" were obtained from ImaGenes. ORFs were amplified by the Expand long template PCR system and cloned into pEGFP-N1 (Clontech) using BamHI and EcoRI or BglI and EcoRI restriction sites. The truncated mutant U1-70KΔ1-197 gene was generated by deleting (using KpnI and BamHI restriction sites) the first 1-197 amino acids from the full-length human U1-70K gene and cloned into pEGFP-C1 (Clontech). The construct hPrp4 GFP-C2 was obtained from David S. Horowitz (Cold Spring Harbor Laboratory, Cold Spring Harbor, NY). The construct MS2-mRED was generated upon sub-cloning the MS2 sequence from pMS2-EYFP-N1 (Huranova, Jablonski et al. 2009) into pDsRed-Monomer-N1 (Clontech) using the XhoI and BamHI restriction sites.

BAC Tagging

BACs harboring the genes encoding human spliceosomal proteins (U1-70K, U2A', hPrp4, hPrp31, hPrp8) and the mouse homolog of the spliceosomal protein, Snu114 were obtained from the BACPAC Resources Center (http://bacpac.chori.org). The EGFP-IRES-Neo cassette (LAP) was inserted into the BAC by recombination as described previously (Zhang, Buchholz et al. 1998; Poser, Sarov et al. 2008). Briefly, the C-terminal tagging cassette (LAP) was polymerase chain reaction (PCR) amplified with gene-specific primers carrying 50 nucleotides of homology to the targeting sequence. Next, purified PCR product was inserted at the C-terminus of the gene of interest using homologous recombination. Correct insertion of the tag was verified by PCR.

Cell cultures and treatments

HeLa cells were cultured in high-glucose DMEM supplemented with 10% fetal calf serum, penicillin and streptomycin (Invitrogen, Carlsbad, CA). Stable cell lines expressing the recombinant BACs were generated by transfection of HeLa cells with Effectene and selected with geneticin. The E3 U2-OS Tet-On cell line was generated by co-integrating the E3 gene (Shav-Tal, Darzacq et al. 2004) lacO repeats and puromycin resistence in U2-OS Tet-On cells. BAC E3 U2-OS cell lines were generated by transfection of E3 U2-OS cell lines with BACs and selecting with hygromycin. E3 cells were cultured in low-glucose DMEM containing 10% fetal calf serum, penicillin, and streptomycin (Invitrogen, Carlsbad, CA). Transient transfections of HeLa and E3 U2-OS cell lines were carried out using Fugene HD (Roche) according to the manufacturer's protocol. Transcription of the transgene in E3 U2-OS cells was induced using 6 μg/ml doxycycline. Doxycycline was added 6-10 h after transfection and cells assayed 12-16 h later. For transcriptional inhibition, cells were treated with 50 μM DRB (Sigma) or 50 μM α-amanitin (Sigma) for 5 h. For splicing inhibition, cells were treated overnight with 100 μM isoginkgetin (LGC standarts).

Antibodies

Goat α-GFP polyclonal antibodies (raised against bacterially expressed full-length EGFP) used for immunoprecipitation were a gift from David Drechsel (MPI-CBG, Dresden, Germany). The Y12 antibody was produced in the IMG antibody facility using a hybridoma cell line. The mouse monoclonal α-BrdU antibody was purchased from Sigma. The mouse monoclonal α-GFP antibody (Santa Cruz Biotech.) and goat anti-mouse antibodies conjugated with horse radish peroxidase (Jackson Lab.) were used for WB analysis.

snRNP immunoprecipitation and Western blot analysis

Hela and Hela BAC cell lines were grown on a 15 cm Petri dish for 28 h. Cells were treated with the aforementioned drugs before harvesting. Immunoprecipitation was performed as described previously (Huranova, Hnilicova et al. 2009) using the mouse α-Sm antibody (Y12) or goat α–GFP antibodies. RNA was extracted using phenol/chloroform, resolved on a 7 M urea denaturing polyacrylamide gel and silver stained. Alternatively, after immunoprecipitation, a fraction of Sepharose beads was resuspended in SDS-PAGE sample buffer and proteins resolved on 8% polyacrylamide

gel. The immunoprecipitated proteins were detected with the α-GFP mouse monoclonal antibody and secondary anti-mouse antibodies conjugated with peroxidase using SuperSignal West Pico (Pierce Chemical).

RT-PCR and qPCR

Total RNA was isolated 24 h after treatment using TRIzol reagent (Invitrogen). cDNA was synthesized using gene-specific reverse primers and reverse transcriptase SuperScript III (Invitrogen). Taq polymerase was used to amplify cDNA. Controls without RT reaction were performed to verify no residual DNA contamination. Quantitative PCR was performed as described previously (Listerman, Sapra et al. 2006), and the ratio of pre-mRNA to mRNA was calculated according to $R_{isoginkgetin} = 2^{(Ctpre\text{-}mRNA - CtmRNA)}$, normalized to DMSO treated cells ($R_n = R_{isoginkgetin}/R_{DMSO}$), and plotted. The following primers were used for RT-PCR and quantitative PCR:

18S - F, 5′-TTGTTGGTTTTCGGAACTGAG;

18S - R, 5′-GCAAATGCTTCGGCTCTGGTC;

HBB ex1 - in1 - F, 5`-CCTGGGCAGGTTGGTATCAAG;

HBB in2 - ex3 - R, 5`-GCCCAGGAGCTGTGGGAGGAA;

HBB ex1 - ex2 - F, 5`-CCTGGGCAGGCTGCTGGTGGT;

HBB ex2 – ex3 - R, 5`-GCCCAGGAGCCTGAAGTTCTC;

LDHA in14 - ex15 - F, 5′-CCTTTCAACTCTCTTTTGGCAACC;

LDHA in14 - ex15 - R, 5′-AATCTTATTCTGGGGGGTCTGTTC;

LDHA ex3 - ex5 - F, 5′-AGAACACCAAAGATTGTCTCTGGC;

LDHA ex3 - ex5 - R, 5′-TTTCCCCCATTAGGTAACGG;

CACNA1G ex13 - in13 - F; 5`-CTTCGGCAACTACGTGCTCT;

CACNA1G ex13 - in13 - R; 5`-AATTGGAAGTGGGACTGCTG;

CACNA1G exon 13 - F, 5′-CCAGGAGGACTGGAACAAAG;

CACNA1G exon 13 - R, 5′-AGAGCACGTAGTTGCCGAAG;

FN1 in14 - ex15 - F, 5′-AAAATGATGTTGGCGACGAG;

FN1 in14 - ex15 - R; 5′-CGTCTCTCCTGTCACGGTGT;

FN1 exon 24 - F; 5′-GGAAGAAGTGGTCCATGCTG;

FN1 exon 24 - R; 5′-GGGACACTTTCCTTGTCATCC.

FCS acquisition, data processing and analysis.

Cells plated on glass bottomed Petri dishes (MatTek, Ashland, MA) were imaged using a MicroTime 200 inverted epifluorescence scanning confocal microscope (Picoquant) equipped with an environmental chamber controlling CO_2 level and temperature. The FCS system contained a pulsed diode laser (LDH-P-C-470, 470 nm; Picoquant) providing 80-psec pulses at up to a 40-MHz repetition rate, a proper filter set (cleanup filter Z470/20, dichroic mirror z490rdc, and bandpass filter HQ515/50; Chroma), a water immersion objective (1.2 NA, 60x; Olympus), 50 μm pinhole and a single SPAD detector. Data were acquired in TTTR mode using SymphoTime200 software (Picoquant) and F(L)CS data analysis was performed using home built routines (DevC++, Bloodshed Software and OriginPro80, OriginLab Corporation). First, standard fluorescence intensity images of the cells using low laser power (1 μW at the back aperture of the objective) were acquired to properly localize the nucleus in all three dimensions. Subsequently, a set of point measurements (120 s each) with optimized power (3.6 μW at the back aperture of the objective – compromise between brightness and minimal photobleaching) were performed at selected locations within the nucleoplasm. FCS analysis of each point measurement consisted of: 1) Filtering out uncorrelated noise contributions (detector after pulsing and dark noise) (Humpolickova, Beranova et al. 2008). 2) Estimation of standard deviation for each lag-time by splitting the measurement into 10 pieces (Benda, Benes et al. 2003). 3) Weighted non-linear least square fit (Levenberg-Marquard routine) by a theoretical model. For fitting the autocorrelation curves we applied the pure diffusion model with one or two components using the standard equation for free 3-dimensional translational diffusion:

$$G(\tau) = 1 + \frac{\sum_{i=1}^{R} \alpha_i^2 \langle N_i \rangle g_{3di}(\tau)}{\left[\sum_{i=1}^{R} \alpha_i \langle N_i \rangle\right]^2} \qquad (1)$$

where $g_{3dim}(\tau) = \left(1 + \frac{\tau}{\tau_{Di}}\right)^{-1} \left(1 + \frac{\tau}{SP^2 \tau_{Di}}\right)^{-1/2}$, α_i is the experimental brightness of i-th species, G(t) is the autocorrelation function, N stands for the number of particles in the effective volume V_{eff}, SP is a structure parameter, a constant for the given experimental setup, defined as the ratio of long and short axis of the ellipsoidal detection volume $SP = z_0/\omega_0$, τ_D is diffusion time. The size of the effective volume is $V_{eff} = \pi^{3/2} \omega_0^2 z_0$.

FRAP acquisition, data processing and analysis

Cells were plated on glass bottomed Petri dishes (MatTek, Ashland, MA) and after 20–24 h they were transfected with the appropriate DNA constructs. The cells were imaged 22–24 h after transfection and drug treatment by using a Leica SP5 confocal microscope equipped with an oil immersion objective (HCX PL APO 633/1,40-0,6 oil, Lbd Blue CS) and an environmental chamber controlling CO_2 level and temperature. Data acquisition was performed using a 512x512 format at a 1400 Hz scan speed and 1,6 Airy pinhole in 16 bit resolution. Bleaching (0.37 s) was performed with a circular spot 1,5 μm in diameter using the 488 nm line of a 100 mW argon laser operating at 100% laser power. Fluorescent recovery was monitored at low laser intensity (5-10% of a 100 mW laser) at 0.37 s intervals at the beginning of the recovery and at 0.37 - 1 s intervals when reaching the plateau of recovery. 10-12 separate FRAP measurements were performed for each experiment and background photobleaching and intensity were subtracted to generate normalized FRAP curves that were fitted either with the pure diffusion model or full model equations.

To fit the FRAP curves with the pure diffusion model (2), we used the following equation derived from (Sprague, Pego et al. 2004).

$$frap(t) = e^{-\frac{\tau_D}{2t}}\left(I_0\left(\frac{\tau_D}{2t}\right) + I_1\left(\frac{\tau_D}{2t}\right)\right) \qquad (2)$$

We calculated the average value of all D_f values and used the average value as an input for full-model FRAP fitting. The full model Laplace transform solution (3) was used according to (Sprague, Pego et al. 2004).

$$\overline{frap(p)} = \left(\frac{1-C_{eq}}{p}\right)\left(1+\frac{k_{on}^{*}}{p+k_{off}}\right)\left(2K_1(qw)I_1(qw)\right) \qquad (3)$$

The actual recovery model is obtained by numerical inversion of transformation (3) using the Matlab routine *invlap.m* (Hollenbeck, 1998) that is used to fit experimental data. Before every fitting we searched both k_{on}^{*} and k_{off} by varying in tenfold increments from 10^{-5} to 10^{2} to find a good guess of both k_{on}^{*} and k_{off}. The weighted Levenberg-Marquardt algorithm was used to cut off points having a big dislocation from the expected course leading to more precise fits.

3.4 Results

In order to describe the dynamic behavior of snRNPs in living cells, we established stable Hela cell lines that express from BACs the GFP-tagged snRNP proteins, U2A' (U2 snRNP), hPrp31 and hPrp4 (U4/U6 snRNP) and Snu114 (U5 snRNP). Previously used Hela cell lines expressing BAC encoded GFP-tagged snRNP proteins, U1-70K (U1 snRNP) and hPrp8 (U5 snRNP) were also used (Sapra, Anko et al. 2009). The advantage of using BACs for gene expression studies is that the endogenous regulatory elements are preserved allowing their expression to be similar to that of the endogenous protein. The expression of GFP-tagged snRNP proteins did not impair co-transcriptional spliceosome formation and haploid yeast cells that express only GFP-tagged snRNP proteins remained viable without any defects in pre-mRNA splicing (Gornemann, Kotovic et al. 2005; Sapra, Anko et al. 2009). GFP-tagged snRNP proteins were properly localized to the cell nucleus and accumulated in Cajal bodies (Fig. 3.1.A). Immunoprecipitation followed by snRNA analysis revealed that the GFP-tagged proteins were properly incorporated into the appropriate snRNPs (Fig. 3.1.B). We concluded that the GFP-tagged snRNP proteins behaved analogous to their endogenous counterparts and were suitable for further investigation.

To analyze the movement of snRNPs in the cell nucleus, we first employed FCS, a tool sensitive enough to detect rapid diffusion and fast interactions (Kim, Heinze et al. 2007). This technique focuses a laser beam on a spot of interest in the nucleoplasm and monitors fluctuations in fluorescence intensity over time. The intensity record is transformed into an autocorrelation function that assesses the diffusion correlation time of the detected molecules. FCS measurements were performed within the nucleoplasm where most pre-mRNA splicing occurs (Fig. 3.2.A) (Neugebauer 2002; Lamond and Spector 2003). By using the pure diffusion model, a satisfactory fit of autocorrelation function was achieved (Kim, Heinze et al. 2007). We detected two moving components in each cell line expressing GFP-tagged snRNP proteins, with diffusion correlation times of around 1 ms for the fast component (τ_{Da}, ~ 40% of all moving proteins) and 20-30 ms for the slow component (τ_{Db}, ~ 60% of all moving proteins) (Fig. 3.2.A, Table 3.1.). The correlation times of the fast component were similar to free GFP and likely reflect free proteins (Fig. 3.2.A, Table 3.1.). To elucidate whether the slower component represented snRNP complexes, we constructed a truncated form of the U1-70K protein lacking the first 1-197 amino acids that contain the U1 snRNA binding motif (Nelissen,

Will et al. 1994). In agreement with previous studies that demonstrated that the C-terminal domain is still able to interact with non-snRNP proteins (Cao and Garcia-Blanco 1998), we observed that the transiently expressed U1-70KΔ1-197-GFP protein partially accumulates in splicing factor compartments (Fig. 3.2.B) but did not incorporate into the U1 snRNP (Supp. Fig. 3.1.). FCS measurements revealed that deletion of the RNA binding motif resulted in the loss of the slower component (Fig. 3.2.B). The calculated diffusion correlation time was higher than the diffusion correlation time of free GFP likely representing the average movement of free mutant and mutant incorporated into non-snRNP complexes (Table 3.1.). We conclude that FCS measurements of wild-type snRNP proteins reveal the diffusion properties of snRNP complexes.

To examine whether the snRNP movement is affected by its interaction with pre-mRNA, we treated cells with 5,6-dichlorobenzimidazole riboside (DRB), a potent inhibitor of RNA polymerase II (Chodosh, Fire et al. 1989). The treatment resulted in an enlargement of splicing factor compartments (Fig. 3.2.C) and inhibited RNA synthesis (Supp. Fig. 3.2.). FCS measurements revealed that transcriptional inhibition had no significant effect on the diffusional behavior of snRNPs (Fig. 3.2.C). In summary, using FCS we showed that individual snRNPs diffused rapidly throughout the nucleoplasm with comparable diffusion correlation times (Table 3.1.). However, we were not able to detect any stable interactions between individual snRNPs and pre-mRNA. We predict that these interactions occur over a longer time scale (seconds and more) beyond the detection limit of FCS.

snRNP diffusion measured by FRAP correlates with FCS data

To overcome the limits of FCS we utilized FRAP to elucidate the relatively slow interaction of snRNPs with pre-mRNA. The FRAP method involves photo-bleaching a small area within the sample and monitoring the recovery of fluorescence intensity over time. Fluorescence recovery reflects the movement of unbleached molecules into the bleached area and is determined by the diffusion and binding characteristics of the analyzed molecules (Sprague, Pego et al. 2004; Sprague and McNally 2005; McNally 2008). Importantly, pre-mRNA splicing is largely co-transcriptional (Neugebauer 2002) and is significantly faster compared to RNA polymerase II elongation (Singh and Padgett 2009). With respect to mobile snRNPs, pre-mRNA represents an immobilized substrate. To dissect diffusion from binding events, we compared the dynamics of

snRNPs in the nucleoplasm before and after transcriptional inhibition (Fig. 3.3.A, B, C and D). FRAP measurements in DRB treated cells showed fast and full fluorescence recovery (Fig. 3.3.B, C and D), indicating that transcriptional inhibition depleted pre-mRNA binding sites. Recovery curves were fitted with the pure diffusion model, supporting the assumption that in the absence of pre-mRNA, snRNPs move rapidly throughout the nucleoplasm. Quantification of FRAP curves yielded effective diffusion coefficients ranging from 0.2 to 0.6 $\mu m^2 s^{-1}$ (Table 3.2.), which were comparable to the diffusion coefficients 0.5 - 0.8 $\mu m^2 s^{-1}$ obtained by FCS (Table 3.1.). These data indicate that in DRB treated cells both FRAP and FCS measured a population of snRNPs that effectively diffuse throughout the cell nucleus.

U4/U6 and U4/U6•U5 snRNP integrity depends on active transcription

In order to characterize the molecular composition of snRNP complexes after transcriptional inhibition, we immunoprecipitated snRNP specific proteins from DRB or α-amanitin treated cells (Fig. 3.3.E). Transcriptional inhibition had no effect on U1 and U2 snRNP integrity. However, we noticed that the small amount of U6 snRNAs that repeatedly co-purified with U2 complexes in non-treated cells were lost after transcriptional inhibition. In addition, after transcriptional inhibition, the levels of co-precipitated U4 and U6 snRNAs with hPrp4 and hPrp8 proteins were reduced, illustrating that di-snRNP and tri-snRNP formation was impaired by this treatment.

snRNPs interact independently with pre-mRNA

To characterize in living cells the interaction of snRNPs with pre-mRNA, we analyzed non-treated cells by FRAP (Fig. 3.3.B, C and D). In order to apply a proper model for data fitting we performed FRAP experiments with two different bleach-spot sizes, 1.5 μm and 2.5μm in diameter (Supp. Fig. 3.3.A). Analysis of each spot size revealed different recovery times, indicating that diffusion significantly contributed to fluorescence recovery and could not be omitted. Thus, FRAP curves were fitted with the full-model comprising both diffusion and binding parameters (Sprague, Pego et al. 2004; McNally 2008). In order to reduce the number of fitted parameters, we used diffusion coefficients measured in DRB treated cells and fitted only parameters that described the binding event - association (k^*_{on}) and dissociation (k_{off}) rates. Since k^*_{on} also depends on the concentration of binding sites, which could not be easily

determined, only k_{off} values were used to describe the interaction between snRNPs and pre-mRNA.

k_{off} values calculated for the U1 snRNP and the U4/U6 snRNP were more than 10 fold higher than k_{off} for the U2 and U5 snRNPs, suggesting that U1 and U4/U6 snRNPs interact with pre-mRNA for a lesser time than U2 and U5 snRNPs (Table 3.2.). A schematic representation of snRNP interactions with pre-mRNA is shown in Fig. 3 F, where the interaction time was calculated as an inversion of k_{off}. The longer association of U2 and U5 snRNPs with pre-mRNA likely reflects the stable interaction of these two snRNPs with pre-mRNA during splicing and is indicative of the *in vivo* splicing rate. Importantly, similar dissociation rates were obtained for different proteins from the same snRNP complex (hPrp8 and Snu114 from the U5 snRNP; hPrp4 and hPrp31 from the U4/U6 snRNP), which convincingly suggests that these values accurately reflect the behavior of snRNP complexes (Table 3.2.). Additionally, by fitting the FRAP data with the diffusion coefficients measured by FCS, similar k_{off} values were calculated (unpublished data). Conclusively, in untreated cells, FRAP measurements revealed that individual snRNPs have distinct dissociation rates, strongly indicating that their interactions with pre-mRNA are independent.

To further show that k_{off} values were indicative of snRNP binding to pre-mRNA, we performed FRAP measurements in cells treated with isoginkgetin, a potent splicing inhibitor. Isoginkgetin prevents U4/U6•U5 tri-snRNP recruitment to the spliceosome *in vitro*, resulting in the accumulation of pre-spliceosomal complex A that contains U1 and U2 snRNPs bound to pre-mRNA (Behzadnia, Golas et al. 2007; O'Brien, Matlin et al. 2008). If k_{off} represents the interaction of snRNPs with pre-mRNA, then stabilization of complex A should decrease the k_{off} value of the U1 snRNP. Splicing inhibition was confirmed by the enlargement of splicing factor compartments (Fig. 3.4.A; (Kaida, Motoyoshi et al. 2007) and the accumulation of pre-mRNA from several genes (Supp. Fig. 3.4.). Importantly, transcription was preserved, as measured by the incorporation of modified nucleotides (Supp. Fig. 3.2.). Splicing inhibition resulted in the elevation of the U1 and U2 snRNP immobile fractions. Quantification of the mobile fraction revealed the dramatic decrease in the U1 snRNP k_{off} value (Fig. 3.4.B and F, Table 3.2.). The *in vivo* formation of a stable U1-U2-pre-mRNA complex was further confirmed by the co-immunoprecipitation of U1 snRNA with the U2A' GFP-tagged protein from isoginkgetin treated cells (Fig. 3.4.C). The prolonged residence time of the U1 snRNP on pre-mRNA complemented our measurements performed after

transcriptional inhibition and demonstrated that the k_{off} values signify snRNP interaction with pre-mRNA.

Splicing inhibition had no effect on the U4/U6 di-snRNP protein dissociation rate and only slightly increased the amount of U4/U6 di-snRNP immobile fraction, suggesting its transient interaction with stalled spliceosomal complexes (Fig. 3.4.D and F, Table 3.2.). U5 snRNP FRAP curves measured in isoginkgetin treated cells showed rapid recovery and their quantification yielded diffusion coefficients that were comparable to the diffusion coefficients measured in DRB treated cells (Fig. 3.4.E, Table 3.2.). Interestingly, we detected an apparent immobile fraction of U5 snRNP that might indicate either stalled spliceosomal complexes containing U5 snRNP or interactions occurring prior to the first step of splicing (Wyatt, Sontheimer et al. 1992).

Taken together, our data showed that snRNP-pre-mRNA interactions can be measured by FRAP. In addition, the snRNPs that form the core active spliceosomal complex exhibited significantly longer interaction times (12-30 s) while U1 and U4/U6 snRNP proteins only transiently interacted with pre-mRNA. This result is consistent with their role during intron definition (U1 snRNP) and spliceosome formation (U4/U6 snRNP).

Splicing inhibition disrupts snRNP complexes

The different dynamic behavior of U4/U6 and U5 snRNP proteins in the presence of isoginkgetin implies impaired tri-snRNP formation. In order to analyze the integrity of tri-snRNP complexes after splicing inhibition, U4/U6 and U5 snRNP specific proteins were immunoprecipitated from isoginkgetin treated cells and co-precipitated snRNAs analyzed (Fig. 3.4.G and H). After splicing inhibition we detected a decrease in the level of U4 and U6 snRNAs associated with hPrp4 and hPrp8 proteins, confirming that di-snRNP and tri-snRNP formation is reduced. Interestingly, we noticed an increase in the association of U1 snRNA with U5 snRNP, possibly reflecting the observed immobilized fraction of U5 snRNP in FRAP measurements after splicing inhibition. Taken together, the immunoprecipitation data demonstrated that active splicing is necessary for di-snRNP and tri-snRNP integrity.

Differential interaction of snRNPs with E3 pre-mRNA

Our results reveal the dynamics of snRNPs in the nucleoplasm and are an average representation of snRNP behavior over numerous gene loci. To analyze snRNP

dynamics at a specific gene locus, we used the inducible E3 U2-OS Tet-On cell system (Fig. 3.5.A; (Shav-Tal, Darzacq et al. 2004; Darzacq, Kittur et al. 2006) that either stably express from BACs, GFP-tagged U1-70K (U1 snRNP) or hPrp8 (U5 snRNP), or transiently express GFP-tagged U2B" (U2 snRNP) or hPrp4 (U4/U6 snRNP). Initially, we determined by FRAP that the average diffusion coefficients and binding constants of individual snRNPs in the nucleoplasm of U2-OS cells are similar to that of Hela cells (Table 3.2.). Doxycycline treatment of cells resulted in the expression of E3 RNA (Fig. 3.5.B), as visualized *in situ* via its interaction with the MS2-mRED protein (Fig. 3.5.C). After induction with doxycycline, snRNP specific proteins localized to the site of active transgene transcription (Fig. 3.5.C). The bleach-spot size test confirmed that the full model could be applied to the E3 gene locus (Supp. Fig. 3.3.B). FRAP measurements performed at the site of transgene transcription revealed a surprising reduction in k_{off} values. The greatest reduction detected was U1 snRNP (~10 fold) and U4/U6 snRNP (~ 30 fold). k_{off} values for U2 snRNP and U5 snRNP dropped only partially (Fig. 3.5.D, Table 3.2.). These data illustrate that the dynamics of snRNPs differ at a specific gene compared to the average values measured in the nucleoplasm. This reflects either massive E3 gene transcription or specific splicing kinetics for E3 pre-mRNA. However, similar to nucleoplasmic spots, the binding rates of snRNPs differed at the artificial gene locus, again indicating the independent interaction of spliceosomal snRNPs with E3 pre-mRNAs.

3.5 Discussion

We have successfully measured the dynamics of snRNP complexes in the cell nucleus and calculated the parameters that describe their movement throughout the nucleoplasm and their interactions with pre-mRNA. By using two different techniques, FRAP and FCS, we show that the diffusion of U1, U2, U4/U6 and U5 snRNPs are comparable and their diffusion rates range between 0.2 - 0.8 $\mu m^2 s^{-1}$. Importantly, similar values were determined from both techniques and in two different cell lines. Our data is consistent with the diffusion rate of U1-70K in plants (D_f = 0.7 $\mu m^2 s^{-1}$) (Ali, Prasad et al. 2008) and humans (D_f = 0.5 $\mu m^2 s^{-1}$) (Grunwald, Spottke et al. 2006) and the common snRNP protein, SmE in human cells (D_f = 0.8 $\mu m^2 s^{-1}$) (Rino, Carvalho et al. 2007). snRNP movement is slower than the movement of non-snRNP splicing

factors U2AF35/65, SF1 or SC35 (D_f = 1.19-1.40 $\mu m^2 s^{-1}$) (Rino, Carvalho et al. 2007). As diffusion efficiency of nuclear factors is largely determined by transient interactions (Phair and Misteli 2001), these data indicate that snRNPs encounter extensive interactions within the nuclear environment.

Surprisingly, in all cases we observed a pool of proteins that were apparently not incorporated into snRNP complexes and diffused rapidly throughout the nucleoplasm. Similarly, two fractions were identified for U1 snRNP, a slower fraction with D_f = 0.5 $\mu m^2 s^{-1}$ and a faster one with D_f = 8.2 $\mu m^2 s^{-1}$ (Grunwald, Spottke et al. 2006). In the case of the exon-junction complex, free proteins were also detected (Schmidt, Im et al. 2009). Together, these observations suggests that a fraction of unbound proteins is a common feature of proteins associated with multi-component complexes.

The mathematical model used for FRAP data analysis not only enabled the estimation of diffusion rates but also allowed the approximation of snRNP binding properties to nuclear components. Treatment of cells with transcriptional and splicing inhibitors demonstrated that in the cell nucleus the dominant interaction partner of snRNPs is pre-mRNA. U1 and U4/U6 snRNP components exhibit fast dynamic exchange with a residence time of ~ 1 s, while U2 and U5 snRNP proteins interact longer with pre-mRNA with a residence time of ~ 12-30 s (Fig. 3.3.F). If the spliceosome interacts with pre-mRNA in a big complex that contains all five snRNPs, then individual snRNPs should have a similar residence time. Therefore, our results are consistent with the step-wise assembly model that proposes the transient interaction of U1 and U4/U6 snRNP proteins with pre-mRNA during the spliceosome formation and the longer association of U2 and U5 snRNP proteins that constitute the activated spliceosome (Rino and Carmo-Fonseca 2009; Wahl, Will et al. 2009).

The residence times of the core splicing components (U2 and U5 snRNPs) can provide us with an estimate of the average splicing rate in living cells. Our results suggest that splicing is accomplished within 30 s. Compared to previous studies that inferred that the splicing rate from intron removal after transcription induction or repression is between 0.5-10 min; our value is much faster (Audibert, Weil et al. 2002; Singh and Padgett 2009). However, the rate of intron removal depends on many factors, including the rate of RNA synthesis and the rate of splice site recognition. Our results provide the first *in vivo* splicing rate estimate in a mammalian system that is independent of the speed of RNA synthesis and involves only the rate of splicing and assembly/disassembly of the spliceosome. Our results correlate well with the analysis of

Miller spreads from Drosophila embryos and ChIP data from yeast that both suggest that splicing is accomplished within a minute after spliceosome formation (Beyer and Osheim 1988; Wetterberg, Zhao et al. 2001; Gornemann, Kotovic et al. 2005). The immobile fractions of U2 and U5 snRNPs (~ 10%) indicate that the splicing of some genes can take significantly longer than 30 s and might reflect delayed or regulated post-transcriptional splicing (LeMaire and Thummel 1990; Wetterberg, Bauren et al. 1996). Interestingly, the interaction of snRNP with β-globin based E3 pre-mRNA differ from the average nucleoplasmic values. It was reported previously that the splicing rates of different introns vary significantly (Audibert, Weil et al. 2002). Therefore, it is plausible that the interaction of individual snRNPs and spliceosome assembly at one or both β-globin introns diverge from the average. In addition, the massive accumulation of snRNPs at the artificial gene loci indicate a high rate of pre-mRNA production. Thus, snRNPs could be reused at this site and be involved in several splicing reactions without leaving the transcription loci, resulting in the observation of a prolonged residence time.

Our comprehensive analysis of snRNP dynamics in the cell nucleus reveals that snRNPs roam throughout the cell nucleus and continuously scan their environment via numerous transient interactions. Once snRNPs encounter a pre-mRNA substrate they assemble the active splicing complex, accomplish the splicing reaction and dissociate to be recycled for another round of splicing. Similar to other active multi-component complexes (e.g. translation or transcription initiation complexes), the active spliceosome is formed from pre-assembled snRNPs only at the time and place of its need, allowing the assembly process to be regulated.

Figures and tables to chapter 3:

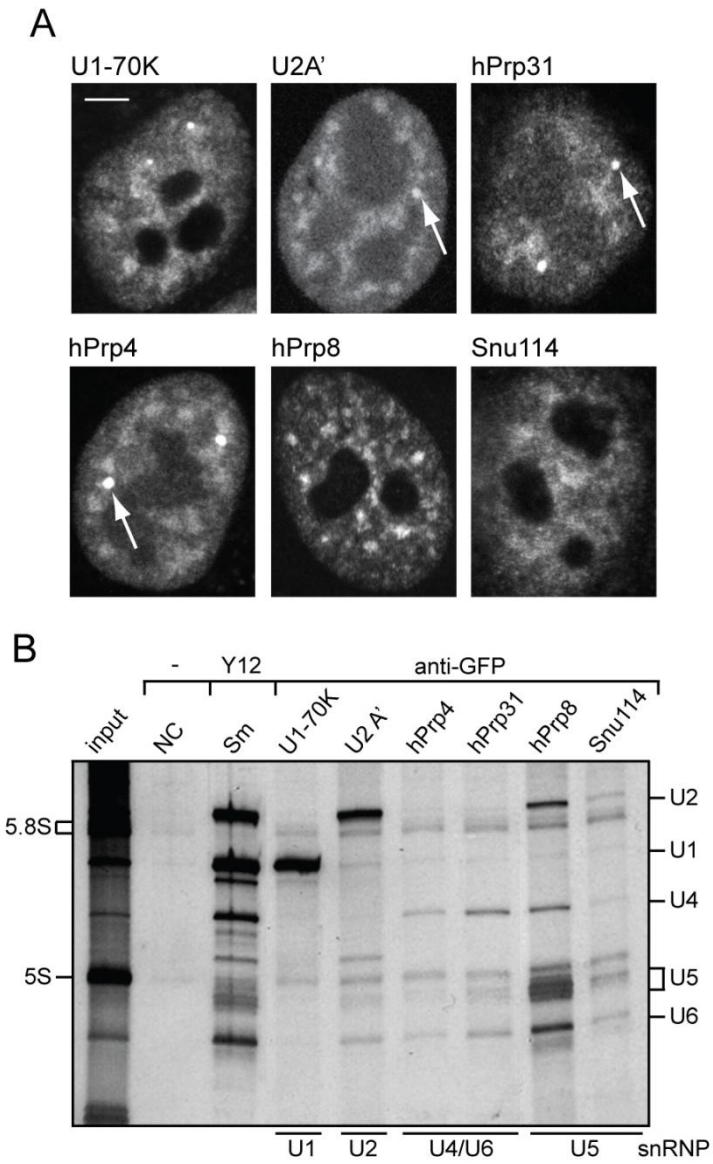

Figure 3.1. GFP-tagged snRNP proteins incorporate into snRNPs. A/ Images of cells expressing GFP-tagged snRNP proteins (scale bar 5 μm). GFP-tagged proteins were localized to the nucleoplasm and enriched in splicing factor compartments and Cajal bodies (*arrows*). B/ snRNPs were immunoprecipitated using anti-GFP or anti-Sm antibodies and co-precipitated RNAs visualized. The position of snRNAs and rRNAs are depicted. Note a small amount of U6 and U5 snRNAs co-precipitate with U2 snRNP (U2A' line) and U2 snRNA associated with U5 snRNP (hPrp8 and Snu114 lines).

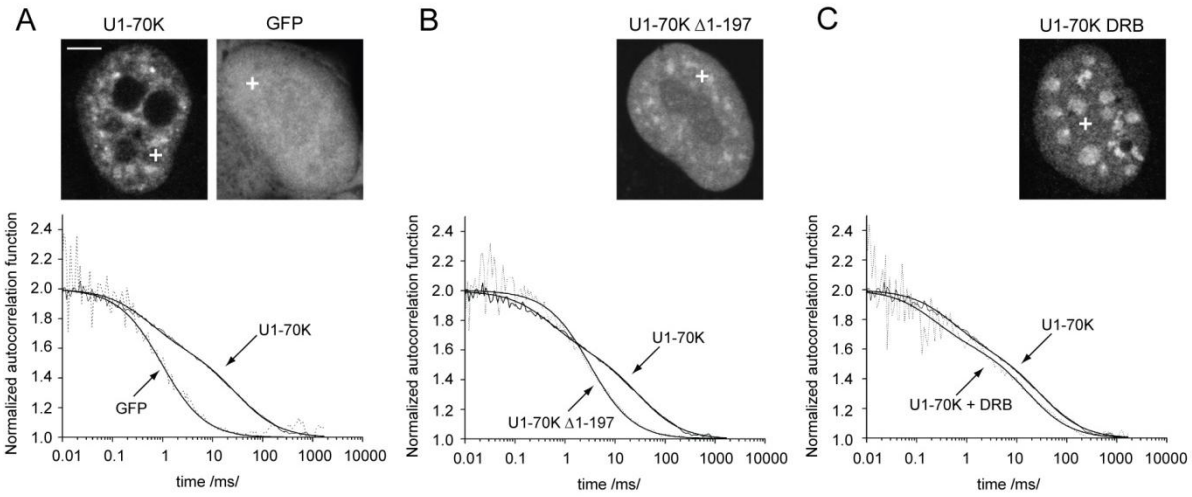

Figure 3.2. FCS measures the *in vivo* mobility of snRNPs. A/ FCS measurements were performed in the nucleoplasm of cells either stably expressing U1-70K-GFP or transiently expressing GFP as depicted by the crosses (scale bar 5 μm). The autocorrelation function of free GFP is fitted with a one-component diffusion model. The autocorrelation function of U1-70K is fitted with a two-component diffusion model. B/ Deletion of the RNA binding domain of U1-70K causes the loss of the slower component and the autocorrelation function of U1-70KΔ1-197 is fitted with a one-component diffusion model. C/ DRB treatment (5 h) inhibits RNA polymerase II and results in the enlargement and rounding up of splicing factor compartments. DRB treatment had only a minimal effect on snRNP diffusion with both fast and slow components still present.

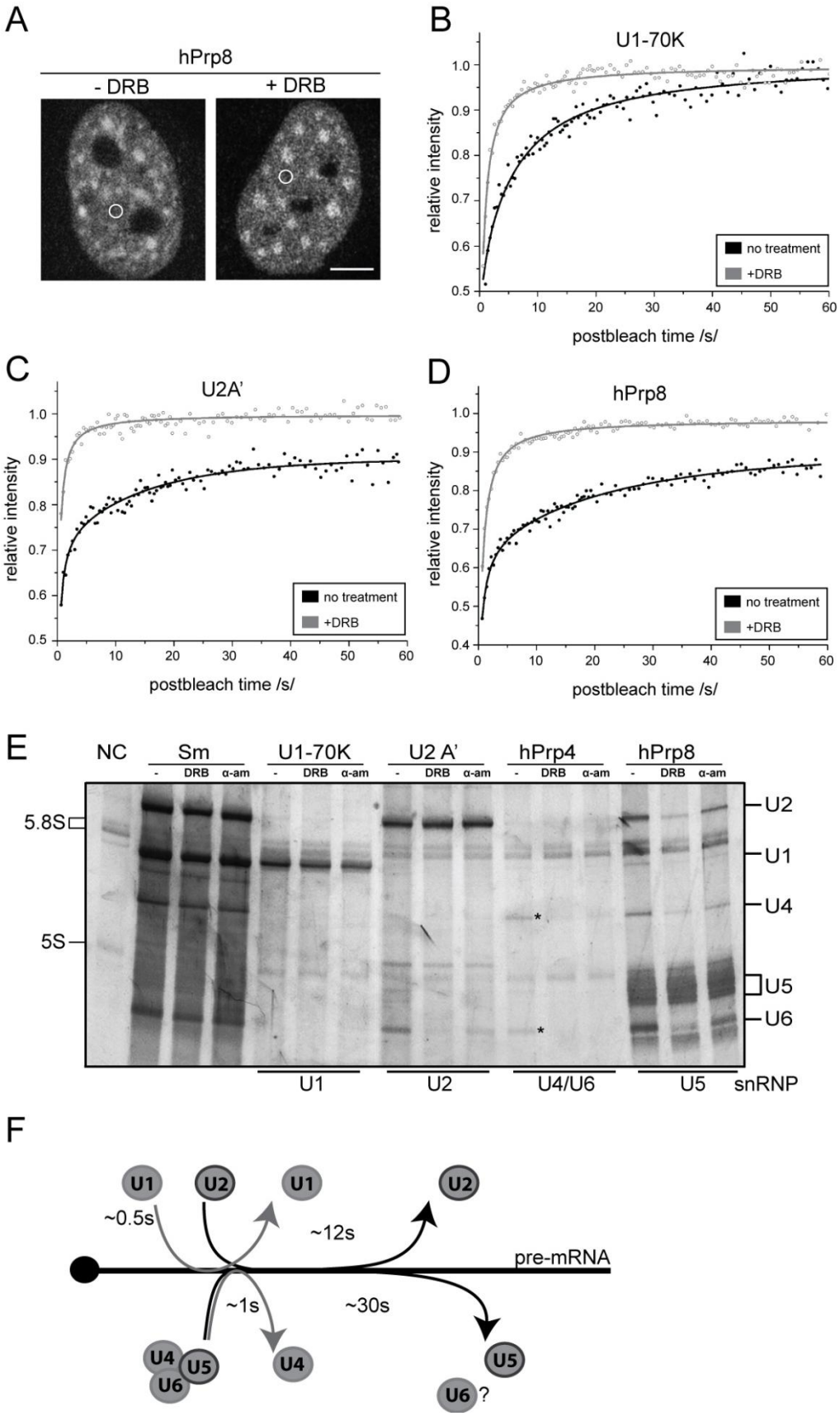
A
hPrp8
- DRB
+ DRB
B
U1-70K
relative intensity
postbleach time /s/
no treatment
+DRB
C
U2A'
relative intensity
postbleach time /s/
no treatment
+DRB
D
hPrp8
relative intensity
postbleach time /s/
no treatment
+DRB
E
NC
Sm
U1-70K
U2 A'
hPrp4
hPrp8
- DRB α-am
5.8S
5S
U2
U1
U4
U5
U6
U1
U2
U4/U6
U5
snRNP
F
U1
U2
U1
U2
~0.5s
~12s
pre-mRNA
~1s
~30s
U4
U5
U6
U4
U5
U6 ?

Figure 3.3. snRNPs interact independently with pre-mRNA as analyzed by FRAP. A/ FRAP measurements were performed in the nucleoplasm as depicted by circles (scale bar 5 μm). B/ U1-70K, C/ U2A', and D/ hPrp8 FRAP curves representing an average of 10-12 measurements before and after DRB treatment. FRAP curves were fitted either with a pure diffusion model (DRB treatment) or the full model (no treatment). Calculated diffusion coefficients and dissociation constants k_{off} are shown in Table 3.2. E/ Co-immunoprecipitation of snRNAs with anti-GFP antibodies from U1-70K-GFP, U2A'-GFP, hPrp4-GFP and hPrp8-GFP cell lines before and after DRB or α-amanitin treatment. Transcriptional inhibition had no effect on the precipitation of U1 and U2 snRNAs but eliminated U6 snRNA association with the U2 snRNP. Transcriptional inhibition reduces the formation of U4/U6 and U4/U6•U5 snRNPs as shown by the decrease of U4 and U6 snRNAs levels in hPrp4 (*stars*) and hPrp8 precipitates. F/ Schematic representation of snRNP interaction times with pre-mRNA. We assume that the U4/U6 proteins hPrp4 and hPrp31 leave and the U4 and U6 snRNPs stay associated with the activated spliceosome.

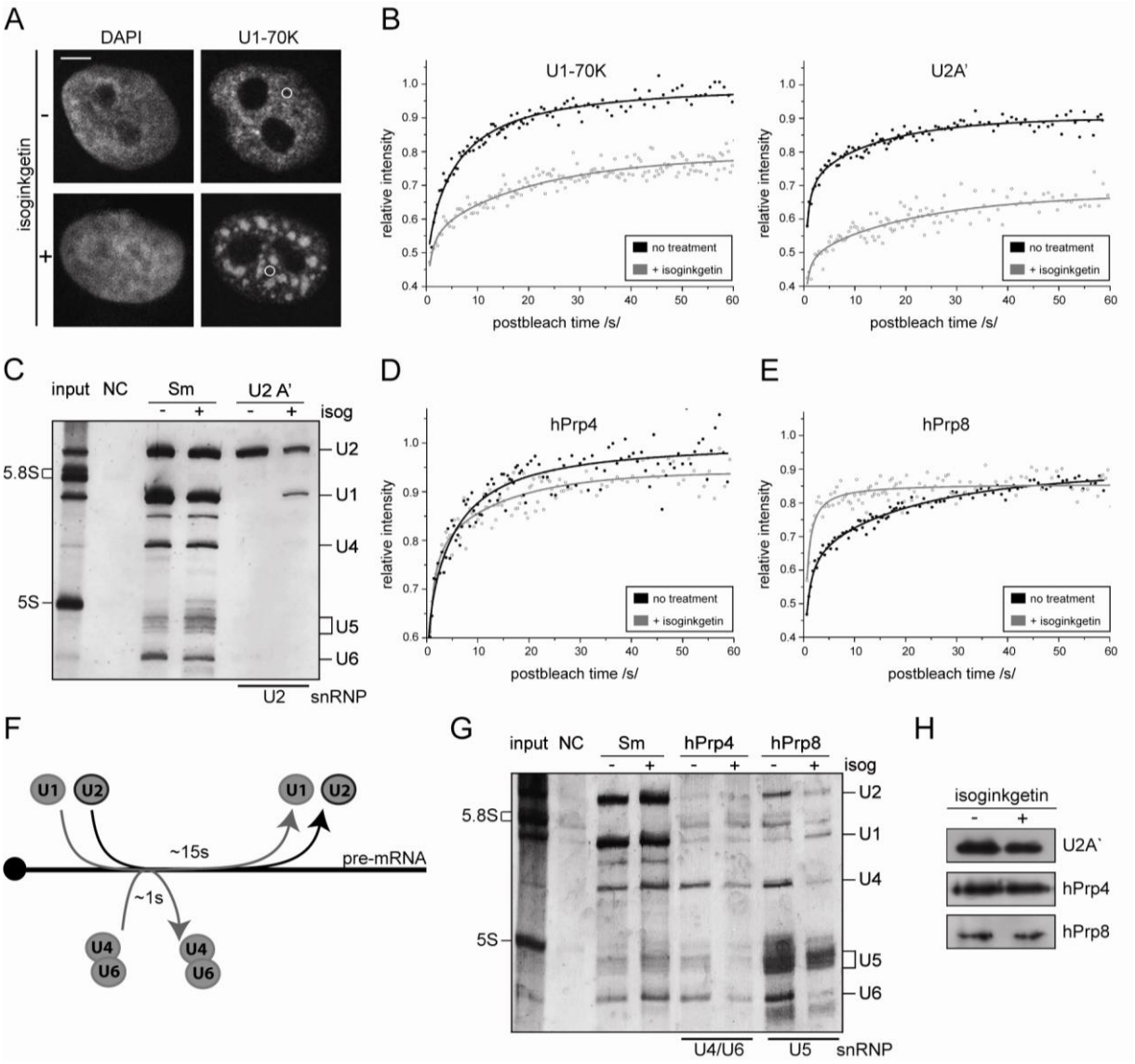

Figure 3.4. The prolonged interaction of U1 and U2 snRNPs with pre-mRNA after splicing inhibition. A/ After isoginkgetin treatment, GFP-tagged snRNP proteins relocalize to enlarged splicing factor compartments. FRAP measurements were performed in the nucleoplasm as depicted by circles (scale bar 5 μm). B/ Splicing inhibition increased the immobile fractions and reduced the mobility of U1-70K and U2A' (see Table 3.2.). The average of 10-12 measurements is shown. C/ Co-immunoprecipitation of U1 snRNA with U2A'-GFP after isoginkgetin treatment. D/ Splicing inhibition had minimal impact on U4/U6 snRNP mobility (see Table 3.2.). E/ Splicing inhibition resulted in increased U5 snRNP mobility that can be described by a pure diffusion model. A portion of U5 snRNPs are bound in an immobile fraction. F/ Schematic representation of snRNP interaction times with pre-mRNA after splicing

inhibition. G/ Co-immunoprecipitation of snRNAs from hPrp4-GFP and hPrp8-GFP cell lines with anti-GFP antibodies before and after isoginkgetin treatment. Splicing inhibition impairs U4/U6 di-snRNP and U4/U6•U5 tri-snRNP formation as shown by the reduced co-precipitation of U4 and U6 snRNAs with hPrp4 and hPrp8 proteins. H/ The efficiency of GFP-tagged protein immunoprecipitation was verified by Western blot analysis.

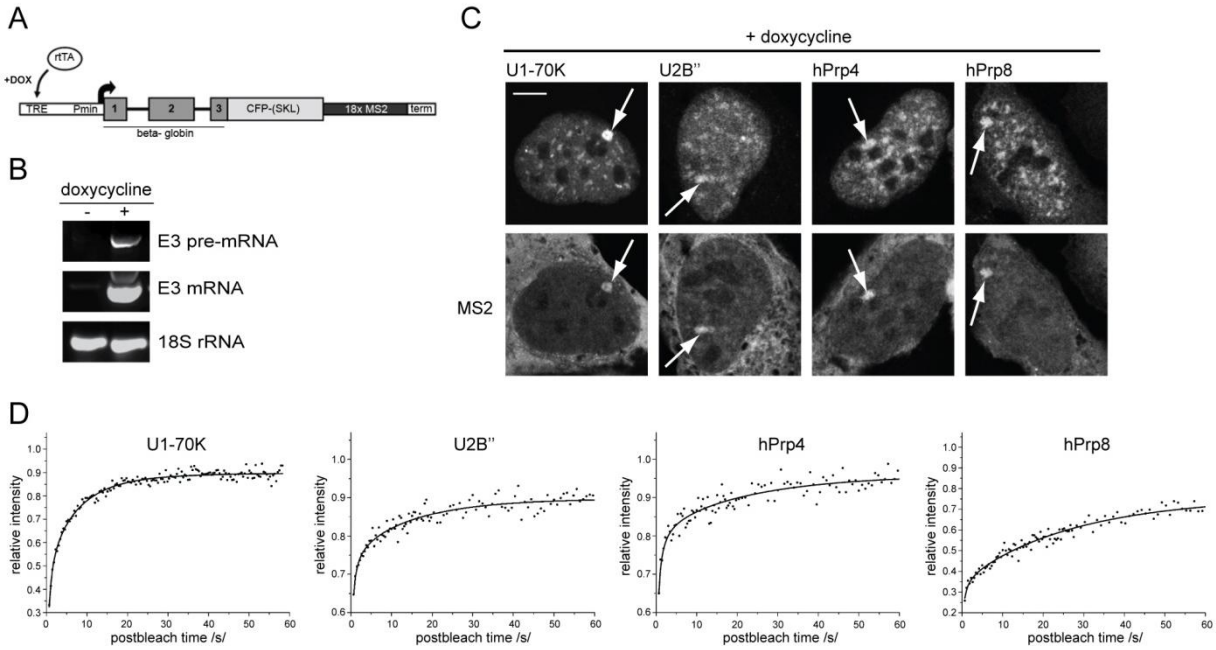

Figure 3.5. snRNP interaction with E3 pre-mRNA. A/ Schematic representation of the E3 gene stably integrated into the genome of the U2-OS Tet-on cell line. Expression of the E3 transgene is driven by a minimal CMV promoter (Pmin) under the control of the tetracycline response element (TRE) and is induced by the presence of doxycycline (DOX) by the transactivator, rtTA. The transgene transcript contains 18x MS2 binding sites and the encoded protein (human β-globin) is fused to CFP-SKL. B/ E3 transgene expression before and after induction. C/ Doxycycline treated E3 cells expressing different GFP-tagged snRNP proteins (*upper panel*) and MS2-mRED protein (*lower panel*). Note the localization of snRNP proteins at the site of active transgene transcription as depicted by MS2-mRED accumulation. D/ FRAP analysis of snRNP dynamics at the active transcription site of the E3 transgene (see Table 3.2.). An average of 10-12 measurements is shown.

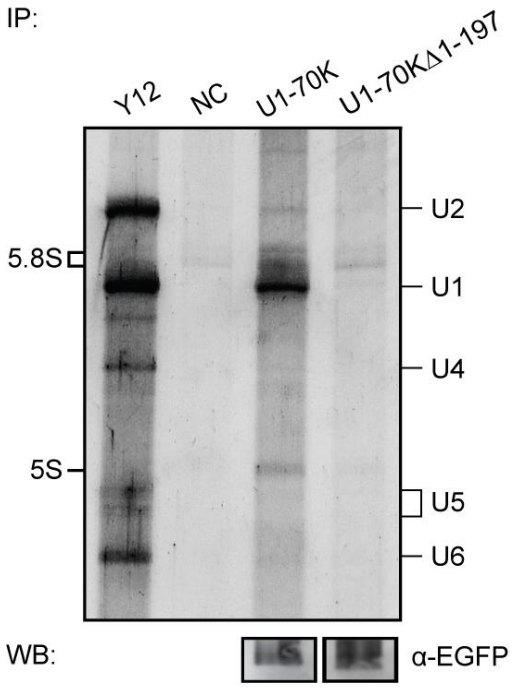

Supplementary figure 3.1. Truncated protein U1-70KΔ1-197 does not co-precipitate U1 snRNA. Co-immunoprecipitation of U1 snRNA was performed from the U1-70K-GFP cell line or HeLa cells transiently expressing U1-70KΔ1-197-GFP using anti-GFP antibodies. Lower panel shows immunoprecipitation efficiency of the GFP-tagged U1-70K and U1-70KΔ1-197 proteins verified by Western blot analysis.

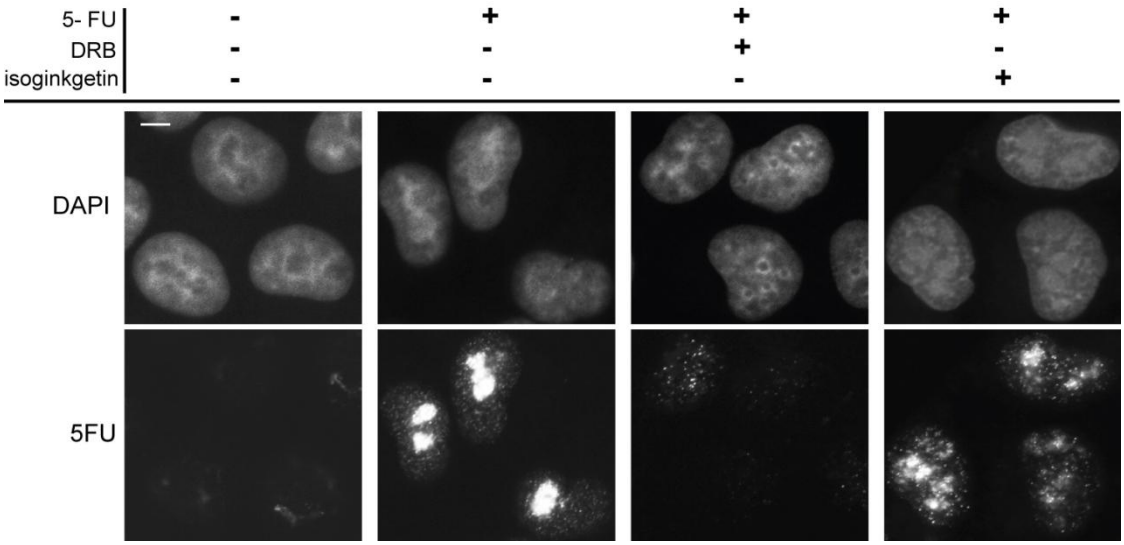

Supplementary figure 3.2. DRB but not isoginkgetin inhibits transcription. Cells were incubated with 5-fluorouridine (5-FU) that was incorporated into newly synthesized RNA. After 30 minutes of treatment cells were fixed and 5-FU labeled RNA detected by indirect immunofluorescence using the anti-bromodeoxyuridine antibody that cross-reacts with 5-FU. Transcription is inhibited by treatment with RNA polymerase II inhibitor DRB, but not by treatment with the splicing inhibitor isoginkgetin (scale bar 5μm).

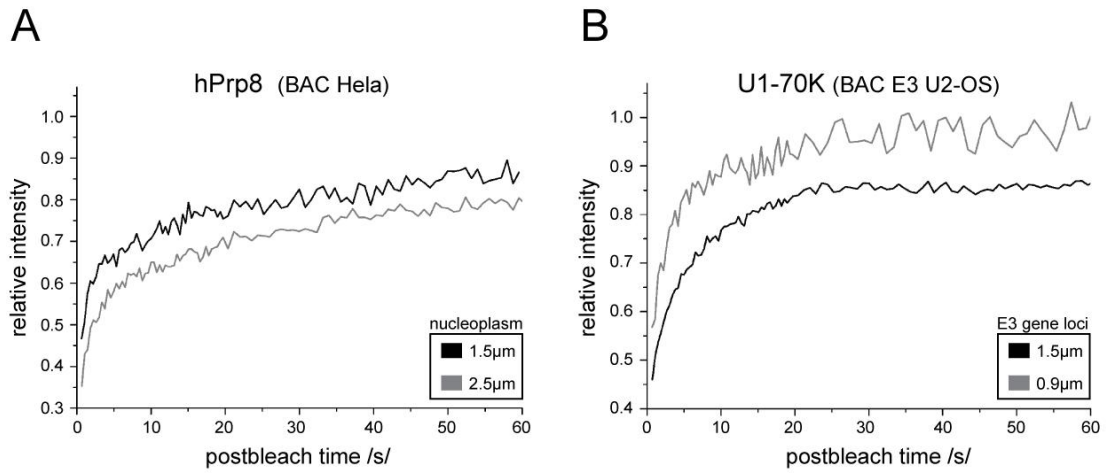

Supplementary figure 2.3. Role of diffusion in FRAP recovery curves of the GFP-tagged snRNP proteins. A/ FRAP measurements with different bleach-spot sizes in the nucleoplasm of the hPrp8-GFP cell line revealed the hPrp8-GFP recovery to be diffusion coupled. B/ FRAP measurements with different bleach-spot sizes on transgene loci in doxycycline treated U1-70K E3 U2-OS cell line revealed the U1-70K-GFP recovery to be diffusion coupled.

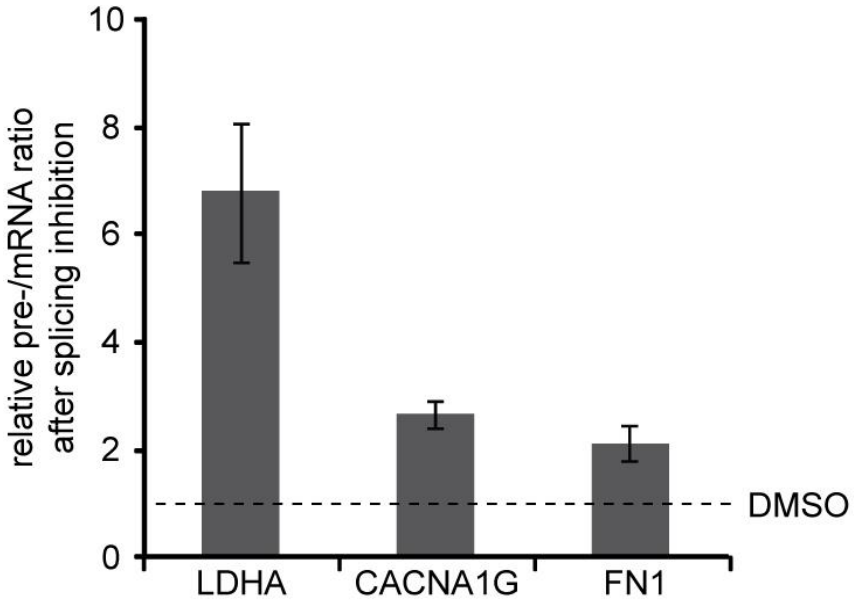

Supplementary figure 3.4. Isoginkgetin inhibits pre-mRNA splicing of several genes. RT-qPCR analysis of pre-mRNA and mRNA abundance was performed in control (DMSO) and isoginkgetin treated cells. Ratio of pre-/mRNA after splicing inhibition was normalized to control cells ratio that was set to one (*dashed line*). Increased pre-/mRNA ratio in isoginkgetin treated cells demonstrates elevated abundace of pre-mRNA.

	τ_{Da} /ms/		τ_{Db} /ms/		Df_b / $\mu m^2 s^{-1}$/	
nucleoplasm	Ave	sd	Ave	sd	Ave	sd
U1-70K	0.56	±0.08	24.92	±3.08	0.63	±0.08
U2 A`	0.67	±0.18	19.91	±4.68	0.82	±0.20
hPrp4	0.76	±0.17	24.68	±3.03	0.64	±0.08
hPrp8	0.64	±0.12	30.29	±1.44	0.54	±0.07
Snu114	0.76	±0.24	26.45	±5.16	0.61	±0.12
EGFP	0.88	±0.07				
U1-70K Δ1-197	3.88	±0.55				

Table 3.1. Calculated parameters derived from FCS measurements. The delay time values τ_{Da} for EGFP are comparable to the values of the fast component detected in the FCS measurements of snRNP proteins. The values for the delay times τ_{Db} describe the diffusion of a slower moving component that reflects snRNP complexes. τ_{Db} was used to calculate the diffusion coefficients Df_b. The average with standard deviations from 8-10 cells is shown.

	Df /μm^{2}s^{-1}/		$k_{off\ nucl\ nt}$ /s^{-1}/		$k_{off\ nucl\ isog}$ /s^{-1}/		Df $_{nucl\ isog}$ /μm^{2}s^{-1}/	
BAC HeLa cells	Ave	SEM	Ave	SEM	Ave	SEM	Ave	SEM
U1-70K	0.24	±0.02	1.87	±0.22	0.062	±0.008		
U2 A`	0.63	±0.04	0.078	±0.006	0.065	±0.009		
hPrp31	0.55	±0.03	0.94	±0.26	0.73	±0.24		
hPrp4	0.47	±0.08	1.16	±0.20	1.01	±0.22		
hPrp8	0.27	±0.02	0.035	±0.006	-	-	0.40	±0.02
Snu114	0.26	±0.02	0.031	±0.008	-	-	0.27	±0.03

	Df /μm^{2}s^{-1}/		$k_{off\ nucl\ nt}$ /s^{-1}/		$k_{off\ E3\ gene\ loci}$ /s^{-1}/	
E3 U2-OS cells	Ave	SEM	Ave	SEM	Ave	SEM
U1-70K *	0.50	±0.05	1.88	±0.15	0.180	±0.031
U2 B``	0.61	±0.07	0.064	±0.005	0.058	±0.008
hPrp4	0.75	±0.08	1.51	±0.20	0.053	±0.007
hPrp8 *	0.37	±0.03	0.040	±0.003	0.025	±0.002

* BAC E3 stable cell line

Table 3.2. Calculated parameters derived from FRAP measurements in BAC Hela (top) and E3 U2-OS (bottom) cell lines. Diffusion coefficients Df were calculated from fits of the FRAP curves measured in the nucleoplasm of DRB treated cells. Dissociation rates $k_{off\ nucl\ nt}$ were derived from fits of the FRAP curves measured in the nucleoplasm of non-treated cells. Kinetic parameters $k_{off\ nucl\ isog}$ and $Df_{nucl\ isog}$ were derived from fits of the FRAP curves measured in the nucleoplasm of isoginkgetin treated cells. Dissociation rates $k_{off\ E3\ gene\ loci}$ were calculated from fits of the FRAP curves measured at the transcription site of the E3 transgene in doxycycline treated E3 U2-OS cells.

CHAPTER 4

A mutation linked to retinitis pigmentosa in HPRP31 causes protein instability and impairs its interactions with spliceosomal snRNPs.

This chapter was reproduced from:
Huranová M., Hnilicová J., Fleischer B., Cvačková Z., Staněk D.: A mutation linked to retinitis pigmentosa in HPRP31 causes protein instability and impairs its interactions with spliceosomal snRNPs. Hum Mol Genet. 2009 Jun 1;18:2014-23

4.1 Abstract

The AD29 mutation in HPRP31 belongs to a series of mutations that were initially linked with the autosomal dominant disorder retinitis pigmentosa (RP) type 11. The HPRP31 gene encodes the hPrp31 protein that specifically associates with spliceosomal small nuclear ribonucleoprotein particles (snRNPs). Despite intensive research it is still unclear how the AD29 (Ala216Pro) mutation causes RP. In this study we report that expression of this mutant protein affects cell proliferation and alters the structure of nuclear Cajal bodies that are connected with snRNP metabolism. Interestingly, these effects can be reversed by the over-expression of the hPrp6 protein, a binding partner of hPrp31. Although Ala216 is not contained within the U4 or U5 snRNP interacting domains we present several lines of evidence that demonstrate that association between the AD29 mutant and snRNPs in the cell nucleus is significantly reduced. Finally, we show that stability of the AD29 mutant is severely affected resulting in its rapid degradation. Taken together, our results indicate that the Ala216Pro mutation destabilizes the hPrp31 protein structure in turn reducing its interaction with snRNP binding partners and leading to its rapid degradation. These findings significantly impact our understanding of the molecular mechanisms underlying RP and suggest that the insufficiency of the functional hPrp31 protein combined with the potential cytotoxicity associated with the expression the AD29 mutant are at least partially causative of the RP phenotype.

4.2 Introduction

Retinitis pigmentosa (RP) is the common name used to describe a group of inherited diseases characterized by the gradual degeneration of retina cells that leads to night blindness and visual field loss. Mutations within a variety of genes have been connected with RP, most of which are specifically expressed in photoreceptor cells. Surprisingly, mutations in three genes directly involved in pre-mRNA splicing have also been linked to autosomal dominant forms of RP. Products of these genes are well characterized components of the spliceosomal small nuclear ribonucleoproteins (snRNP) ((McKie, McHale et al. 2001; Vithana, Abu-Safieh et al. 2001; Chakarova, Hims et al. 2002) reviewed in (Mordes, Luo et al. 2006)). Of these proteins, hPrp8 is a key protein of the U5 snRNP that lies within the catalytic center of the spliceosome (Grainger and Beggs 2005; Pena, Rozov et al. 2008). hPrp3 and hPrp31 (also known as 61K) are components of the U4/U6 snRNP involved in the formation and stability of U4/U6 and U4/U6•U5 tri-snRNPs (Will and Luhrmann 2006). In addition, a mutation in a tentative splicing factor PAP-1 has also been linked to RP (Keen, Hims et al. 2002).

Initially the hPrp31 protein directly binds both the U4 snRNA and the U4 snRNP protein 15.5K to create the core of the U4 snRNP (Nottrott, Urlaub et al. 2002; Liu, Li et al. 2007). This interaction is followed by U4 and U6 snRNAs annealing to form the U4/U6 snRNP. Finally, the key interaction for the formation of the U4/U6•U5 tri-snRNP is the interaction of hPrp31 with the U5 snRNP-specific protein hPrp6 (Makarova, Makarov et al. 2002). During the splicing reaction the tri-snRNP undergoes dramatic rearrangements that result in disintegration of the tri-snRNP into individual snRNP components. In a process called the spliceosomal cycle, tri-snRNPs are re-assembled in a step wise manner similar to *de novo* formation described above (Will and Luhrmann 2006). U4/U6 and U4/U6•U5 snRNP formation and recycling occur primarily in the nuclear inclusion called the Cajal body that accelerates the snRNP assembly reaction ((Stanek, Rader et al. 2003; Schaffert, Hossbach et al. 2004; Stanek and Neugebauer 2004; Klingauf, Stanek et al. 2006; Stanek, Pridalova-Hnilicova et al. 2008) reviewed in (Stanek and Neugebauer 2006)). The Cajal body is a dynamic structure whose integrity depends on transcription/splicing activity as well as snRNP biogenesis (Carmo-Fonseca, Pepperkok et al. 1992; Sleeman, Ajuh et al. 2001; Stanek, Rader et al. 2003; Lemm, Girard et al. 2006; Stanek, Pridalova-Hnilicova et al. 2008).

It is largely unknown why mutations in snRNP-specific proteins cause RP

symptoms. It was reported that expression of hPrp31 mutants in retina cells negatively influences splicing of retina specific genes (Yuan, Kawada et al. 2005; Mordes, Yuan et al. 2007). However, most mutations in the HPRP31 gene result in the destabilization of hPrp31 mRNA that leads to a decrease in the synthesis of functional protein (Rio Frio, Wade et al. 2008). Moreover, RP affected families with large deletions of the HPRP31 gene have been identified (Abu-Safieh, Vithana et al. 2006; Kohn, Bowne et al. 2008). Together these observations suggest a haploinsufficiency model that predicts that there is a critical concentration of snRNP protein necessary to support retina cell survival (Vithana, Abu-Safieh et al. 2003; Rivolta, McGee et al. 2006; Rio Frio, Wade et al. 2008). Therefore, expression from only one allele may not be sufficient to achieve this critical level of expression in retina cells. This model however does not apply to all snRNP mutations, as depletion of one HPRP3 allele does not trigger RP in mouse or zebrafish (Graziotto, Inglehearn et al. 2008). In addition, it was shown that RP associated mutations in yeast Prp8 and hPrp3 influence snRNP assembly (Boon, Grainger et al. 2007; Gonzalez-Santos, Cao et al. 2008) and thus might trigger the death program in sensitive cells.

In this study we have concentrated on the hPpr31 point mutant, AD29 that contains an Ala216Pro substitution that does not apparently trigger a non-sense mediated decay. It was recently shown that the expression of the AD29 mutant, while affecting the splicing of mini-gene reporter plasmids, had no effect on the splicing of a full-length gene derived reporter (Wilkie, Vaclavik et al. 2008). Here, we have investigated whether the expression of the AD29 mutant has any effect on cell proliferation and snRNP assembly. Further, we have used co-immunoprecipitation, glycerol gradient ultracentrifugation and Förster resonance energy transfer (FRET) to map the interaction of this mutant protein with other snRNP proteins. Finally, we have probed the stability of the mutant protein and tested whether overexpression of hPrp31s major interacting partner in the tri-snRNP, hPrp6, can reverse phenotypes generated by AD29 expression.

4.3 Material and methods

Cells and antibodies

HeLa cells were cultured in Dulbecco's modified Eagle medium supplemented with

10% fetal calf serum, penicillin and streptomycin (Gibco BRL). Cells were transfected with Fugene HD (Roche) according to the manufacture's protocol. Stable HeLa cell lines were created by transfecting cells with the hPrp31-YFP (Stanek and Neugebauer 2004) or AD29-YFP plasmids. To obtain individual YFP positive cells G418 resistant cells were sorted by FACS. After selection, the antibiotics were omitted from the cell culture medium.

The following antibodies were used: rabbit anti-SART3/p110 antibodies (Stanek, Rader et al. 2003), mAb anti-coilin (5P10) (Almeida, Saffrich et al. 1998) kindly provided by M. Carmo-Fonseca, rabbit antibodies against hPrp31 (U4/U6-61K) (Makarova, Makarov et al. 2002), hPrp4 (U4/U6-60K) (Lauber, Plessel et al. 1997), hSnu114 (U5-116K) (Fabrizio, Laggerbauer et al. 1997) and hPrp3 kindly provided by R. Lührmann. Monoclonal antibodies against U2B" were purchased from Progen and anti-hPrp6 antibodies (H-300) from Santa Cruz Biotechnology.

Mutation and protein tagging

SART3-YFP-C3, hPrp4-YFP-C1, hPrp31-CFP-C3 and hPrp31-YFP-C3 were described previously (Stanek and Neugebauer 2004). The full-length hPrp6 was amplified by high fidelity PCR (Phusion, Finnzymes) from an EST clone and subsequently sub-cloned into ECFP-C3 or EYFP-C3 vectors derived from EGFP-C3 (Clontech) by using EcoRI/HindIII restriction sites. Correct sequences were confirmed by sequencing.

The point G646C mutation within the hPrp31 sequence was introduced by PCR mutagenesis using the ExSite Mutagenesis kit (Stratagene), primers 646-For: 5'-TTCATCCCACCCAACCTGTCCATCAT and 646-Rev: 5'-GGACATCCGGGACTC CACATACTC and hPrp31-CFP-C3 as a template (Stanek and Neugebauer 2004). The correct sequence was verified by sequencing. Subsequently, the AD29 mutant was re-cloned into the EYFP-C3 vector using EcoRI/BamHI restriction sites.

Indirect immunofluorescence

Cells were fixed in 4% paraformaldehyde/PIPES (Sigma) for 10 min, permeabilized for 5 min with 0.2% Triton X-100 (Sigma) and incubated with the appropriate primary antibodies. Secondary anti-rabbit antibodies conjugated with FITC or TRITC and anti-mouse antibodies conjugated with TRITC or Cy5 (Jackson ImmunoResearch Laboratories) were used. Images were collected using the DeltaVision microscope system (Applied Precision) coupled with the Olympus IX70 microscope equipped with

an oil immersion objective 60x 1.42NA using the same settings for each sample. Stacks of 25 z-sections with 200nm z-step were collected per sample and subjected to mathematical deconvolution using the measured point spread function (SoftWorx, Applied Precision). Mean intensities in Cajal bodies and nucleoplasm were quantified using SoftWorx as described previously (Stanek and Neugebauer 2004). 20-40 cells containing ~40-100 Cajal bodies were analyzed in each experiment.

Live cell imaging

Cells were plated on glass bottomed Petri dishes (MatTek) and after 20-24 h imaged using the DeltaVision microscope system coupled with the Olympus IX70 microscope equipped with an oil immersion objective 40x 1.3NA and an environmental chamber controlling CO_2 level and temperature. Images were taken every 30 min for 24 h using YFP excitation and emission filters (Applied Precision). To measure the effects of hPrp6-CFP expression on AD29 cell growth the same microscope set up was used except YFP and CFP filters were used. 8-12 positions were imaged simultaneously using the Multi-point visiting function. There were ~30-75 cells per experiment at time 0 h. The number of YFP or YFP/CFP positive cells were counted at each time point and plotted accordingly.

For protein stability measurements cells were placed under the DeltaVision microscopic system as descried above and images were taken every 15 min for 75 min using YFP filters. Cycloheximide was added to the medium at a final concentration of 30 µg/ml and cells were imaged as before for an additional 5 h. Relative YFP fluorescence of each cell with respect to the start point was calculated and an average of all cells was plotted.

Western blotting

Cells were washed with ice-cold PBS, scraped and pelleted at 1,000 g for 5 min before being resuspended in 30 µl PBS. This was followed by the addition of 30 µl of 2x protein sample buffer and incubation at 95ºC for 5 min. Cell extracts were subsequently homogenized by passage through a 22 G needle. Proteins were resolved on a 10% polyacrylamide gel, blotted onto a nitrocellulose membrane and incubated with anti-hPrp31 antibodies followed by incubation with goat anti-rabbit antibodies coupled with horseradish peroxidase (Jackson ImmunoResearch Laboratories). The SuperSignal West Pico/Femto Chemiluminiscent Substrate (Pierce) was used to generate luminiscence.

FRET measurement

HeLa cells were transfected with constructs encoding fluorescently tagged proteins using Fugene HD, grown for 24-26 h and fixed at room temperature in 4% paraformaldehyde/PIPES (Sigma) for 10 min. After rinsing with Mg-PBS (PBS supplemented with 10mM Mg^{2+}) and water, cells were embedded in glycerol containing DABCO. FRET was measured by the acceptor photobleaching method as previously described (Stanek and Neugebauer 2004) using the Leica SP5 confocal microscope. Intensities of CFP (excited by 405nm laser set to 5-10% of maximum power) and YFP (excited by 514nm laser line set to 2% of maximum power) were measured. Following this,, YFP was bleached in a region of interest by 3-5 intensive (30% maximum power) pulses of 514 nm laser line and CFP and YFP fluorescence measured again. Apparent FRET efficiency was calculated according to the equation $FRET_{efficiency}\{\%\} = (CFP_{after} - CFP_{before})x100/ CFP_{after}$. Unbleached regions of the same cell were used as a negative control. Ten cells were measured per each FRET pair.

Immunoprecipitation

HeLa, WT31 or AD29 cells were grown on 15 cm Petri dishes, placed on ice, washed 3 times with ice cold Mg-PBS and harvested into NET-2 buffer (50 mM TRIS-Cl pH 7.5, 150 mM NaCl, 0.05% Nonidet P-40) supplemented with a complete mix of protease inhibitors (Roche) and pulse-sonicated for 90 s on ice. Cell extracts were centrifuged at 13,000 rpm and the supernatant incubated with Protein-G Sepharose beads (GE Healthcare) coated with goat anti-GFP antibodies (raised against bacterially expressed full-length EGFP and obtained from David Drechsel, MPI-CBG, Dresden, Germany) for 4 h at 4ºC. Captured complexes were extracted by bead incubation in protein sample buffer for 5 min at 95ºC and the precipitated proteins were detected by Western blotting.

Glycerol gradient ultracentrifugation

Nuclear extracts were prepared according to (Dignam, Lebovitz et al. 1983), diluted in gradient buffer (20 mM HEPES/KOH pH 8, 150 mM NaCl, 1.5 mM MgCl2, 0.5mM dithiothreitol) and fractionated in a linear 10-30% glycerol gradient by centrifugation at 32,000 rpm for 17 h using the SW-41 rotor (Beckman). The gradient was divided into 20 fractions (~620 µl) and proteins from these fractions analyzed by Western blotting.

4.4 Results

Cells expressing the AD29 mutant exhibit slower proliferation

It has been shown that RP linked mutations in the splicing factor Prp8 cause disruption of U5 snRNP biogenesis in yeast (Boon, Grainger et al. 2007). In a human cell line a mutation in hPrp3 has been shown to have a negative effect on snRNP assembly (Gonzalez-Santos, Cao et al. 2008). In this study, we decided to analyze the effects of expression of a hPrp31 mutant on cell growth and snRNP assembly in human cells. To achieve this, we established two stable cell lines that expressed either YFP tagged wild-type hPrp31 (WT31 cells) or mutant AD29 tagged with YFP (AD29 cells) (Fig. 4.1.). Similar to endogenous protein (data not shown; see also (Schaffert, Hossbach et al. 2004; Stanek, Pridalova-Hnilicova et al. 2008)) the wild-type hPrp31-YFP (WT31-YFP) localized to the cell nucleus and accumulated in Cajal bodies and splicing factor compartments (Fig. 4.1.A). The localization pattern of the AD29-YFP mutant (AD29-YFP) was more diverse (Fig. 4.1.B). In most cells analyzed AD29-YFP localized to the cell nucleus and the cytoplasm, however cells displaying a mostly cytoplasmic or nuclear accumulation were also presented. In comparison with the localization of WT31-YFP, AD29-YFP exhibited a more diffuse nuclear staining pattern and weak accumulation in Cajal bodies. A similar localization pattern has previously been observed in cells transiently expressing a AD29-GFP mutant (Deery, Vithana et al. 2002). Of note, nucleolar accumulation was observed in cells highly expressing either of the YFP tagged proteins.

In order to test the effects of AD29 mutant expression on cell proliferation AD29 cells were observed for 24 h and their growth compared with WT31 cells (Fig. 4.1.C). Cells expressing the mutant protein divided 10% slower than cells expressing the wild-type protein. As both stable cell lines expressed the same amounts of endogenous hPrp31 and expression of WT31-YFP and AD29-YFP were comparable (see below Fig. 4.3.) these data indicate that AD29 expression has a dominant negative effect on cell proliferation.

During live-cell imaging we noticed that the localization of AD29-YFP changes during cell cycle. At early G1 phase AD29-YFP was found mainly in the cytoplasm and only gradually accumulated in the nucleus during interphase. This observation explains the diverse localization of AD29 in an unsynchronized cell population. In contrast

WT31-YFP accumulated in the cell nucleus as soon as the nuclear membrane was formed after mitosis.

The AD29 mutant disrupts formation of Cajal bodies

As described above, our data indicates that the expression of AD29-YFP has a negative effect on cell growth (Fig. 4.1.C). Given that hPrp31 is necessary for tri-snRNP formation we decided to investigate snRNP metabolism in cells expressing the mutant protein. First, we analyzed cells for the presence of Cajal bodies because these bodies facilitate certain steps in tri-snRNP assembly (Stanek and Neugebauer 2006) and their integrity depends on ongoing snRNP biogenesis and/or splicing (Carmo-Fonseca, Pepperkok et al. 1992; Lemm, Girard et al. 2006). Staining cells with the Cajal body marker coilin revealed that the expression of AD29-YFP altered the structure of Cajal bodies (Fig. 4.2.). Further, a significant fraction of AD29-YFP expressing cells did not have apparent Cajal bodies (Fig. 4.2.C) and if Cajal bodies were present they were often smaller than in WT31 cells. In the population of AD29 cells that did contained Cajal bodies we analyzed the localization of snRNP specific proteins within Cajal bodies. Interestingly, we observed in AD29 cells that accumulation of SART3, a marker of U4/U6 snRNP is reduced while the localization of the U5-specific protein hSnu114 and the U2-specific U2B" were not significantly altered (Fig. 4.2.D). As Cajal body integrity is sensitive to snRNP metabolism and splicing these data indicate that expression of the AD29 mutant impacts upon snRNP metabolism and/or splicing.

Interaction between AD29 and snRNPs is significantly reduced

To analyze AD29 association with snRNP specific proteins we first employed the technique of FRET to detect protein complexes *in situ*. Either AD29-CFP or WT31-CFP were co-expressed with the YFP-tagged snRNP specific protein SART3, hPrp4 or hPrp6 (Fig. 4.3.A) and FRET was measured by acceptor photobleaching (Fig. 4.3.B). We analyzed these snRNP proteins because they mark different stages of tri-snRNP formation: SART3 is specifically found in the U4/U6 snRNP intermediate, hPrp4 is a component of the U4/U6 snRNP and the tri-snRNP while hPrp6 is the U5-specific protein that interacts with hPrp31 to facilitate U4/U6•U5 tri-snRNP assembly. Cells co-expressing WT31-CFP and SART3-YFP exhibited a high FRET signal specifically within Cajal bodies that is consistent with previously published data that demonstrated that the U4/U6 snRNP is highly concentrated in Cajal bodies (Stanek and Neugebauer

2004). A high FRET signal between hPrp6-YFP and WT31-CFP in the nucleoplasm indicates that there is a higher concentration of tri-snRNPs in the nucleoplasm than in Cajal bodies. Finally, the FRET signal between WT31-CFP and hPrp4-YFP was similar in the Cajal body and the nucleoplasm reflecting the localization of both U4/U6 and U4/U6•U5 snRNPs. Notably, the association between the AD29 mutant and U4/U6 snRNP proteins SART3 and hPrp4 (as measured by FRET) was reduced by approximately 40 to 50%. In contrast, the interaction between AD29 and hPrp6 was lowered only in the nucleoplasm whilst this interaction in Cajal bodies was similar to wild-type hPrp31. These data indicate that the mutant protein is still able to partially integrate into snRNPs but its association with snRNPs is compromised.

To further test the interaction between AD29 and snRNPs, immunoprecipitation assays were carried out on WT31 or AD29 cells. As a negative control the parental cell line was used. WT31 and AD29 cell lines expressed a similar amount of YFP-tagged proteins and their levels were lower than the level of endogenous hPrp31 (Fig. 4.3.C). Co-precipitated proteins were analyzed by Western blotting. Both hPrp3 and hPrp4 (proteins found in U4/U6 and U4/U6•U5 snRNPs) along with hSnu114 and hPrp6 (U5 and U4/U6•U5 snRNP specific proteins) were co-precipitated with WT31-YFP illustrating that WT31-YFP is properly incorporated into U4/U6 and U4/U6•U5 snRNPs. In contrast, AD29-YFP did not pull-down any of the tested U4/U6 specific proteins signifying that the single point mutation is sufficient to disrupt the interaction between AD29 and the U4/U6 snRNP. However, AD29 precipitated with its U5-specific binding partner hPrp6. This finding extends the *in vitro* binding studies (Liu, Li et al. 2007; Wilkie, Vaclavik et al. 2008) and shows in human cells that AD29 interacts with hPrp6. Of interest, we repeatedly detected limited amounts of hSnu114 pulled down by AD29-YFP suggesting that under the immunoprecipitation assay conditions the AD29 mutant might still be capable of interaction with the U5 snRNP.

To confirm that the AD29 mutant is impaired in its ability to incorporate into snRNPs we prepared nuclear extracts from AD29 or WT31 stable cell lines. These extracts were subjected to glycerol gradient fractionation and the presence of AD29-YFP or WT31-YFP in individual fractions analyzed (Fig. 4.3.D). Consistent with our previous findings, the AD29 mutant was mainly restricted to the top of the gradient and its sedimentation behavior was similar to bovine serum albumin that has a comparable molecular weight (data not shown). These data further demonstrate that the mutant is not a stable component of snRNP complexes.

Over-expression of hPrp6 is able to rescue some defects in AD29 expressing cells

Although the interaction between AD29 and snRNPs is dramatically reduced this mutant is still able to instigate a dominant negative effect on both cell growth and Cajal body formation (Figs. 4.1. and 4.2.). It has been shown that AD29 binds strongly to hPrp6 *in vitro* (Wilkie, Vaclavik et al. 2008) and our data shows that AD29 is able to interact with hPrp6 *in vivo* (Fig.4.3.). Thus, it is plausible that AD29 might sequester free U5 snRNP or hPrp6 and that in turn changes the dynamics of tri-snRNP formation. To test this hypothesis we expressed hPrp6-CFP in AD29 cells and measured the appearance of Cajal bodies (Fig. 4.4.A-C). Expression of hPrp6-CFP but not CFP alone increased the number of cells that contained Cajal bodies to a level comparable to parental HeLa or WT31 cells. This result indicates that the negative effect AD29 has on Cajal body formation can be overcome by expression of hPrp6.

To further test whether hPrp6 can also rescue the AD29 induced growth phenotype, AD29 cells were transfected with hPrp6-CFP and their proliferation measured as described previously (Fig. 4.4.D). Neighboring AD29 cells that did not express hPrp6-CFP served as an internal negative control. Although the transfection procedure had a general negative effect on cell proliferation (compare fig. 4.4.D with fig. 4.1.C) AD29 cells expressing hPrp6-CFP divided faster than their non-transfected neighbors.

The AD29 mutation destabilizes the hPrp31 protein

During live cell observations we noticed that the amount of AD29-YFP in individual cells changed significantly during the 24 h observation period. The observed changes in AD29-YFP accumulation were not connected with any particular cell cycle phase and instead exhibited a rather stochastic behavior indicating that this effect might be a reflection on the dynamics of AD29 expression and degradation. To test the stability of the AD29-YFP protein cells were treated with the translation inhibitor cycloheximide and YFP fluorescence monitored for 5 h (Fig. 4.5.). While the WT31-YFP fluorescence decreased only marginally, the level of AD29-YFP fluorescence dropped rapidly after only 1 to 2 h incubation in cycloheximide (Fig. 4.5.A-C). The fluorescent signal decreased both in the nucleus and the cytoplasm and no preferential degradation was observed in either of these cell compartments. Similar results were observed when the degradation of the AD29 mutant was analyzed by Western blotting

(Fig. 4.5.D). While endogenous hPrp31 and WT31-YFP were stably present in cells during the 5 h treatment, AD29-YFP protein disappeared within a couple of hours. Together these data suggest that the Ala216Pro substitution causes a conformational change that negatively affects the stability of the protein.

4.5 Discussion

Retinitis pigmentosa is a heritable disease that affects 1 in 4000 people. So far there have been over 40 loci identified that carry mutations that cause RP. Generally, most of these genes are directly involved in controlling retina cell metabolism. However, three genes that encode general RNA splicing factors that are ubiquitously expressed have also been implicated in RP. In addition, the gene encoding the putative splicing factor PAP1 is also mutated in RP (Mordes, Luo et al. 2006). The mechanism underlying how mutations in splicing factors trigger RP has been extensively investigated during the last couple of years. Such studies has shown that mutations in HPRP3 and HPRP8 can influence snRNP assembly and that many mutations in HPRP31 lead to the degradation of its mRNA by the non-sense mediated decay pathway, consequently lowering the expression of functional hPrp31 protein.

Here we investigated the hPrp31 point mutation found in the AD29 family that does not apparently activate the mRNA degradation pathway but instead codes for an alanine to proline substitution at residue 216. It has been shown *in vitro* and by two-hybrid analysis that this amino acid change does not interfere with the hPrp31-hPrp6 interaction (Liu, Li et al. 2007; Wilkie, Vaclavik et al. 2008). In addition, a structural analysis of the U4snRNA/15.5K/hPrp31 complex revealed that the Ala216 residue is not directly involved in the interaction between hPrp31 and U4 snRNA or 15.5K however, the effect of the AD29 mutation on the hPrp31 and U4 snRNP interaction has never been tested (Liu, Li et al. 2007). Here we have demonstrated that the AD29 mutation dramatically alters the ability of hPrp31 to interact with U4/U6 snRNPs. Analysis of the association of AD29 and U4/U6 snRNPs *in situ* by FRET revealed that this association was reduced by half. Further, the AD29 mutant precipitated the U5 snRNP, specifically the hPrp6 and hSnu114 proteins but not any of the tested U4/U6 markers. Finally, the AD29 mutant was mainly concentrated at the top of a glycerol gradient indicating that it is not a stable component of snRNPs. These data together

indicate that the mutant has a limited ability to associate with U4/U6 snRNPs. In addition, the interaction between AD29 and snRNPs is weak and does not withstand the conditions during snRNP immunoprecipitation and gradient centrifugation. As the mutant protein is partially localized in the cytoplasm, one explanation for reduced interaction with snRNPs could be a defect in nuclear import. However, the Ala216Pro substitution does not affect the nuclear localization signal or interaction with importin β1 and direct measurements of nuclear import did not reveal any differences between wild-type and mutant proteins (Deery, Vithana et al. 2002; Wilkie, Morris et al. 2006). Therefore we assume that reduced nuclear localization is rather an effect than a cause of reduced AD29 binding to snRNPs.

To date, it is unclear whether the AD29 mutant can bind U4/U6 and U5 snRNPs simultaneously and form the tri-snRNP or whether the mutant binds U4/U6 and U5 snRNPs independently and prevents tri-snRNP formation. Based on the fact that AD29 interacts with hPrp6 *in vivo* as assayed by both FRET and immunoprecipitation (Fig. 4.3.) and that over-expression of hPrp6 is able to rescue the AD29 phenotype we speculate that free AD29 transiently binds via hPrp6 to the U5 snRNP. This interaction prevents the proper association with the U4/U6 snRNP and changes the dynamics of tri-snRNP formation resulting in the observed phenotypes: reduced cellular proliferation (Fig. 4.1.) and disruption of Cajal body formation (Fig. 4.2.). Both phenotypes are likely to be dominant as we did not observe any changes in the expression of endogenous hPrp31 or other tested snRNP proteins (Fig. 4.3. and data not shown).

Besides the effects of AD29 expression on cell growth and nuclear morphology we also observed the rapid degradation of the AD29 mutant in HeLa cells. Despite the fact that these results were acquired using cell culture expressing normal levels of endogenous hPrp31, such observation raise two alternative models for RP. The first model predicts that the AD29 mutant is rapidly degraded in all cell types including retina cells and RP symptoms are caused by the insufficiency of functional hPrp31. This hypothesis would be in accordance with previous findings that demonstrated that large deletions of the HPRP31 gene and mutations that destabilize hPrp31 mRNA cause RP (Abu-Safieh, Vithana et al. 2006; Kohn, Bowne et al. 2008; Rio Frio, Wade et al. 2008). Additionally, this model would also explain the incomplete penetrance of the AD29 mutation (Vithana, Abu-Safieh et al. 2001).

An alternative hypothetical model would require specific stabilization and/or high expression of the mutant in retina cells. In this case the mutant would only be able

to exert its dominant negative effect on snRNP metabolism and cell viability when it is present in cells as is the case of our model system. These defects can be reverted by over-expressing the hPrp31 binding partner, hPrp6 whose expression might represent an additional factor that determines whether RP symptoms are manifested in affected individuals. To distinguish between these two models further investigation is required to determine whether the AD29 mutant is present in targeted retina cells.

Figures to chapter 4:

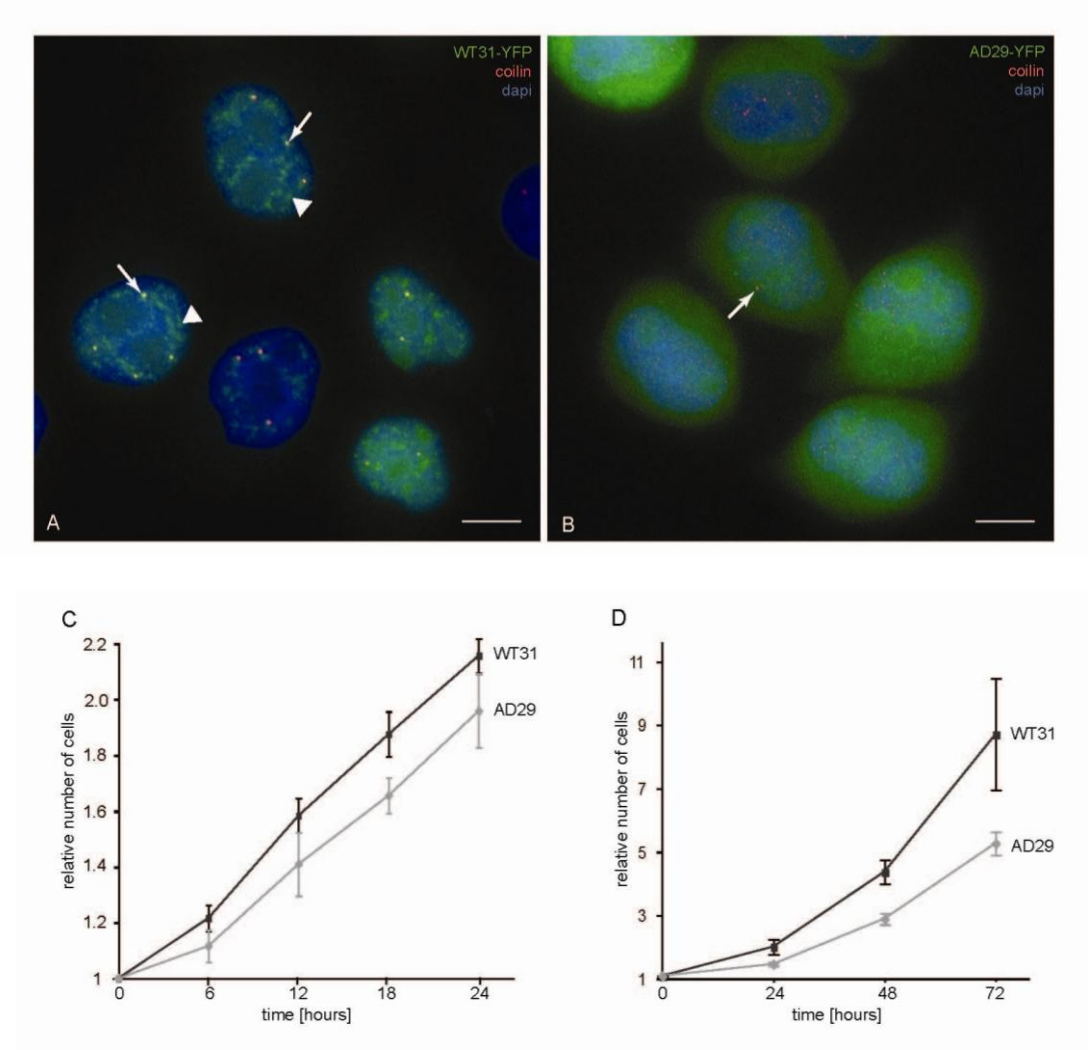

Figure 4.1. The AD29 mutant is aberrantly localized in the cytoplasm and inhibits cell growth. Stable cell lines expressing either the AD29-YFP mutant or wild-type hPrp31-YFP (WT31-YFP) were created from parental HeLa cells. A/ WT31-YFP was localized in the nucleus within splicing factor compartments (arrowheads) and Cajal bodies (*arrows*). B/ The AD29-YFP mutant was found abnormally localized within both the nucleus and cytoplasm. In the cell nucleus AD29-YFP exhibited a more diffuse staining than wild-type protein and was only weakly accumulated in Cajal bodies (*arrows*). Cajal bodies were visualized by immunodetection of coilin (shown in red) that preferentially accumulates in Cajal bodies. DNA is visualized by dapi staining (blue). Bars represent 10 μm. C, D/ Proliferation of WT31 and AD29. C/ WT31 and AD29 cell growth was monitored on the microscope for 24 h and their proliferation graphically represented. D/ WT31 and AD29 cells were plated to the same density and their number calculated every 24 h for three days. The average of two experiments and SEM are shown.

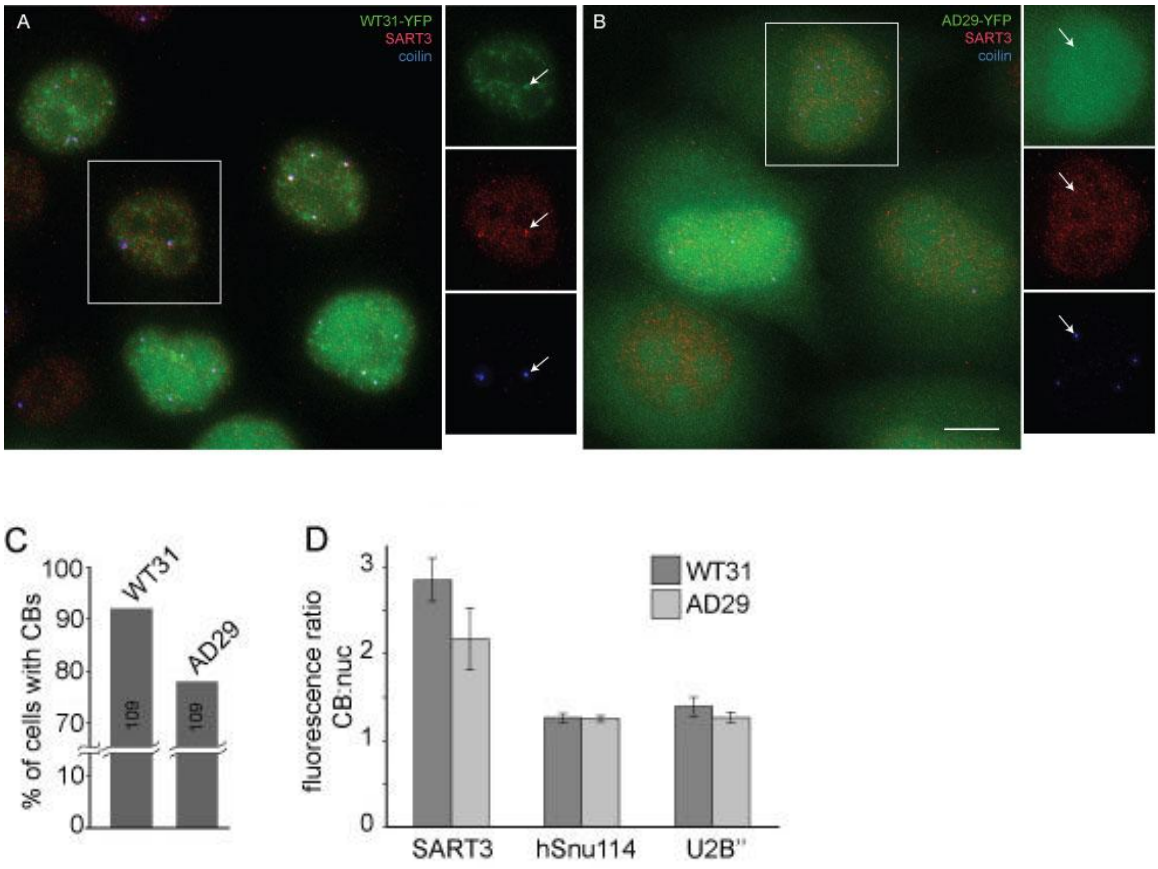

Figure 4.2. Expression of AD29-YFP affects the formation of Cajal bodies. To reveal how the expression of AD29-YFP affects the formation of Cajal bodies WT31 /A/ and AD29 /B/ cells were stained for the Cajal body marker coilin (blue) and SART3 (red), a marker of the U4/U6 snRNP. Cajal bodies are marked by arrows. Bars represent 10 μm. C/ Cells containing Cajal bodies were counted (number of cells counted is given within bars). D/ To analyze whether the AD29 mutant influences the localization of snRNPs in Cajal bodies, AD29 and WT31 cells were stained for coilin as a marker of Cajal bodies and either SART3 (U6 and U4/U6 snRNPs), hSnu114 (U5 snRNP and tri-snRNP) or U2B" (U2 snRNP) and the fluorescence ratio of Cajal bodies to nucleoplasm calculated. Expression of AD29 affected accumulation of SART3 in Cajal bodies. The average of three experiments and SEM are shown.

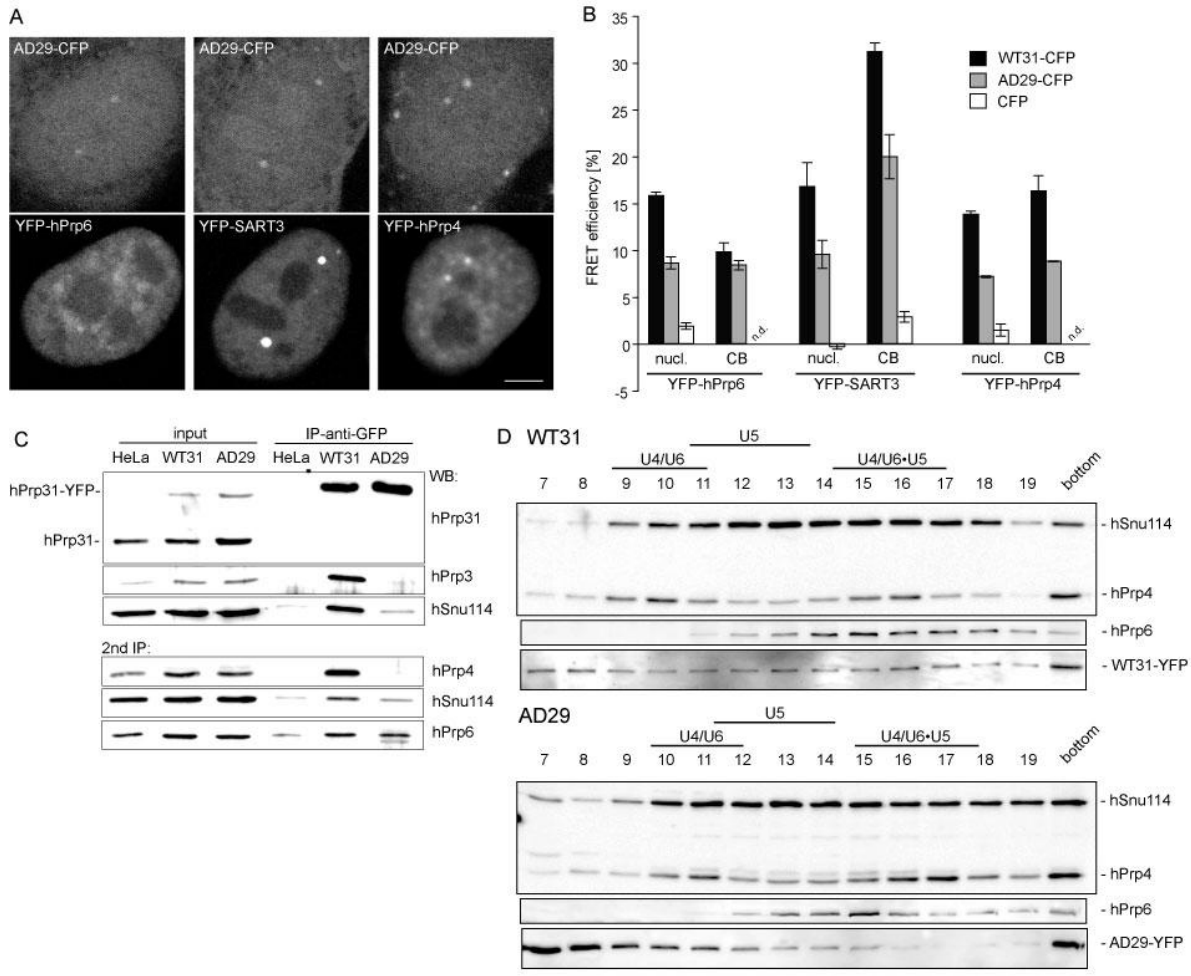

Figure 4.3. The interaction between AD29 and snRNPs is weakened. A/ AD29-CFP was co-expressed with markers of different snRNPs tagged with YFP and their association in the nucleoplasm and Cajal bodies measured by FRET. Bars represent 5 µm. B/ FRET efficiency indicates the association of wild-type protein (WT31) or AD29 mutant protein with hPrp6, SART3 or hPrp4. The AD29 mutant exhibited a significantly lower FRET signal with U4/U6 snRNP markers (SART3 and hPrp4) than wild-type protein. FRET measurements of cells expressing an empty CFP vector were used as a negative control. The average of two independent experiments and SEM are plotted. C/ AD29-YFP or WT31-YFP was precipitated from extracts made from the WT31 or AD29 stable cell lines using anti-GFP antibodies that cross-react with the YFP variant. Parental HeLa cells (HeLa) were used as a negative control. Two independent immunoprecipitations are shown. WT31-YFP co-precipitated efficiently with U4/U6 (hPrp3 and hPrp4) and U5 (hSnu114 and hPrp6) snRNP specific proteins demonstrating

that it is incorporated into the U4/U6 and U4/U6•U5 snRNPs. In contrast, AD29-YFP co-precipitated U5-specific hPrp6 and also a smaller amount of hSnu114 but none of the tested U4/U6 specific proteins. D/ Nuclear extracts were prepared from WT31 or AD29 cells, resolved on glycerol gradients and the position of snRNP specific proteins visualized by Western blotting. In comparison to the wild-type protein the AD29 mutant does not co-migrate with snRNPs but is instead concentrated at the top of the gradient signifying that it is not stably incorporated into snRNP complexes.

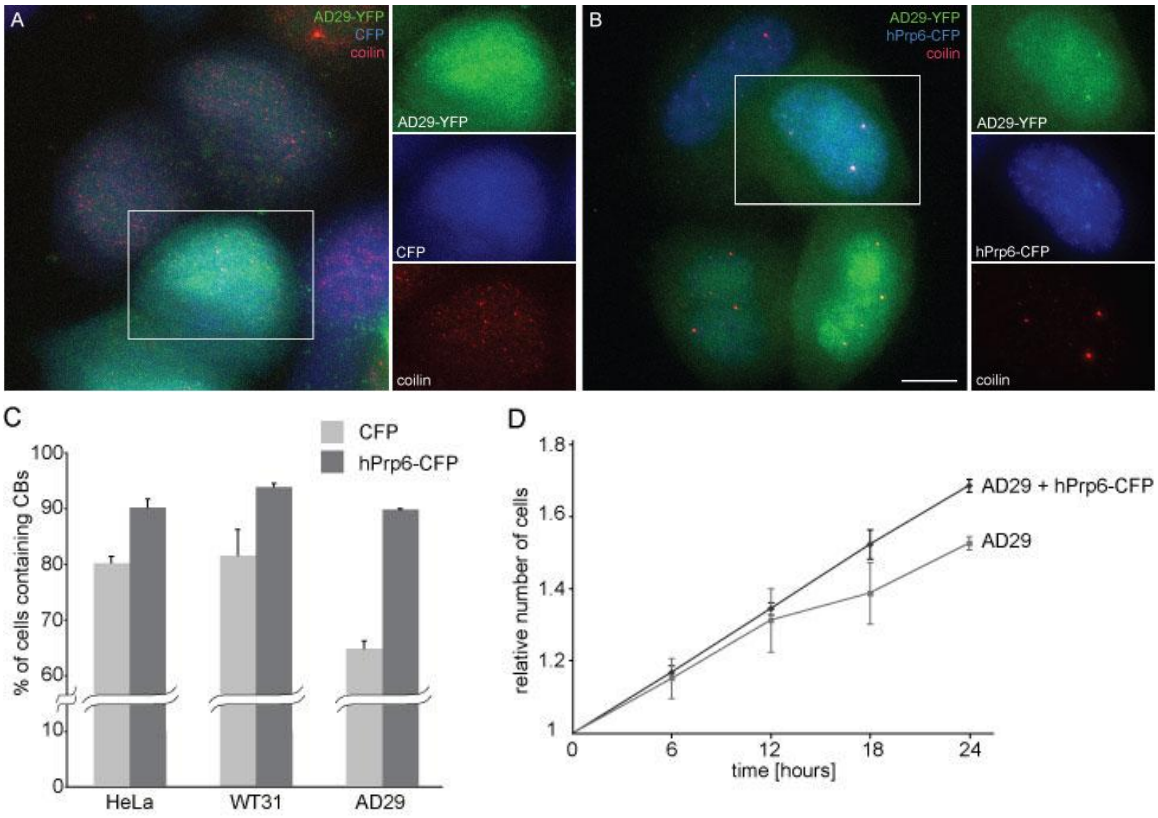

Figure 4.4. Expression of hPrp6 rescues the AD29 phenotype. The AD29 cell line was transfected with /A/ CFP or /B/ hPrp6-CFP. 24 h post-transfection cells were fixed and stained for the Cajal body marker coilin. In CFP transfected cells, Cajal bodies were smaller and coilin was often dispersed throughout the nucleoplasm with no obvious accumulation. Expression of hPrp6 led to the re-formation of Cajal bodies. Bar represents 10 μm. C/ Parental HeLa cells, WT31 or AD29 cells were transfected with CFP or hPrp6-CFP, stained for coilin and the number of cells with Cajal bodies determined. The average and SEM of two independent experiments are shown. D/ The AD29 cells were transfected with hPrp6-CFP and their proliferation measured 20-24 h after transfection. Although transfection conditions negatively affected cell growth, the AD29 cells expressing hPrp6-CFP divided faster than non-transfected cells. An average of three experiments with SEM is shown.

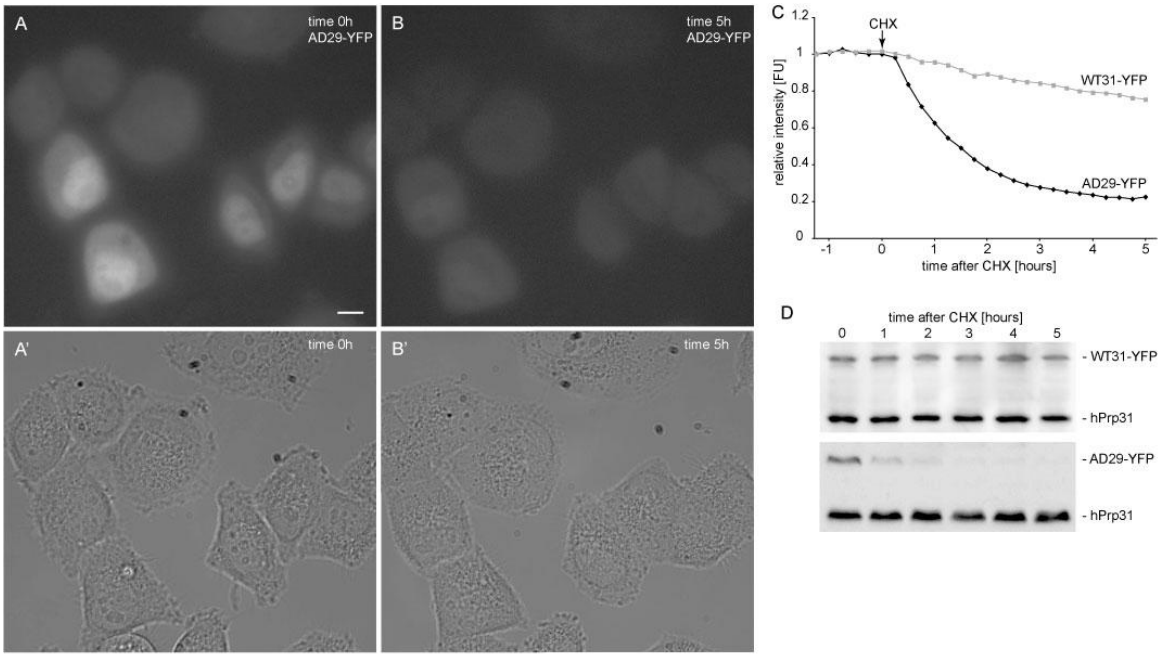

Figure 4.5. The AD29 protein is rapidly degraded inside cells. A, B and C/ To compare the stability of AD29-YFP to WT31-YFP proteo-synthesis was inhibited by cycloheximide in WT31 or AD29 cell lines and YFP fluorescence measured every 15 min for 5 h. /A,A'/ AD29 cells at time 0 h and /B,B'/ 5 h after cycloheximide addition. /A,B/ YFP fluorescence /A',B'/ bright-field images. C/ Graph of relative YFP fluorescence after protein synthesis inhibition. YFP fluorescence did not exhibit any significant decrease before addition of cycloheximide, 15 min post addition of cycloheximide AD29-YFP fluorescence (n=28 cells) began decreasing indicative of the rapid degradation of the AD29-YFP protein. In contrast, WT31-YFP protein (n=22 cells) exhibited only a slow decay during the course of the 5 h experiment. D/ Protein synthesis was inhibited as before and proteins detected by Western blotting using anti-hPrp31 antibodies that recognize both endogenous and tagged hPrp31 variants. The results show the relative stability of WT31-YFP compared to AD29-YFP that is rapidly degraded after 2 hours.

CHAPTER 5

In vivo detection of RNA-binding protein interactions with cognate RNA sequences by fluorescence resonance energy transfer.

This chapter was reproduced from:
Huranová M., Jablonski J.A., Benda A., Hof,M., Staněk D. and Caputi M. A method to visualize the interaction of RNA-binding proteins to their cognate RNA binding site in cells by fluorescence resonance energy transfer. RNA 2009 Nov; 15:2063-71

5.1 Abstract

Expression of the nascent RNA transcript is regulated by its interaction with a number of proteins. The misregulation of such interactions can often result in impaired cellular functions that can lead to cancer and a number of diseases. Thus, our understanding of RNA-protein interaction within the cellular context is essential for the development of novel diagnostic and therapeutic tools. While there are many *in vitro* methods that analyze RNA-protein interactions *in vivo* approaches are scarce. Here we established a method based on fluorescence resonance energy transfer (FRET), we termed RNA-binding mediated FRET (RB-FRET), which determines RNA-protein interaction inside cells and tested it on hnRNP H protein binding to its cognate RNA. Using two different approaches we provide evidence that RB-FRET is sensitive enough to detect specific RNA-protein interactions in cell, providing a powerful tool to study spatial and temporal localization of specific RNA-protein complexes.

5.2 Introduction

Up to 40% of mutations leading to genetic diseases and cancer cause post-transcriptional misregulation of gene expression that often correlate with splicing defects, RNA editing errors and altered mRNA stability or localization. Several diseases such as Frontotemporal Dementia with Parkinsonism (FTDP) (D'Souza, Poorkaj et al. 1999) or Spinal Muscular Atrophy (SMA) (Lorson, Hahnen et al. 1999) originate from a single nucleotide mutation in the pre-mRNA resulting in an imbalanced ratio between alternatively spliced protein variants. A majority of these mutations are speculated to weaken critical interactions with cellular splicing factors. The identification of such factors is often a cumbersome process that requires *in vitro* assays and several multiple biochemical purification steps. Furthermore, the complex set of interactions within the cellular environment can hardly be mimicked *in vitro*. Within the cell RNA - proteins interactions may be influenced by: i) the relative concentrations of competing factors, ii) the secondary structure of the target RNA, which might be influenced by its interaction with a number of RNA binding proteins, iii) the phosphorylation state of the RNA binding protein, iv) ion concentrations and v) intracellular localization.

hnRNP H is the prototypical member of a highly homologous, ubiquitously expressed protein family of RNA binding proteins constituted by hnRNPs H, H', F, 2H9 and GRSF-1. These proteins have been shown to regulate several aspects of mRNA biogenesis. In particular, members of this protein family have been shown to activate splicing in several systems (Min, Chan et al. 1995; Chou, Rooke et al. 1999; Hastings, Wilson et al. 2001; Caputi and Zahler 2002; Garneau, Revil et al. 2005; Han, Yeo et al. 2005; Marcucci, Baralle et al. 2006; Schaub, Lopez et al. 2007) while acting as splicing repressors in others (Chen, Kobayashi et al. 1999; Fogel and McNally 2000). Members of the hnRNP H family share similar binding specificities for the consensus sequence DGGGD (were D is A, G or C) (Schaub, Lopez et al. 2007). NMR studies also indicate that hnRNP F, one of the hnRNP H family members, interacts with a poly G sequence via two quasi RNA recognition motifs (qRRMs) (Dominguez and Allain 2006). Genomic studies have shown that G-runs are found preferentially in intronic sequences immediately flanking the splice sites and appear to facilitate splicing of the intron (McCullough and Berget 1997; Yeo, Hoon et al. 2004). Nevertheless, functional studies indicate that mutation of only few of the potential hnRNP H binding sites within a gene transcript may alter splicing (Schaub, Lopez et al. 2007), suggesting that interaction

with other regulatory elements and/or proper positioning within a higher order RNA structure may be required for splicing control by hnRNPs of the H family. Thus, the ability of hnRNP H to functionally interact with a target sequence *in vivo* appears to differ from its ability to bind a RNA substrate *in vitro*. The same is likely to be true for most RNA binding proteins, which recognize their target RNA in a complex environment where several other factors may compete or aide in the interaction and structural elements within the RNA itself might alter the stability of the RNA-protein complex. Furthermore, the interaction between a given RNA binding protein and its target may drastically change in response to intracellular signaling and changes in key physiological conditions.

A wide array of techniques has been developed to study the spatial distribution and interactions of proteins in cellular systems. More recently, single mRNA molecules, tagged with a fluorescent reporter, have been visualized and their localization in living cells studied (Shav-Tal, Singer et al. 2004; Rodriguez, Shenoy et al. 2006; Boireau, Maiuri et al. 2007; Rodriguez, Condeelis et al. 2007), while other reporter systems allowed for the direct visualization of RNA transcription (Darzacq, Shav-Tal et al. 2007; Endoh, Mie et al. 2008). However, specific techniques aimed at the direct detection of protein RNA interactions within cells need to be fully developed. Recent studies have utilized fluorescence resonance energy transfer (FRET) and fluorescence complementation (TriFC) to study the interaction between the RNA binding proteins PTB, Raver1, FMRP and IMP1 and their cognate RNA targets (Rackham and Brown 2004; Lorenz 2009). Although useful, such techniques have limitations, as they lack either specificity for the recognition by the protein of a specific mRNA (the former) or the ability to detect temporal and spatial regulation (the latter).

FRET is a photophysical phenomenon in which energy is transferred between two appropriate fluorophores called donor and acceptor that are in proper orientation and distance (usually less than 10 nm). In cell biology, fluorophores are often attached to proteins and their proximity is achieved by interaction of tagged proteins. However, the tagged proteins do not have to interact directly. It is often enough when FRET partners are part of the same macromolecular complex, as for the spliceosome where FRET was successfully used for measuring dynamic protein-protein interactions between splicing factors (Stanek and Neugebauer 2004; Chusainow, Ajuh et al. 2005; Ellis, Lleres et al. 2008; Rino, Desterro et al. 2008). In this work we describe a novel technique to detect specific RNA-protein interaction within cells by FRET-FLIM

utilizing the MS2 coat protein-RNA operator interaction as a molecular marker. This technique, we termed RNA-binding mediated FRET (RB-FRET), allows for quantitative and dynamic analysis of the association of a given RNA binding protein with its cognate RNA target inside cells and overcomes the shortcomings of *in vitro* studies and previous *in vivo* techniques.

5.3 Materials and Methods

Plasmids construction.

Construct pECFP-hnH was obtained by cloning the hnRNP H coding sequence downstream the ECFP coding sequence in the vector pECFP-C3 (Clontech) or Cerulean. The construct pMS2-EYFP- was obtained by cloning the coding sequence for the MS2 coat protein upstream the EYFP gene in the pEYFP-N1 vector (Clontech). pRed-M1x and pRed-M4x were obtained by inserting either 1 or 4 MS2 coat protein binding sites (AAACAAGAGGATTACCCTTGT) into the 3' UTR of the vector pHC-Red-C1 (Clontech). pRed-M6x was obtained by inserting 6 MS2 coat protein binding sites derived from the construct pSL-MS2-6x donated by R.H. Singer (Albert Einstein College of Medicine). Vectors pRed-M4x-H5', pRed-M4x-H3' and pRed-M6x-H5' were obtained by inserting the double hnRNP H binding site GGGGAGGGGA 50 nt upstream (pRed-M4x-H5', pRed-M6x-H5') or downstream (pRed-M4x-H3') the MS2 binding sites. Vector pRed-M1x-H1x was obtained by inserting the single hnRNP H binding site GGGGA 10 nt upstream the MS2 binding site in pRed-M1x.

Cells and transfections.

HeLa cells were cultured in Dulbecco's modified Eagle medium supplemented with 10% fetal calf serum, penicillin and streptomycin (Gibco BRL). Cells were transfected with fluorescent protein-tagged constructs with Fugene HD (Roche) according to the manufacture's protocol. Cell were grown for 24–28h and fixed in 4% paraformaldehyde/PIPES (Sigma) for 10 min at room temperature. After rinsing with Mg–PBS (PBS supplemented with 10 mM Mg^{2+}) and water, cells were embedded in glycerol containing 2.5% 1,4-Diazabicyclo [2.2.2]octane (DABCO; Sigma Aldrich) as an antifade reagent.

Western blot analysis.

HeLa cells were transfected with the indicated plasmids and 24 hours later lysed in NP-40 buffer (50 mM Tris-HCl [pH 7.4], 150 mM KCl, 10% glycerol, 1% NP-40, 2 mM EDTA, 1 mM PMSF). The cell extract was denatured, separated on a 10% polyacrylamid gel and blotted to nitrocellulose membrane. hnRNP H was detected with a polyclonal antibody donated by D.Black (University of California at Los Angeles). MS2 coat protein was stained with a polyclonal antibody donated by Peter G. Stockley (University of Leeds). GFP variants were detected with the monoclonal antibody B-2 (SC-9996, Santa Cruz Biotech). The bands were visualized by chemiluminiscence of the peroxidase activity of a peroxidase-conjugated secondary antibody by using ECL.

RNA-affinity chromatography (RAC) assays.

Substrate RNAs for RAC were generated by PCR amplification of the sequences contained within the corresponding pRed 3'UTR. The 5' primer utilized for the amplification contained the minimal T7 promoter sequence. RNAs were synthesized utilizing T7 RNA polymerase. RNAs were covalently linked to adipic acid dihydrazide agarose beads as previously described (Caputi, Mayeda et al. 1999). The beads containing immobilized RNA were incubated in a reaction mixture containing HeLa extracts dialyzed in a final volume of 400 µl (20 mM HEPES-KOH pH 7.9, 5% Glycerol, 0.1 M KCl, 0.2 mM EDTA, 0.5 mM DTT, 4mM ATP, 4mM $MgCl_2$) for 1 hour at 30°C. HeLa extracts were obtained upon lysis of $4x10^5$ cells transfected with the indicated plasmids. Beads were then washed and the proteins specifically bound to the immobilized RNA eluted in 2% SDS, separated on polyacrylamide SDS-gels, electroblotted and probed with the indicated antibody.

Fluorescence resonance energy transfer.

FRET was measured by acceptor photobleaching method. FRET measurement was performed on the Leica TCS SP5 confocal microscope using the FRET acceptor photobleaching protocol (Leica). The HCX PL APO 63x/1,40-0,6 oil, Lbd Blue CS objective, 50 mW diode laser (405 nm) and 100mW Ar laser were used. The data acquisition was performed in 512x512 format with 400Hz scan speed and 1,6Airy pinhole in 16bit resolution. The gain of the photomultiplier detectors was adjusted to obtain the optimal dynamic range. The 405nm laser line with 5-10% of maximum power was used for CFP detection in wavelenght range 446-506nm. The laser line

514nm was used for YFP detection with 2% of laser intensity and YFP photobleaching with 30% of laser intensity in 3-5 consecutive scans. Detected wavelength range for YFP was 526-568nm. Minimal CFP bleaching (0–2%) was observed and was not taken into account for the calculation of FRET efficiency. The CFP fluorescence was measured before (CFP_{before}) and after (CFP_{after}) the YFP bleaching using Leica software (FRET photobleaching wizard) and apparent FRET efficiency directly without any background subtraction calculated according to the equation $FRET_{efficiency}[\%] = (CFP_{after} - CFP_{before}) \times 100/CFP_{after}$. A region in the nucleoplasm was bleached and FRET efficiency calculated as an average of the whole area. Values for all cells were averaged and standard error of the mean calculated. Unbleached region of the nucleoplasm of the given cell was used as a negative control. Average of unbleached regions were −10–0% for each pair tested. Number of analyzed cells is given in graphs.

Fluorescence lifetime imaging microscopy.

The FLIM was carried out according to (Wahl, Koberling et al. 2004) on a MicroTime 200 inverted epifluorescence scanning confocal microscope (Picoquant, Germany). The configuration contained a pulsed diode laser (LDH-P-C-440, 440 nm, Picoquant, Germany) providing 80 ps pulses at up to a 40 MHz repetition rate, a proper filter set (a clean up filter Z438/10, a dichroic mirror z440rdc, and a band-pass filter HQ480/40) (Chroma), a water immersion objective (1.2 NA, 60×) (Olympus), and two SPAD detectors (MPD, Italy) with polarization beam splitter. FWHM of the overall IRF is 300 ps. Data acquisition was performed in TTTR mode, an advanced mode of TCSPC. The data were acquired and analyzed in SymphoTime200 software (Picoquant, Germany). A pixel size was 100 x100 nm, time per pixel 1,2 ms and the size of the image varied between 100 – 200 pixels per dimension depending on the imaged cell size. Under the used average intensity of 2 μW at the back aperture of the objective each pixel of selected ROI contained between 500 to 1500 photons, fulfilling the TCSPC condition for maximum countrate (max. 5% of laser repetition rate). The TCSPC histograms were a priori corrected for anisotropy effect by proper summing of signals from two SPADs with orthogonal polarizations. The average lifetime for selected ROI was determined by tail-fitting of the overall TCSPC histogram (cca. 10^7 photons). The FLIM images were prior analysis binned 2x2 and analyzed by tail-fitting FLIM approach using two exponentiels. The presented average lifetime is an intensity weighted average of both

contributions. The mean and standard error of the mean of the average lifetimes were determined. Number of assayed cells is given in graphs.

5.4 Results

Our basic experimental approach we carried out is summarized in Figure 5.1. The RNA binding protein of interest is tagged with an enhanced cyan fluorescent protein (ECFP) and utilized as FRET donor, while the bacteriophage MS2 coat protein is tagged with the enhanced yellow fluorescent protein (EYFP) and utilized as FRET acceptor. A target RNA containing the binding site for the protein of interest in the proximity of the high affinity MS2 RNA-operator is generated by a third construct. Upon simultaneous binding of the protein of interest-ECFP and MS2-EYFP fusion protein to the target RNA proximity of the acceptor ECFP and the acceptor EYFP will result in FRET.

Utilizing the outlined strategy we analyzed the binding of hnRNP H to its putative RNA binding site. The hnRNP H was tagged at its NH2 terminus with ECFP obtaining the clone pECFP-hnH (Fig. 5.2.A), while the bacteriophage MS2 coat protein gene was tagged at its COOH terminus with EYFP (pMS2-EYFP). Expression of the fusion proteins ECFP-hnH and MS2-EYFP was confirmed by western blot analysis of the lysates from HeLa cells transfected with the pECFP-hnH and pMS2-EYFP constructs (Fig. 5.2.B). Antibodies against hnRNP H, MS2 and ECFP/EYFP indicated that the fusion proteins were properly expressed.

Next we obtained a series of constructs expressing mRNA substrates carrying the binding sites for hnRNP H and the MS2 coat protein by inserting either one or two copies of the high affinity hnRNP H binding site (GGGGA) (Schaub, Lopez et al. 2007) in proximity of 1, 4 or 6 copies of the sequence-specific stem loop recognized by the MS2 coat protein (Fig. 5.2.A, pRed vector series). The binding sites separated by a 50 nt spacer sequence were inserted within the 3' UTR of the HcRed1 gene. Expression of the HcRed1 gene allowed for control of expression of the target mRNA.

To show that the ECFP-hnH and MS2-EYFP fusion proteins can be efficiently recruited onto the target RNAs *in vitro* we utilized an RNA affinity chromatography (RAC) technique that allows for efficient detection of RNA-protein interactions in complete cell extracts. RNA substrates containing the sequences within the 3' UTR of

the pRed-M4x-H3' and pRed-M4x constructs and a control sequence derived from the parental pHcRed1-C1 vector were synthesized in vitro (Fig. 5.3.A). RNAs were than incubated with total extracts from HeLa cells transfected with pMS2-EYFP, pECFP-hnH or the combination of the two. Proteins specifically bound to the bait RNAs were than eluted and analyzed by western blotting. Western blot analysis of the eluate shows that both endogenous hnRNP H and the fusion protein ECFP-hnH are recruited by the M4x-H3' RNA, containing both the MS2 coat protein and the hnRNP H consensus binding site (Fig. 5.3.B lanes 2-4). The RNA substrate carrying only the MS2 coat protein binding sites showed a lower affinity for both the ECFP-hnH fusion protein and the endogenous hnRNP H (Fig. 5.3.B lanes 5-8). The MS2-EYFP fusion protein was efficiently recruited by the substrates containing the MS2 coat protein RNA binding sites (lanes 3,4,7,8). The control RNA sequence (RNA_Cont) exhibited only a residual affinity for the fusion proteins present in the cell extracts, this was likely due to the low stringency washing steps utilized in the elution process.

Next we tested the ability of RNA-binding mediated FRET (RB-FRET) to generate efficient FRET signals between the ECFP-hnH donor and the MS2-EYFP acceptor when the two molecules were brought in proximity by their association to their target RNA sequences. HeLa cells were co-transfected with pMS2-EYFP, pECFP-hnH and the indicated pRed vector (Fig. 5.4.). Expression of the transfected plasmids was monitored by visualizing the ECFP, EYFP and HcRed1 tags (Fig. 5.4.A). FRET signals between ECFP-hnH and MS2-EYFP pairs were measured by the acceptor photobleaching method that relies on detection of quenched donor fluorophores (Bastiaens, Majoul et al. 1996; Karpova, Baumann et al. 2003). FRET was detected as an increase of the donor (ECFP) fluorescence after acceptor (EYFP) photodestruction (Fig. 5.4.A). As a positive control for FRET efficiency, we examined the Cajal body-specific protein p80 coilin, which has previously been shown to interact with itself both *in vitro* and *in vivo* (Hebert and Matera 2000) The coilin NH2 terminus was tagged with either ECFP or EYFP (ECFP-p80, EYFP-p80) and pairs of tagged variants were co-expressed in HeLa cells (Fig. 5.4.B). FRET efficiency between MS2-EYFP/ECFP-hnH correlated with expression of substrate RNA containing both MS2 and hnRNP H binding sites and was comparable to the coilin positive control. FRET signal was significantly lower when MS2-EYFP/ ECFP-hnH were co-expressed with a RNA substrate containing MS2 binding sites but no high affinity hnRNP H binding sites. In addition, only a marginal increase of ECFP fluorescence was observed when the YFP

acceptor was omitted. These results indicate that FRET is strictly dependent on the binding of the tagged hnRNP H to its RNA target. Thus, RB-FRET can efficiently measure binding of the hnRNP H and MS2 tagged proteins to their respective binding sites within the target RNA.

Next we confirmed the FRET measurements obtained via acceptor photobleaching utilizing fluorescence lifetime imaging microscopy (FLIM). The FLIM-FRET approach is robust, quantitative and less sensitive to artifacts with respect to concentration of fluorophores. FLIM estimates FRET efficiency by measuring the donor fluorescence lifetime, which shortens in the presence of an acceptor fluorophore. Thus, the more FRET, the greater reduction in the donor lifetime. Co-expression of the pECFP-p80/pEYFP-p80 pair positive control (Fig. 5.5.A and 5.5.C) showed a strong decrease in lifetime of the donor with respect to the expression of pECFP-p80 alone (Fig. 5.5.A, 5.5.C and supplementary table 5.1.). Similarly, in the RB-FRET assay expression of pRed-M4x-H3' (2.88 ns), pRed-M4x-H-5' (2.75 ns) or pRed-M6x-H5' (2.65 ns) caused a decrease in fluorescence lifetime of the donor ECFP-hnH with respect to the expression of the control substrate pRed-M4x (2.98 ns; Fig. 5.5.B, 5.5.C and supplementary table 5.1.). Alternatively, the fluorescent protein Cerulean was used as a donor (Rizzo, Springer et al. 2004) and FRET measured by FLIM as previously. Similar results were obtained for CFP/YFP and Cerulean/YFP FRET pairs (Fig. 5.5.C, 5.6.B and supplementary table 5.1.). In addition, similar lifetime decrease was observed when the pRed-M1x-H1x substrate with only one of each binding sites was used (Fig. 5.6.B and supplementary table 5.1.). These data confirmed the results obtained using the acceptor-photobleaching method, thus validating this novel approach for the analysis of RNA-protein interactions *in situ*.

5.5 Discussion

The post-transcriptional processing and regulation of RNAs are key mechanisms in the control of gene expression. So far biochemical studies have not elucidated the complex set of interactions that govern the association of RNA and proteins and could not provide spatial and temporal information about where and when they occur within the cellular environment. Furthermore, recent work uncovered the multifaceted nature of the different mechanisms regulating the processing and the expression of cellular

mRNAs, suggesting that such events are intimately coupled and need to be studied within a functional cellular environment to be fully understood.

The RB-FRET method described here enables the detection and localization of RNA-protein interactions within cells and is specifically useful for studying RNA binding proteins with known RNA target sequence. As the RNAs and proteins studied can be expressed within a living cell, both the physical and biological properties of these complexes can be faithfully investigated. Furthermore, the tagged RNA binding protein studied is expressed at physiological relevant levels. Indeed, endogenous and tagged hnRNP H are expressed in comparable amounts (Fig. 5.3.B), indicating that this technique allows for the detection of interactions when components are expressed at low, physiologically relevant levels. The ability to study RNA-protein interactions inside cells enables the identification those interactions that are likely to be biologically relevant from those that are not, a limitation of *in vitro* assays. In this case, although hnRNP H binding to the high affinity binding site (GGGGA) had been reported in vitro (Schaub, Lopez et al. 2007) it is unclear if this interaction happens *in vivo*, since the mutation of only a few of the numerous hnRNP H binding sites predicted within a given pre-mRNA appears to affect its splicing.

Trimolecular fluorescence complementation (TriFC) has been recently utilized to detect RNA-protein interaction in live cells (Rackham and Brown 2004). In this approach the MS2 coat protein and the protein of interest are fused to two complementary portions of the Venus fluorescent protein. Binding of the two fusion proteins to a substrate RNA containing the RNA sequence of interest and the MS2 binding site allows for the two portions of Venus to come in close proximity and generate a fluorescent complex. Although this method is able to detect RNA-protein interactions *in situ* its major pitfall is the permanent cross-link beween the studied RNA-binding protein, MS2–protein and likely the target RNA. In addition, the maturation of BiFC protein after formation of the protein-protein complex takes a considerable amount of time (Hu, Chinenov et al. 2002). Therefore, temporal and spatial regulation in response to physiological events cannot be observed with this method. Our technique overcomes these limitations since FRET is generated by close proximity between the donor and acceptor molecule and no stable complex is formed; furthermore, there is no lag time for the formation of the interaction. This allows for the characterization of interactions over time and in response to intra-cellular signals.

Utilizing YFP tagged RNA binding proteins and SytoxOrange stained cellular RNA, Lorenz has recently utilized FRET-FLIM to detect the dynamic, temporal, spatial regulation of the binding of the RNA binding protein of interest to cellular RNA (Lorenz 2009). Since SytoxOrange labels indiscriminately the RNA within the cell this technique cannot determine if the RNA binding protein studied is able to associate with the RNA sequence of interest. On the contrary, our methodology generates FRET only if the protein studied interacts with a specific substrate RNA. In summary, RB-FRET can determine RNA-proteins interactions in living cells with high temporal and spatial resolution, allowing for the detection of the specific interaction between a known RNA binding protein with a RNA sequence of interest.

Figures and tables to chapter 5:

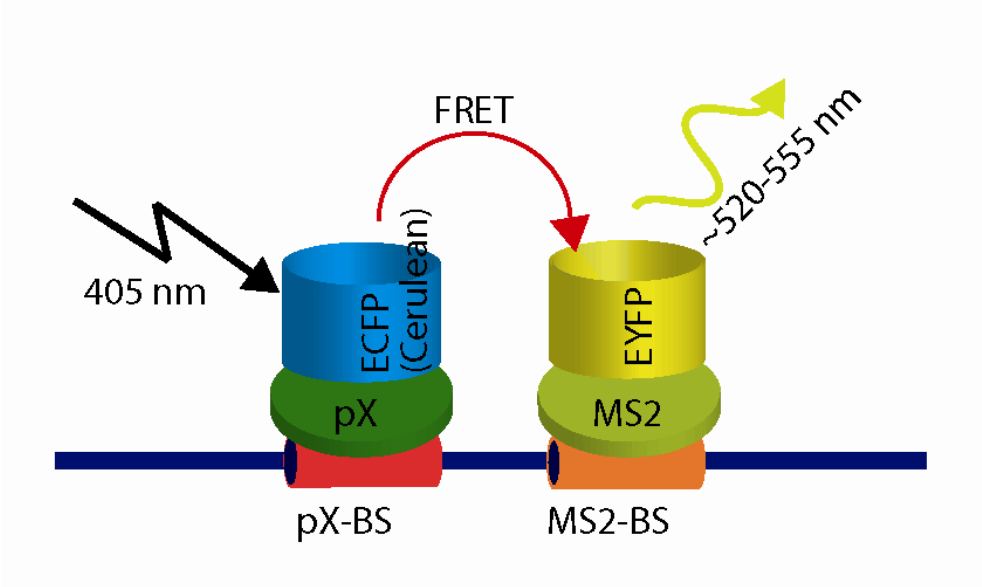

Figure 5.1. Schematic representation of the strategy utilized to visualize RNA-protein interaction inside cells.

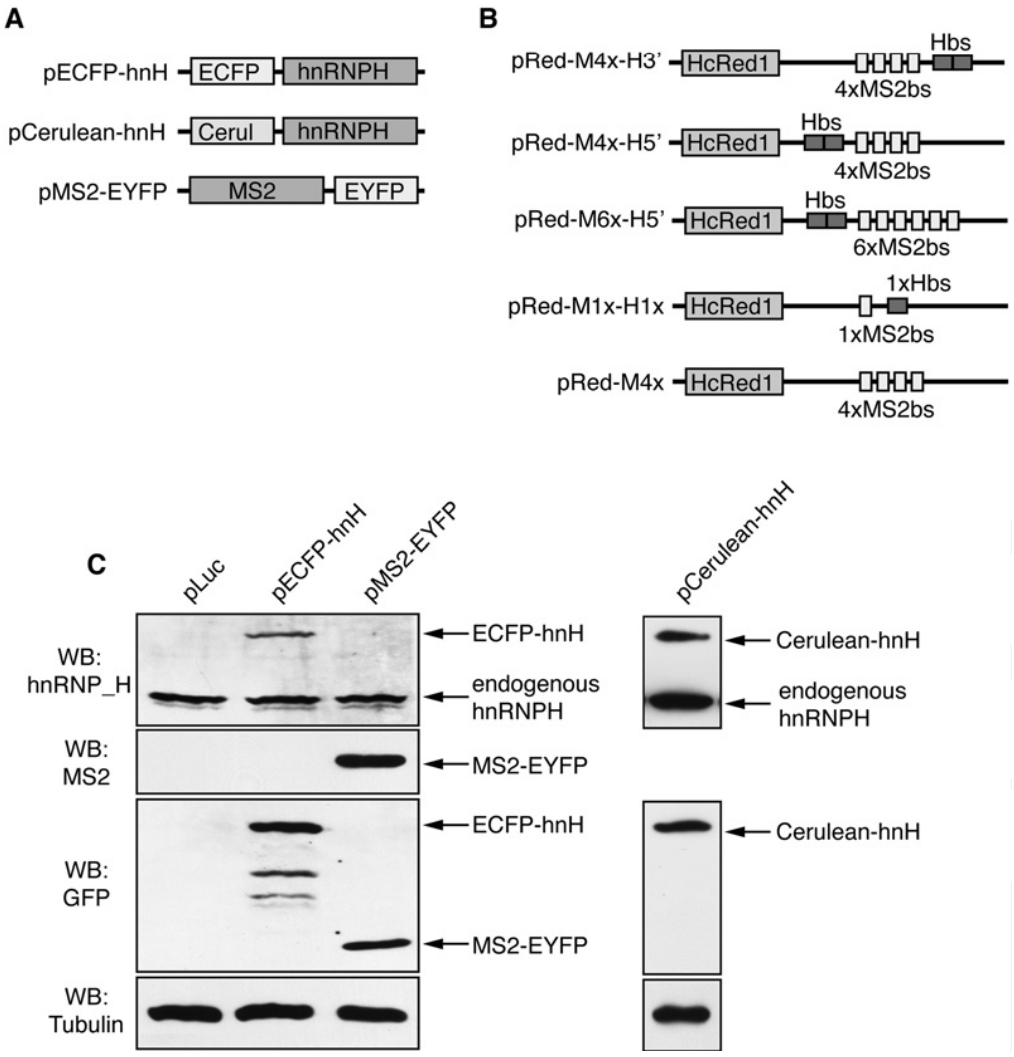

Figure 5.2. Validation of vector expression utilized in this study. A/ Schematic representation of the protein expression vectors utilized in the study. B/ Schematic representation of the constructs generating RNA substrates utilized in the study. C/ Expression of the key fusion proteins utilized in the study. HeLa cells were transfected the indicated expression plasmid (top). The total cell lysates were analyzed by western blot with the indicated antibody. Identity of the various fusion proteins is indicated on the right. Endogenous hnRNP H is also marked.

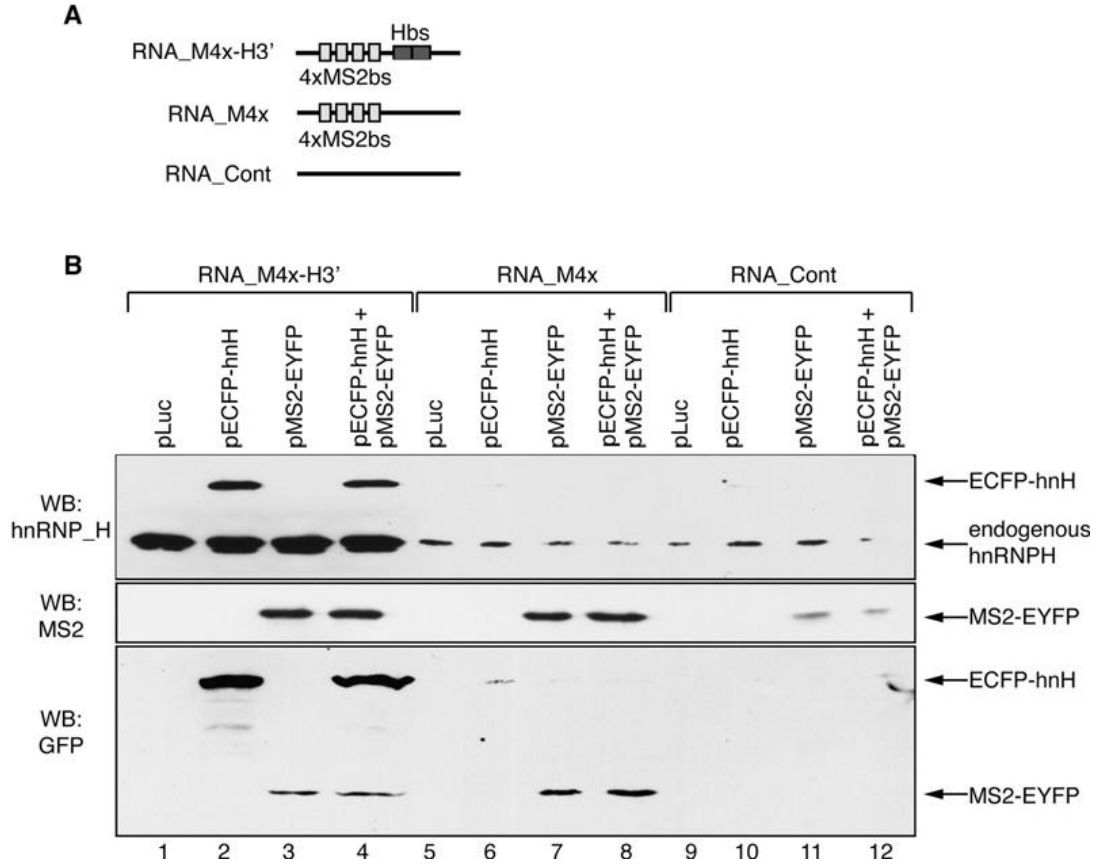

Figure 5.3. The fusion proteins specifically bind their target RNA *in-vitro*. A/ Schematic representation of the RNA substrates utilized in the RNA affinity chromatography (RAC) assay. B/ Analysis of the fusion proteins bound to the substrate RNAs by RAC. The substrates schematically represented in A were covalently linked to agarose beads and incubated in extracts derived from HeLa cells transfected with the indicated plasmids (top of the figure). Proteins bound to the substrates were eluted and immunoblotted with the indicated antibodies. Identity of the various fusion proteins is indicated on the right.

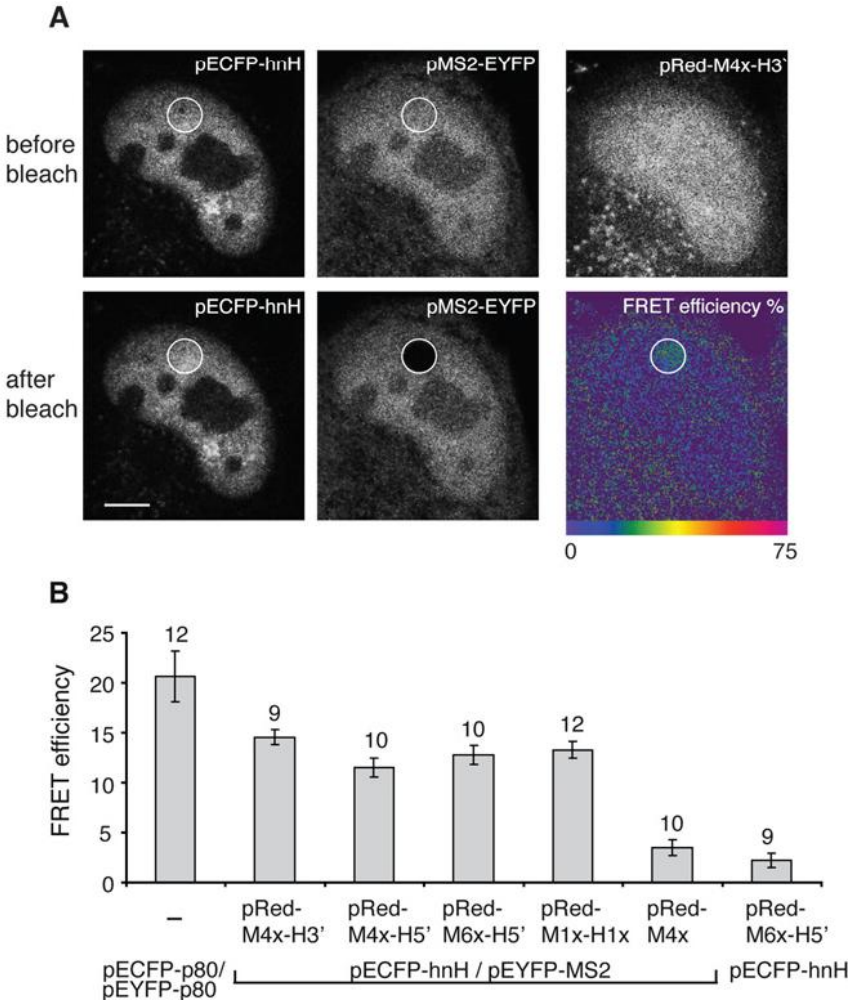

Figure 5.4. Detection of hnRNP H binding to its RNA binding site by FRET. A/ ECFP tagged hnRNP H (ECFP-hnH) and EYFP tagged MS2 (MS2-EYFP) proteins were co-expressed with HcRed1 containing MS2 and hnRNP H binding sites within its 3' UTR. Each protein tag was imaged and visualized as indicated in each panel. EYFP was photobleached in a specific region (circled) and FRET efficiency measured as an increase of ECFP fluorescence after EYFP photodestruction. Bars 5 μm. B/ Quantification of FRET between ECFP-hnRH and MS2-EYFP co-expressed with different RNA binding targets. FRET between ECFP-p80 and EYFP-p80 served as a positive control and co-expression of target RNA containing only MS2 biding sites (pRed-M4x) as a negative control. Cells expressing RNA with both target sequences (pRed-M6x-H5') and ECFP-hnH only were analyzed as additional negative control. The average and SEM are shown and number of assayed cells indicated above bars.

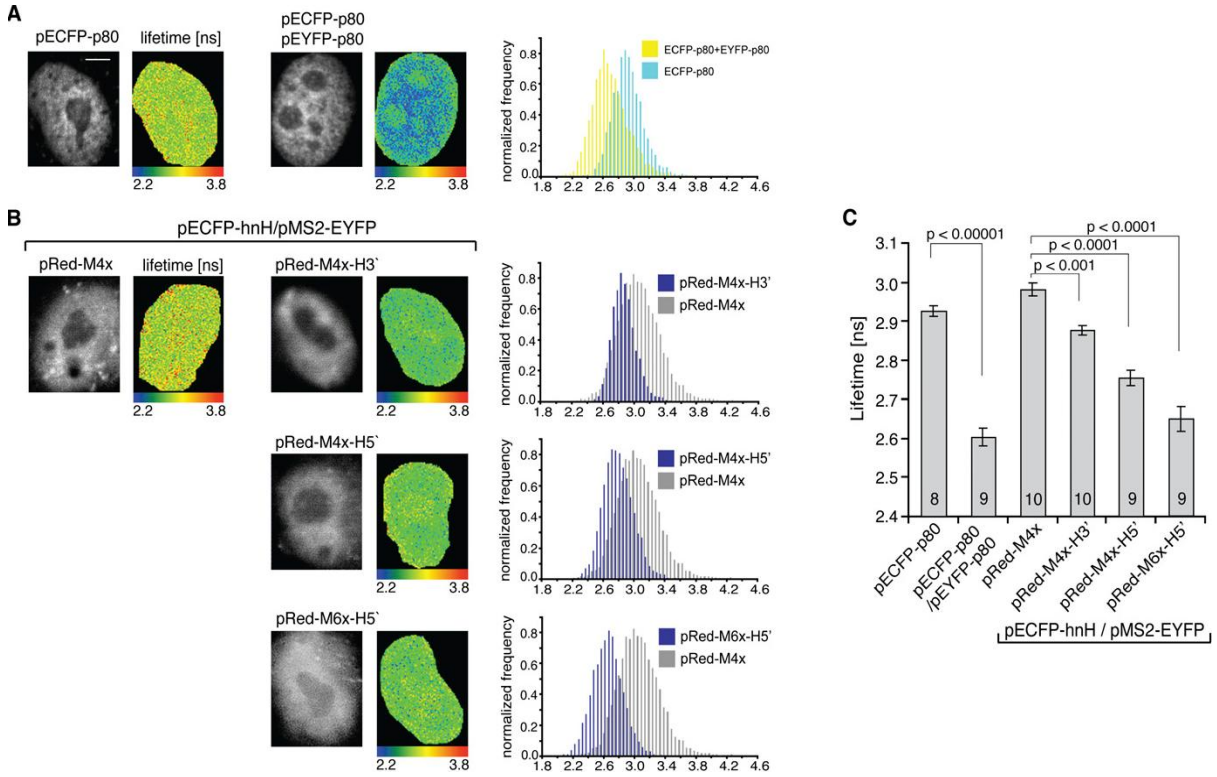

Figure 5.5. Binding of ECFP- hnH to its RNA binding site by FRET-FLIM *in situ*. A/ Lifetime of ECFP fluorescence was measured for ECFP-p80 as a negative control and ECFP-p80 co-expressed with EYFP-p80 as a positive control. Lifetimes within cells are shown in false colors: blue - short lifetime, red - long lifetime. Notice shortening of ECFP fluorescence lifetime, which is indicative of FRET. B/ ECFP-hnH and MS2-EYFP were co-expressed with constructs containing different binding sites and ECFP fluorescence lifetime was measured for each construct. pRed-M4x served as a negative control. ECFP fluorescence, lifetime heat-maps and histograms of lifetime distributions are shown. C/ Quantification of lifetimes shown in A and B. Decrease of lifetimes indicates FRET between ECFP and EYFP constructs. The average and SEM are shown and number of assayed cells indicated within bars.

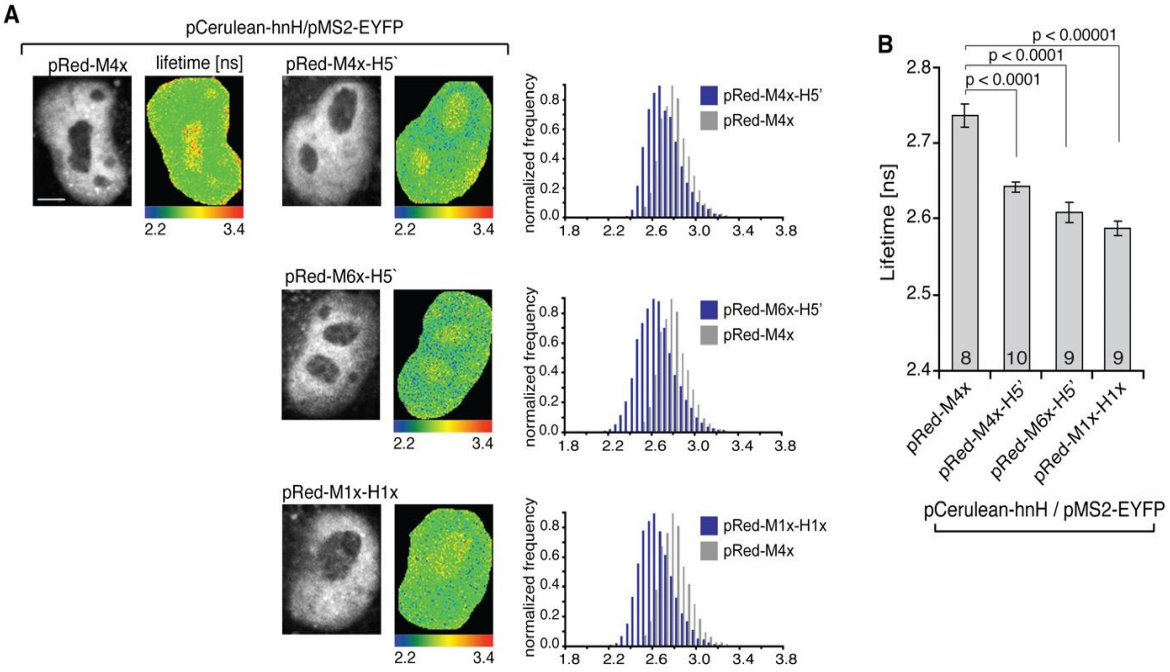

Figure 5.6. Quantification of lifetimes using Cerulean instead of ECFP as a FRET donor. A/ Cerulean-hnH and MS2-EYFP were co-expressed with constructs containing different binding sites and Cerulean fluorescence lifetime was measured for each construct. pRed-M4x served as a negative control. Cerulean fluorescence, lifetime heat-maps and histograms of lifetime distributions are shown. B/ Quantification of lifetimes shown in A. Decrease of lifetimes indicates FRET between Cerulean and EYFP constructs. The average and SEM are shown and number of assayed cells indicated within bars.

Values for the assays in Figure 5												
	ECFP		ECFP-p80/EYFP-p80		M4x/ECFP-hnH/EYFP-MS2		M4x-H3′/ECFP-hnH/EYFP-MS2		M4x-H5′/ECFP-hnH/EYFP-MS2		M6x-H5′/ECFP-hnH/EYFP-MS2	
	Mean	SD	Mean	SD	Mean	SD	Mean	SD	Mean	SD	Mean	SD
tau1	3.35	±0.10	2.89	±0.05	3.49	±0.08	3.28	±0.07	3.27	±0.06	3.13	±0.10
tau2	1.58	±0.13	1.62	±0.06	1.57	±0.08	1.43	±0.05	1.39	±0.08	1.37	±0.06
x1	0.75	±0.03	0.77	±0.01	0.73	±0.02	0.78	±0.03	0.73	±0.04	0.72	±0.03
Mean tau	2.92	±0.04	2.60	±0.07	2.98	±0.05	2.88	±0.04	2.75	±0.06	2.65	±0.10

Values for the assays in Figure 6								
	M4x/Cerul-hnH/EYFP-MS2		M6x-H5′/Cerul-hnH/EYFP-MS2		M4x-H5′/Cerul-hnH/EYFP-MS2		M1x-H1x/Cerul-hnH/EYFP-MS2	
	Mean	SD	Mean	SD	Mean	SD	Mean	SD
tau1	3.13	±0.03	3.00	±0.06	3.06	±0.02	2.97	±0.10
tau2	1.26	±0.05	1.29	±0.03	1.25	±0.03	1.29	±0.06
x1	0.79	±0.01	0.77	±0.01	0.77	±0.01	0.77	±0.00
Mean tau	2.74	±0.04	2.61	±0.04	2.64	±0.02	2.59	±0.03

Table 5.1. Summary of the fit parametres from the biexponential fits of lifetime histograms using Cerulean and ECFP as a FRET donor in Fig. 5.5 and 5.6.. Shown are mean values and their standard errors of mean from multiple measurements for individual lifetimes tau1, tau2 and average lifetime, which is an intensity weighted average of both contributions (x1 is the relative amplitude contribution of tau1).

CHAPTER 6

General Discussion

In this thesis I presented results that contribute to understanding the dynamic behaviour and assembly of the spliceosomal complexes in the context of the cell nucleus. I showed how the disease linked mutation in a particular splicing factor affects the dynamic interactions between the spliceosomal subcomplexes. In addition, I introduced a novel method for studying RNA-protein interactions in living cells. The results were separately described and discussed in chapter 2, 3, 4, and 5.

Mature splicing machinery is exclusively restricted to the cell nucleus, where the pre-mRNA processing takes place. Here snRNPs localize to three distinct compartments: the nucleoplasm, the splicing factor compartments (SFC) and the Cajal bodies (CB). These nuclear structures are dynamic and reflect diverse processes occuring throughtout the snRNPs life-span. While in the nucleoplasm snRNPs carry out splicing, those snRNPs that are not involved in splicing are localized to splicing factor compartments or „speckles“ (Lamond and Spector 2003). Cajal bodies host the snRNP biogenesis and final steps of maturation (Will and Luhrmann 2001; Jady, Darzacq et al. 2003) and also serve as an assembly station for U2 snRNP, U4/U6 di-snRNP and U4/U6 tri-snRNP (Nesic, Tanackovic et al. 2004; Schaffert, Hossbach et al. 2004; Stanek and Neugebauer 2004).

The pre-mRNA splicing is accomplished by the dynamic network of snRNPs within spliceosome. Once the intron is defined by interactions of U1 and U2 snRNPs, the pre-assembled U4/U6.U5 tri-snRNP joins this complex and after extensive rearrangements the active spliceosome core is generated (Wahl, Will et al. 2009). Recently two models of spliceosome assembly were proposed based mostly on *in vitro* approches (reviewed in (Rino and Carmo-Fonseca 2009)). One model proposes a step-wise assembly of the spliceosome exerted by sequential association and dissociation of snRNPs with pre-mRNA, while the second one proposes that spliceosome is already a pre-assembled complex and in the form of `penta-snRNP` associates with pre-mRNA to promote splicing.

In this thesis I addressed the question how the spliceosome assembles *in vivo* by analysing and quantifying snRNP interactions with pre-mRNA. The dynamic behaviour of snRNPs in the nucleoplasm reflects their splicing activity and so is determined by their diffusion and interactions with pre-mRNA. Inhibition of transcription leads to relocalization of snRNPs to speckles implying that inactive snRNPs are stored to these structures. The fraction of snRNPs that remained in the nucleoplasm showed faster movement which indicated a lack of a substrate to bind. Similarly faster movement of several splicing factors due to transcription inhibition was already reported (Rino, Carvalho et al. 2007). This movement is characterized as an effective diffusion, because even in the absence of pre-mRNA the snRNPs scan and transiently interact with the nuclear environment (Phair and Misteli 2001). I quantified diffusion rates describing snRNPs effective diffusion ranging between 0.2 - 0.8 $\mu m^2 s^{-1}$. These values are approximately 100 times lower that the diffusion of free GFP emphasizing the strenght of the snRNP transient interactions, which also goes together with the conception of stochastic view of spliceosome assembly suggested previouly (Rino, Carvalho et al. 2007). This model assumes that the snRNPs move randomly throughout the nucleus and when necessary they assemble the spliceosome and promote splicing.

While measurements performed after transcription inhibition provide an information about snRNPs movement, it does not answer the question how the spliceosome assembles on the pre-mRNA. Here, I quantified the interactions of individual snRNPs with pre-mRNA in cells with ongoing transcription. The strenght of a particular interaction is characterized by the dissociation constant, which specifies the time the snRNP is bound to the pre-mRNA and released afterwards – the residence time. I found that U1 and U4/U6 snRNPs stay bound to the pre-mRNA around 1s, but U2 and U5 snRNPs associated with pre-mRNA at least 10 times longer, approximately tens of seconds. Thus, these differantial interactions between snRNPs and pre-mRNA let me assume that snRNPs interact with pre-mRNA independently, which supports the step-wise model of spliceosome assembly.

Importantly, the residence time of the core spliceosomal components U2 and U5 snRNPs provided me also the estimate of an average splicing rate, as the aforementioned 12-30s reflect the time the U2 and U5 snRNPs stay associated with pre-mRNA till it is spliced. Taking into account the average RNA polymerase II synthesis rate (~ 4kb per minute), 30 seconds would be enough to generate one exon (~ 200-300bp) or intron (~ 1000bp and more), which would be spliced within this time period

supporting the co-transcriptional pre-mRNA splicing (Neugebauer 2002; Singh and Padgett 2009). This data are consistent with previous studies from Miller spreads from Drosophila embryos and ChIP data from yeast, where both show that splicing is accomplished within a minute after spliceosome formation (Beyer and Osheim 1988; Wetterberg, Zhao et al. 2001; Gornemann, Kotovic et al. 2005). Conclusivelly, I showed that individual snRNPs and pre-assembled snRNPs move throughout the nucleoplasm and in an ordered pathway assemble the spliceosome, which likely allows to accomodate many regulatory events to control the process of pre-mRNA splicing.

When the spliceosome carries out splicing, it is disassembled by assistance of hPrp22 and the hPrp43/Ntr1/Ntr2 complex (Company, Arenas et al. 1991; Arenas and Abelson 1997; Tsai, Tseng et al. 2007). It has not been shown so far, what happens with the disassembled U2, U5 and U6 snRNPs. In addition, snRNPs dissociate from the RNA substrate independently (discussed above) and three of them U4, U5 and U6 must be re-assembled again into the tri-snRNP to participate in the splicing process, which implies for possible recycling events in the snRNP lifecycle.

In this thesis I presented a study showing an additional „recycling“ role for CBs in the snRNP metabolism pathway. As mentioned at the beginning, CBs are the sites of snRNPs biogenesis and maturation. There are two to four CBs per one cell and it was reported that the size and number of CBs depend on the cell metabolic activity and cell cycle (Andrade, Tan et al. 1993; Boudonck, Dolan et al. 1998). It was shown that snRNPs do not accumulate in CBs, when transcription or splicing is inhibited (Carmo-Fonseca, Pepperkok et al. 1992; Kaida, Motoyoshi et al. 2007), which was consistent with our data showing that CBs accomodate also mature snRNPs and that these snRNPs rapidly exchange between them. This raised a question, why the recruitment of snRNPs to CBs depends on ongoing transcription. Probably, the cycling of snRNPs through CBs could reflect snRNPs reassembly after pre-mRNA splicing. I inhibited spliceosome disassembly by depleting cells of hPrp22 or Ntr1, which resulted in accumulation of U4/U6 di-snRNP and decreased levels of U5 snRNP in CBs implying for impaired tri-snRNP formation, fenotype recently demonstrated by depleting either of hPrp31 and hPrp6 proteins (Schaffert, Hossbach et al. 2004). The impaired formation of tri-snRNP likely reflected the lack of U5 snRNP, which might be entrapped in the stalled post-spliceosomal complexes (Turner, Norman et al. 2004). The fact that di-snRNP is still formed in CBs is the result of high levels of U6 snRNPs present in the cell and fast dissociation of U4 snRNP from pre-mRNA during splicing (mentioned above). Thus,

the nuclear CBs serve as the major sites of repeated di-snRNP and tri-snRNP reassembly throughout the snRNPs life-span (Fig. 6.1.).

Surprisingly, the basal tri-snRNP metabolism seems to have an important role in development of such a specific disease like retinitis pigmentosa (RP), which affects only rod cells in eye retina. Although it is a heterogenous disease and many mutations are located in retina metabolism linked genes, mutations in tri-snRNP specific proteins were discovered to initiate this disease, too. In this thesis, I present results showing how the AD29 (A216P) mutant variant of hPrp31 protein affects tri-snRNP metabolism and possibly causes the RP. We expressed AD29 in cells and found that the cell proliferation was reduced. Beside its nuclear localization, this protein was also present in cytoplasm, which was similar to A194E mutant form of the hPrp31 protein (Deery, Vithana et al. 2002). Unlike the wildtype U4/U6 snRNP specific proteins, AD29 was only little accumulated in CBs suggesting its inability to be incorporated into U4/U6 di-snRNP based on the results discussed above. We confirmed that interactions between AD29 and U4/U6 snRNP specific proteins were reduced. Interestingly, interactions with U5 specific proteins Snu114 and hPrp6 were stronger and this stronger interaction of AD29 and hPrp6 was previously shown also *in vitro* (Wilkie, Vaclavik et al. 2008). AD29 likely inhibits tri-snRNP assembly by retaining U5 snRNP and preventing its association with U4/U6 di-snRNP. Overexpression of hPrp6 in AD29 cells compensated the AD29 induced phenotype and resulted in rescue of CBs morphology and increased cell proliferation rate.

The rapid degradation of AD29 raises a question how this protein initiates the disease. Is it the hPrp31 insufficiency, which is consistent with studies showing that also deletions in hPrp31 and destabilizing mutation cause RP (Abu-Safieh, Vithana et al. 2006; Rio Frio, Wade et al. 2008). Or is the AD29 function specific only in retina cells, where the efficiency of hPrp6 compensation could play a role. Neither AD29 nor other mutant forms of the tri-snRNP specific proteins were linked to decreased splicing efficiency in model cell systems (Deery, Vithana et al. 2002; Wilkie, Vaclavik et al. 2008), which suggests that their cytotoxicity may only be exerted specifically in retina rod cells. Here, the signal transduction system, mainly the flexuous membrane with embedded rhodopsin undergoes constant renewal and this puts a substantial demand on the splicing machinery. This suggestion goes together with the fact, that also the mutations in retina specific proteins cause RP and calls for experiments in animal models. However, recent study showed no RP degenerative phenotype in heterozygous

knock-in mouse Prp31 (A216P/+) carrying the AD29 mutation (Bujakowska, Maubaret et al. 2009), therefore further investigation is required to elucidate the molecular mechanisms of RP development.

Future experiments should involve detailed analysis of AD29 interaction with U4/U6 and U5 snRNPs. Particularly the AD29-hPrp6 and AD29-SART3 interactions need to be resolved. It is not clear, whether AD29 and hPrp6 form AD29-U5 snRNP complex, albeit U5 snRNP specific protein hSnu114 was also detected in the AD29 precipitate. Additionally, AD29 was shown to interact with U4/U6 di-snRNP *in situ* (interaction with SART3 measured by FRET, Fig. 4.3.B), however, we did not pull-down with AD29 neither hPrp3 nor hPrp4 (U4/U6 di-snRNP specific proteins). Thus, it is of importance to examine also the interactions between AD29 and U5, U4 and U6 snRNAs. As the fast degradation of AD29 could make the complexes sensitive for any *in vitro* analysis, we need an aproach, which would enable us to vizualize RNA-protein interactions *in vivo*.

In this thesis I present a study employing the FRET based method (RB FRET) for studying RNA-protein interactions *in situ*. I tested RB-FRET approach on the previously shown interaction of hnRNP H protein with its cognate RNA sequence and confirmed that *in vitro* interaction happens also *in situ* (Schaub, Lopez et al. 2007). I tagged hnRNP H protein with CFP and the RNA sequence with YFP using the MS2 system, which is an elegant tool for RNA labeling (Querido and Chartrand 2008). This approach allows to examine interactions over time and in response to cellular signals. The previously shown trimolecular fluorescence complementation assay (TriFC) also allows for RNA-protein interactions *in vivo* (Hu, Chinenov et al. 2002), however lacks the temporal resolution because of the permanent cross-link among the tagged molecules and the time needed for the maturation of the fluorescent protein. Another recently presented work studying RNA-protein interactions employed the FRET-FLIM approach and introduced RNA labeling with SytoxOrange (Lorenz 2009). Since SytoxOrange labels all RNA within the cell, using this methods we cannot determine the direct target RNA sequence of the studied protein. As the RNA-protein interactions rule almost all cellular processes, like transcription, splicing, translation, RNA editing, iRNA, etc., my technique allows for labeling of a particular RNA sequence and a particular protein of interest, and detect the RNA-protein interaction *in vivo* with high temporal and spatial resolution.

Figures to chapter 6:

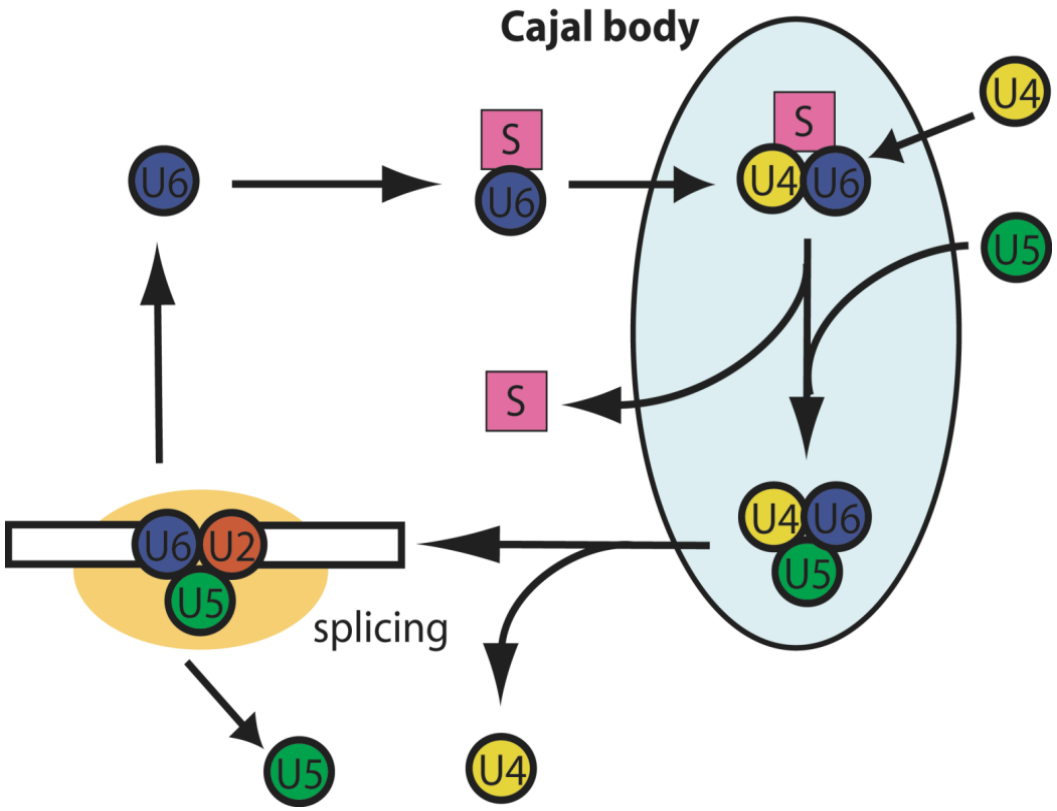

Figure 6.1. Recycling of spliceosomal snRNPs. In Cajal bodies, SART3 (S) promotes U4 and U6 snRNAs annealing (U4/U6 di-snRNP assembly) and moves away upon binding of U5 snRNP. The mature U4/U6.U5 tri-snRNP is released from the Cajal body into the nucleoplasm and participates in pre-mRNA splicing. U4 snRNP is released and U5 and U6 snRNPs form together with U2 snRNP the active spliceosome. U6 and U5 snRNPs are released from the postspliceosomal complex and go to Cajal bodies to enter again the pathway of di- and tri-snRNP assembly.

Conclusions

Following conclusions were reached in Chapter 2:

- In contrast to previous studies that viewed CBs as sites of newly synthetized snRNP accumulation we showed that CBs consist mainly of mature snRNPs.

- We showed that snRNPs constantly cycle between CBs. We photoactivated SmD1-PA-GFP or SmB-PA-GFP in one CB and observed rapid accumulation of fluorescence in the other CBs. Co-transfection with CB markers SART3 or coilin was performed to properly localize CBs.

- We demonstrated that CBs are the sites of snRNP recycling and repeated tri-snRNP formation. Inhibition of spliceosome disassembly resulted in accumulation of U4/U6 di-snRNP components in CBs reflecting the lack of U5 snRNP stalled in post-spliceosomal complexes.

- We demonstrated that continuous snRNPs cycling is important for maintaining the CB structure. Inhibition of spliceosome disassembly resulted in CBs enlargement due to U4/U6 di-snRNP accumulation.

Following conclusions were reached in Chapter 3:

- GFP-tagged snRNP specific proteins expressed from recombineered BACs are properly incorporated into snRNPs.

- FCS measurements revealed diffusion properties of snRNPs mobile fraction. We found that snRNPs diffuse throught nucleoplasm with comparable diffusion times and that this movement is not affected by interactions with pre-mRNA.

- Quantification of FRAP curves obtained from untreated cells revealed differential interaction of snRNPs with pre-mRNA and supported ordered model of spliceosome assembly.

- Based on residence times of individual snRNPs on pre-mRNA we estimated average splicing rate in living cells (approximately 30s) and found that not the intron recognition, but the splicing reaction is the rate limiting step of pre-mRNA splicing process.

- Inhibition of splicing with isoginkgetin compound increased levels of pre-spliceosomal complex A (containing U1 and U2 snRNPs) and revealed their higher residence time on pre-mRNA, which clarified the proper use of k_{off} value for description of snRNPs interaction with pre-mRNA.

- Employing snRNA co-immunoprecipitation we found that spliceosome as well as di-snRNP and tri-snRNP integrity depends on ongoing transcription and splicing.

- Employing FRAP we found that snRNPs interact independently also with transcripts in a specific gene loci further supporting the step-wise assembly model of the spliceosome.

Following conclusions were reached in Chapter 4:

- We compared the growth rate of the WT31 and AD29 cell lines and found that AD29 has a dominant negative effect on cell proliferation. AD29 cell line divided 10% slower compared to WT31.

- We analysed CBs integrity and found that CBs are smaller or even disappear in AD29 cell line. We showed reduced localization of U4/U6 di-snRNP in AD29 cell line, whereas localization of U5 and U2 snRNPs stayed unchanged.

- We employed FRET and immunoprecipitation and analysed AD29 association with tri-snRNP proteins. We found that AD29 interaction with U4/U6 proteins decreased, while it increased in the case of U5 specific proteins Snu114 and hPrp6.

- Analysis of the AD29 association with snRNP complexes using gradient centrifugation revealed that AD29 exists predominantly in free form, little associates with U4/U6 and U5 snRNPs, but does not associate with tri-snRNP.

- Overexpression of hPrp6 in AD29 cell line compensated the AD29 induced phenotype. We detected more CBs and proliferation rate was similar to WT31 cells.

- Inhibition of translation enabled us to vizualize and examine the stability of AD29 protein. We found that AD29 protein is rapidly degraded compared to hPrp31 protein.

Following conclusions were reached in Chapter 5:

- We employed RNA affinity chromatography and confirmed that ECFP-hnH and MS2-EYFP are efficiently recruited onto the target RNAs *in vitro.*

- We used FRET acceptor photobleaching approach and FLIM approach to test the RNA-protein interaction *in situ.* In both cases we used control sample expressing CFP and YFP tagged protein coilin, which is known to self-interact.

- FRET efficiency between MS2-YFP/ECFP-hnH correlated with expression of substrate containing binding sites for both proteins and was comparable to the coilin positive control.

- FLIM approach validated the results obtained by acceptor photobleaching approach. We detected decrease in ECFP-hnH or Cerulean-hnH lifetime in presence of MS2-YFP indicating the stable interaction occuring between hnRNP H and its binding sequence in the pRed constructs.

Summary

Pre-mRNA splicing is a key step in gene expression, which occurs in the cell nucleus. It is accomplished by a huge complex called the spliceosome. Within the spliceosome five major snRNPs U1, U2, U4, U5, U6 and additional splicing factors undergo dynamic interactions and rearrangements to define and excise the intronic sequences from pre-mRNA to generate translatable mRNA. Although the whole splicing machinery is localized to the cell nucleus, some steps in snRNPs maturation occur also in the cytoplasm. snRNPs continuously cycle through nucleoplasm and nuclear compartments, like CBs and speckles to fullfill their functions. In CBs snRNPs obtain the necessary posttranscriptional modifications (pseudouridinylation, 2‘-O-ribose methylation) and some get pre-assembled to U4/U6 di-snRNP and U4/U6 tri-snRNP.

Pre-mRNA splicing occurs in an ordered association and dissocation of snRNPs with pre-mRNA. In the nucleoplasm the U1 and U2 snRNPs scan and recognize the intronic sequences. I showed that U1 snRNP association with 5‘ splice site is characteristic for a rapid exchange rate of 0.5 s. After the 3‘ splice site is synthetized U2 snRNP comes and this way the intron is defined. By engagement of U4/U6.U5 tri-snRNP the catalytic spliceosomal core U2.U5.U6 is generated. I showed that compared to the dynamic and fast intron recognition, the splicing reaction is the rate limiting step, which is accomplished within 30 seconds before the spliceosome disassembles.

The disassembled snRNPs are recycled and participate in the splicing process again. We showed that repeated formation of U4/U6.U5 tri-snRNP occurs mainly in CBs, where the free U5 snRNP joins the pre-assembled U4/U6 di-snRNP. This process is very dynamic and encounters productive interaction between U5 and U4/U6 snRNP specific proteins, hPrp6 and hPrp31 respectivelly. Mouse knockout of hPrp31 is lethal and knockdown leads to impaired formation of tri-snRNP and enlarged CBs.

Several mutations within hPrp31 protein were linked to cell specific disease retinitis pigmentosa, which affects rod cells in retina and ultimately leads to total blindness. I showed that Ala216Pro mutation in hPrp31 (AD29) impairs integration of this mutant form to U4/U6 di-snRNP, but streghtens its interaction with hPrp6 protein. Deeper study of AD29 interactions with U4/U6.U5 tri-snRNP proteins and snRNAs might bring more insights to the molecular mechanisms initiating this disease. RB-

FRET approach, which I introduced would be in this case an ideal tool for analysing RNA-protein interactions in living cells.

References

Abu-Safieh, L., E. N. Vithana, et al. (2006). "A large deletion in the adRP gene PRPF31: evidence that haploinsufficiency is the cause of disease." Mol Vis **12**: 384-8.

Achsel, T., H. Brahms, et al. (1999). "A doughnut-shaped heteromer of human Sm-like proteins binds to the 3'- end of U6 snRNA, thereby facilitating U4/U6 duplex formation in vitro." Embo J **18**(20): 5789-802.

Ali, G. S., K. V. Prasad, et al. (2008). "Analyses of in vivo interaction and mobility of two spliceosomal proteins using FRAP and BiFC." PLoS One **3**(4): e1953.

Almeida, F., R. Saffrich, et al. (1998). "Microinjection of anti-coilin antibodies affects the structure of coiled bodies." J Cell Biol **142**(4): 899-912.

Andrade, L. E., E. M. Tan, et al. (1993). "Immunocytochemical analysis of the coiled body in the cell cycle and during cell proliferation." Proc Natl Acad Sci U S A **90**(5): 1947-51.

Arenas, J. E. and J. N. Abelson (1997). "Prp43: An RNA helicase-like factor involved in spliceosome disassembly." Proc Natl Acad Sci U S A **94**(22): 11798-802.

Audibert, A., D. Weil, et al. (2002). "In vivo kinetics of mRNA splicing and transport in mammalian cells." Mol Cell Biol **22**(19): 6706-18.

Azubel, M., N. Habib, et al. (2006). "Native spliceosomes assemble with pre-mRNA to form supraspliceosomes." J Mol Biol **356**(4): 955-66.

Bastiaens, P. I., I. V. Majoul, et al. (1996). "Imaging the intracellular trafficking and state of the AB5 quaternary structure of cholera toxin." Embo J **15**(16): 4246-53.

Behzadnia, N., M. M. Golas, et al. (2007). "Composition and three-dimensional EM structure of double affinity-purified, human prespliceosomal A complexes." EMBO J **26**(6): 1737-48.

Behzadnia, N., K. Hartmuth, et al. (2006). "Functional spliceosomal A complexes can be assembled in vitro in the absence of a penta-snRNP." RNA **12**(9): 1738-46.

Bell, M., S. Schreiner, et al. (2002). "p110, a novel human U6 snRNP protein and U4/U6 snRNP recycling factor." Embo J **21**(11): 2724-35.

Benda, A., M. Benes, et al. (2003). "How to determine diffusion coefficients in planar phospholipid systems by confocal fluorescence correlation spectroscopy." Langmuir **19**(10): 4120-4126.

Beyer, A. L. and Y. N. Osheim (1988). "Splice site selection, rate of splicing, and alternative splicing on nascent transcripts." Genes Dev **2**(6): 754-65.

Bindereif, A. and M. R. Green (1987). "An ordered pathway of snRNP binding during mammalian pre-mRNA splicing complex assembly." EMBO J **6**(8): 2415-24.

Black, D. L. and A. L. Pinto (1989). "U5 small nuclear ribonucleoprotein: RNA structure analysis and ATP-dependent interaction with U4/U6." Mol Cell Biol **9**(8): 3350-9.

Blencowe, B. J. (2006). "Alternative splicing: new insights from global analyses." Cell **126**(1): 37-47.

Blencowe, B. J., M. Carmo-Fonseca, et al. (1993). "Interaction of the human autoantigen p150 with splicing snRNPs." J Cell Sci **105**(Pt 3): 685-97.

Boireau, S., P. Maiuri, et al. (2007). "The transcriptional cycle of HIV-1 in real-time and live cells." J Cell Biol **179**(2): 291-304.

Boon, K. L., T. Auchynnikava, et al. (2006). "Yeast ntr1/spp382 mediates prp43 function in postspliceosomes." Mol Cell Biol **26**(16): 6016-23.

Boon, K. L., R. J. Grainger, et al. (2007). "prp8 mutations that cause human retinitis pigmentosa lead to a U5 snRNP maturation defect in yeast." Nat Struct Mol Biol **14**(11): 1077-83.

Boudonck, K., L. Dolan, et al. (1998). "Coiled body numbers in the Arabidopsis root epidermis are regulated by cell type, developmental stage and cell cycle parameters." J Cell Sci **111**(Pt 24): 3687-94.

Brody, E. and J. Abelson (1985). "The "spliceosome": yeast pre-messenger RNA associates with a 40S complex in a splicing-dependent reaction." Science **228**(4702): 963-7.

Bujakowska, K., C. Maubaret, et al. (2009). "Study of gene-targeted mouse models of splicing factor gene Prpf31 implicated in human autosomal dominant retinitis pigmentosa (RP)." Invest Ophthalmol Vis Sci **50**(12): 5927-33.

Caceres, J. F. and A. R. Kornblihtt (2002). "Alternative splicing: multiple control mechanisms and involvement in human disease." Trends Genet **18**(4): 186-93.

Cao, W. and M. A. Garcia-Blanco (1998). "A serine/arginine-rich domain in the human U1 70k protein is necessary and sufficient for ASF/SF2 binding." J Biol Chem **273**(32): 20629-35.

Caputi, M., A. Mayeda, et al. (1999). "hnRNP A/B proteins are required for inhibition of HIV-1 pre-mRNA splicing." EMBO J. **18**(14): 4060-4067.

Caputi, M. and A. M. Zahler (2002). "SR proteins and hnRNP H regulate the splicing of the HIV-1 tev-specific exon 6D." Embo J **21**(4): 845-55.

Carmo-Fonseca, M., R. Pepperkok, et al. (1992). "Transcription-dependent colocalization of the U1, U2, U4/U6, and U5 snRNPs in coiled bodies." J Cell Biol **117**(1): 1-14.

Carvalho, T., F. Almeida, et al. (1999). "The spinal muscular atrophy disease gene product, SMN: A link between snRNP biogenesis and the Cajal (coiled) body." J Cell Biol **147**(4): 715-28.

Company, M., J. Arenas, et al. (1991). "Requirement of the RNA helicase-like protein PRP22 for release of messenger RNA from spliceosomes." Nature **349**(6309): 487-93.

D'Souza, I., P. Poorkaj, et al. (1999). "Missense and silent tau gene mutations cause frontotemporal dementia with parkinsonism-chromosome 17 type, by affecting multiple alternative RNA splicing regulatory elements." Proc Natl Acad Sci U S A **96**(10): 5598-603.

Darzacq, X., B. E. Jady, et al. (2002). "Cajal body-specific small nuclear RNAs: a novel class of 2'-O- methylation and pseudouridylation guide RNAs." Embo J **21**(11): 2746-2756.

Darzacq, X., N. Kittur, et al. (2006). "Stepwise RNP assembly at the site of H/ACA RNA transcription in human cells." J Cell Biol **173**(2): 207-18.

Darzacq, X., Y. Shav-Tal, et al. (2007). "In vivo dynamics of RNA polymerase II transcription." Nat Struct Mol Biol **14**(9): 796-806.

Deery, E. C., E. N. Vithana, et al. (2002). "Disease mechanism for retinitis pigmentosa (RP11) caused by mutations in the splicing factor gene PRPF31." Hum Mol Genet **11**(25): 3209-19.

Dignam, J. D., R. M. Lebovitz, et al. (1983). "Accurate transcription initiation by RNA polymerase II in a soluble extract from isolated mammalian nuclei." Nucleic Acids Res **11**(5): 1475-89.

Dominguez, C. and F. H. Allain (2006). "NMR structure of the three quasi RNA recognition motifs (qRRMs) of human hnRNP F and interaction studies with Bcl-x G-tract RNA: a novel mode of RNA recognition." Nucleic Acids Res **34**(13): 3634-45.

Dundr, M., M. D. Hebert, et al. (2004). "In vivo kinetics of Cajal body components." J Cell Biol **164**(6): 831-42.

Dundr, M., U. Hoffmann-Rohrer, et al. (2002). "A kinetic framework for a mammalian RNA polymerase in vivo." Science **298**(5598): 1623-6.

Ellis, J. D., D. Lleres, et al. (2008). "Spatial mapping of splicing factor complexes involved in exon and intron definition." J Cell Biol **181**(6): 921-34.

Endoh, T., M. Mie, et al. (2008). "Direct detection of RNA transcription by FRET imaging using fluorescent protein probe." J Biotechnol **133**(4): 413-7.

Fabrizio, P., B. Laggerbauer, et al. (1997). "An evolutionarily conserved U5 snRNP-specific protein is a GTP-binding factor closely related to the ribosomal translocase EF-2." Embo J **16**(13): 4092-106.

Faustino, N. A. and T. A. Cooper (2003). "Pre-mRNA splicing and human disease." Genes Dev **17**(4): 419-37.

Fogel, B. L. and M. T. McNally (2000). "A cellular protein, hnRNP H, binds to the negative regulator of splicing element from Rous sarcoma virus." J Biol Chem **275**: 32371-32378.

Garneau, D., T. Revil, et al. (2005). "Heterogeneous Nuclear Ribonucleoprotein F/H Proteins Modulate the Alternative Splicing of the Apoptotic Mediator Bcl-x." J Biol Chem **280**(24): 22641-50.
Gerlich, D., J. Beaudouin, et al. (2003). "Global chromosome positions are transmitted through mitosis in mammalian cells." Cell **112**(6): 751-64.
Ghetti, A., M. Company, et al. (1995). "Specificity of Prp24 binding to RNA: a role for Prp24 in the dynamic interaction of U4 and U6 snRNAs." Rna **1**(2): 132-45.
Girard, C., H. Neel, et al. (2006). "Depletion of SMN by RNA interference in HeLa cells induces defects in Cajal body formation." Nucleic Acids Res **34**(10): 2925-32.
Gonzalez-Santos, J. M., H. Cao, et al. (2008). "Mutation in the splicing factor Hprp3p linked to retinitis pigmentosa impairs interactions within the U4/U6 snRNP complex." Hum Mol Genet **17**(2): 225-39.
Gornemann, J., K. M. Kotovic, et al. (2005). "Cotranscriptional spliceosome assembly occurs in a stepwise fashion and requires the cap binding complex." Mol Cell **19**(1): 53-63.
Gorski, S. A., S. K. Snyder, et al. (2008). "Modulation of RNA polymerase assembly dynamics in transcriptional regulation." Mol Cell **30**(4): 486-97.
Grainger, R. J. and J. D. Beggs (2005). "Prp8 protein: at the heart of the spliceosome." RNA **11**(5): 533-57.
Graziotto, J. J., C. F. Inglehearn, et al. (2008). "Decreased levels of the RNA splicing factor Prpf3 in mice and zebrafish do not cause photoreceptor degeneration." Invest Ophthalmol Vis Sci **49**(9): 3830-8.
Grunwald, D., B. Spottke, et al. (2006). "Intranuclear binding kinetics and mobility of single native U1 snRNP particles in living cells." Mol Biol Cell **17**(12): 5017-27.
Han, K., G. Yeo, et al. (2005). "A combinatorial code for splicing silencing: UAGG and GGGG motifs." PLoS Biol **3**(5): e158.
Hastings, M. L., C. M. Wilson, et al. (2001). "A purine-rich intronic element enhances alternative splicing of thyroid hormone receptor mRNA." Rna **7**(6): 859-74.
Hebert, M. D. and A. G. Matera (2000). "Self-association of coilin reveals a common theme in nuclear body localization." Mol Biol Cell **11**(12): 4159-71.
Hentze, M. W. and A. E. Kulozik (1999). "A perfect message: RNA surveillance and nonsense-mediated decay." Cell **96**(3): 307-10.
Hu, C. D., Y. Chinenov, et al. (2002). "Visualization of interactions among bZIP and Rel family proteins in living cells using bimolecular fluorescence complementation." Mol Cell **9**(4): 789-98.
Huang, S. and D. L. Spector (1991). "Nascent pre-mRNA transcripts are associated with nuclear regions enriched in splicing factors." Genes Dev **5**(12A): 2288-302.
Humpolickova, J., L. Beranova, et al. (2008). "Fluorescence lifetime correlation spectroscopy reveals compaction mechanism of 10 and 49 kbp DNA and differences between polycation and cationic surfactant." J Phys Chem B **112**(51): 16823-9.
Huranova, M., J. Hnilicova, et al. (2009). "A mutation linked to retinitis pigmentosa in HPRP31 causes protein instability and impairs its interactions with spliceosomal snRNPs." Hum Mol Genet **18**(11): 2014-23.
Huranova, M., J. A. Jablonski, et al. (2009). "In vivo detection of RNA-binding protein interactions with cognate RNA sequences by fluorescence resonance energy transfer." RNA **15**(11): 2063-71.
Chakarova, C. F., M. M. Hims, et al. (2002). "Mutations in HPRP3, a third member of pre-mRNA splicing factor genes, implicated in autosomal dominant retinitis pigmentosa." Hum Mol Genet **11**(1): 87-92.
Chan, S. P., D. I. Kao, et al. (2003). "The Prp19p-associated complex in spliceosome activation." Science **302**(5643): 279-82.
Chen, C. D., R. Kobayashi, et al. (1999). "Binding of hnRNP H to an exonic splicing silencer is involved in the regulation of alternative splicing of the rat beta-tropomyosin gene." Genes Dev. **13**(5): 593-606.
Chen, C. H., D. I. Kao, et al. (2006). "Functional links between the Prp19-associated complex, U4/U6 biogenesis, and spliceosome recycling." Rna **12**(5): 765-74.

Chodosh, L. A., A. Fire, et al. (1989). "5,6-Dichloro-1-beta-D-ribofuranosylbenzimidazole inhibits transcription elongation by RNA polymerase II in vitro." J Biol Chem **264**(4): 2250-7.

Chou, M. Y., N. Rooke, et al. (1999). "hnRNP H is a component of a splicing enhancer complex that activates a c-src alternative exon in neuronal cells." Mol. Cell. Biol. **19**(1): 69-77.

Chusainow, J., P. M. Ajuh, et al. (2005). "FRET analyses of the U2AF complex localize the U2AF35/U2AF65 interaction in vivo and reveal a novel self-interaction of U2AF35." RNA **11**(8): 1201-14.

Jady, B. E., X. Darzacq, et al. (2003). "Modification of Sm small nuclear RNAs occurs in the nucleoplasmic Cajal body following import from the cytoplasm." Embo J **22**(8): 1878-1888.

Jurica, M. S., L. J. Licklider, et al. (2002). "Purification and characterization of native spliceosomes suitable for three-dimensional structural analysis." RNA **8**(4): 426-39.

Jurica, M. S. and M. J. Moore (2003). "Pre-mRNA splicing: awash in a sea of proteins." Mol Cell **12**(1): 5-14.

Kaida, D., H. Motoyoshi, et al. (2007). "Spliceostatin A targets SF3b and inhibits both splicing and nuclear retention of pre-mRNA." Nat Chem Biol **3**(9): 576-83.

Kambach, C., S. Walke, et al. (1999). "Crystal structures of two Sm protein complexes and their implications for the assembly of the spliceosomal snRNPs." Cell **96**(3): 375-87.

Karpova, T. S., C. T. Baumann, et al. (2003). "Fluorescence resonance energy transfer from cyan to yellow fluorescent protein detected by acceptor photobleaching using confocal microscopy and a single laser." J Microsc **209**(Pt 1): 56-70.

Keen, T. J., M. M. Hims, et al. (2002). "Mutations in a protein target of the Pim-1 kinase associated with the RP9 form of autosomal dominant retinitis pigmentosa." Eur J Hum Genet **10**(4): 245-9.

Kim, S. A., K. G. Heinze, et al. (2007). "Fluorescence correlation spectroscopy in living cells." Nat Methods **4**(11): 963-73.

Kiss, T. (2002). "Small nucleolar RNAs: an abundant group of noncoding RNAs with diverse cellular functions." Cell **109**(2): 145-8.

Kiss, T. (2004). "Biogenesis of small nuclear RNPs." J Cell Sci **117**(Pt 25): 5949-51.

Klingauf, M., D. Stanek, et al. (2006). "Enhancement of U4/U6 small nuclear ribonucleoprotein particle association in Cajal bodies predicted by mathematical modeling." Mol Biol Cell **17**(12): 4972-81.

Kohn, L., S. J. Bowne, et al. (2008). "Breakpoint characterization of a novel approximately 59 kb genomic deletion on 19q13.42 in autosomal-dominant retinitis pigmentosa with incomplete penetrance." Eur J Hum Genet.

Konarska, M. M. and P. A. Sharp (1986). "Electrophoretic separation of complexes involved in the splicing of precursors to mRNAs." Cell **46**(6): 845-55.

Konarska, M. M. and P. A. Sharp (1988). "Association of U2, U4, U5, and U6 small nuclear ribonucleoproteins in a spliceosome-type complex in absence of precursor RNA." Proc Natl Acad Sci U S A **85**(15): 5459-62.

Kotovic, K. M., D. Lockshon, et al. (2003). "Cotranscriptional recruitment of the U1 snRNP to intron-containing genes in yeast." Mol Cell Biol **23**(16): 5768-79.

Lacadie, S. A. and M. Rosbash (2005). "Cotranscriptional spliceosome assembly dynamics and the role of U1 snRNA:5'ss base pairing in yeast." Mol Cell **19**(1): 65-75.

Lamond, A. I. and D. L. Spector (2003). "Nuclear speckles: a model for nuclear organelles." Nat Rev Mol Cell Biol **4**(8): 605-12.

Lauber, J., G. Plessel, et al. (1997). "The human U4/U6 snRNP contains 60 and 90kD proteins that are structurally homologous to the yeast splicing factors Prp4p and Prp3p." Rna **3**(8): 926-41.

LeMaire, M. F. and C. S. Thummel (1990). "Splicing precedes polyadenylation during Drosophila E74A transcription." Mol Cell Biol **10**(11): 6059-63.

Lemm, I., C. Girard, et al. (2006). "Ongoing U snRNP Biogenesis Is Required for the Integrity of Cajal Bodies." Mol Biol Cell **17**(7): 3221-31.

Licatalosi, D. D. and R. B. Darnell (2006). "Splicing regulation in neurologic disease." Neuron **52**(1): 93-101.
Lippincott-Schwartz, J., E. Snapp, et al. (2001). "Studying protein dynamics in living cells." Nat Rev Mol Cell Biol **2**(6): 444-56.
Listerman, I., A. S. Bledau, et al. (2007). "Extragenic Accumulation of RNA Polymerase II Enhances Transcription by RNA Polymerase III." PLoS Genet **3**(11): e212.
Listerman, I., A. K. Sapra, et al. (2006). "Cotranscriptional coupling of splicing factor recruitment and precursor messenger RNA splicing in mammalian cells." Nat Struct Mol Biol **13**(9): 815-22.
Liu, J. L. and J. G. Gall (2007). "U bodies are cytoplasmic structures that contain uridine-rich small nuclear ribonucleoproteins and associate with P bodies." Proc Natl Acad Sci U S A **104**(28): 11655-9.
Liu, S., P. Li, et al. (2007). "Binding of the human Prp31 Nop domain to a composite RNA-protein platform in U4 snRNP." Science **316**(5821): 115-20.
Lorenz, M. (2009). "Visualizing protein-RNA interactions inside cells by fluorescence resonance energy transfer." RNA **15**(1): 97-103.
Lorson, C. L., E. Hahnen, et al. (1999). "A single nucleotide in the SMN gene regulates splicing and is responsible for spinal muscular atrophy." Proc Natl Acad Sci U S A **96**(11): 6307-11.
Makarov, E. M., O. V. Makarova, et al. (2002). "Small nuclear ribonucleoprotein remodeling during catalytic activation of the spliceosome." Science **298**(5601): 2205-8.
Makarova, O. V., E. M. Makarov, et al. (2002). "Protein 61K, encoded by a gene (PRPF31) linked to autosomal dominant retinitis pigmentosa, is required for U4/U6center dotU5 tri-snRNP formation and pre-mRNA splicing." Embo J **21**(5): 1148-1157.
Malca, H., N. Shomron, et al. (2003). "The U1 snRNP base pairs with the 5' splice site within a penta-snRNP complex." Mol Cell Biol **23**(10): 3442-55.
Marcucci, R., F. E. Baralle, et al. (2006). "Complex splicing control of the human Thrombopoietin gene by intronic G runs." Nucleic Acids Res.
Martin, A., S. Schneider, et al. (2002). "Prp43 is an essential RNA-dependent ATPase required for release of lariat-intron from the spliceosome." J Biol Chem **277**(20): 17743-50.
Matera, A. G. and K. B. Shpargel (2006). "Pumping RNA: nuclear bodybuilding along the RNP pipeline." Curr Opin Cell Biol **18**(3): 317-24.
Mayes, A. E., L. Verdone, et al. (1999). "Characterization of Sm-like proteins in yeast and their association with U6 snRNA." Embo J **18**(15): 4321-31.
McCullough, A. J. and S. M. Berget (1997). "G triplets located throughout a class of small vertebrate introns enforce intron borders and regulate splice site selection." Mol Cell Biol **17**: 4562-4571.
McKie, A. B., J. C. McHale, et al. (2001). "Mutations in the pre-mRNA splicing factor gene PRPC8 in autosomal dominant retinitis pigmentosa (RP13)." Hum Mol Genet **10**(15): 1555-62.
McNally, J. G. (2008). "Quantitative FRAP in analysis of molecular binding dynamics in vivo." Methods Cell Biol **85**: 329-51.
Meister, G., C. Eggert, et al. (2002). "SMN-mediated assembly of RNPs: a complex story." Trends Cell Biol **12**(10): 472-8.
Min, H., R. C. Chan, et al. (1995). "The generally expressed hnRNP F is involved in a neural-specific pre-mRNA splicing event." Genes Dev. **9**(21): 2659-2671.
Misteli, T., J. F. Caceres, et al. (1997). "The dynamics of a pre-mRNA splicing factor in living cells." Nature **387**(6632): 523-7.
Mordes, D., X. Luo, et al. (2006). "Pre-mRNA splicing and retinitis pigmentosa." Mol Vis **12**: 1259-71.
Mordes, D., L. Yuan, et al. (2007). "Identification of photoreceptor genes affected by PRPF31 mutations associated with autosomal dominant retinitis pigmentosa." Neurobiol Dis **26**(2): 291-300.
Narayanan, U., T. Achsel, et al. (2004). "Coupled in vitro import of U snRNPs and SMN, the spinal muscular atrophy protein." Mol Cell **16**(2): 223-34.

Narayanan, U., J. K. Ospina, et al. (2002). "SMN, the spinal muscular atrophy protein, forms a pre-import snRNP complex with snurportin1 and importin beta." Hum Mol Genet **11**(15): 1785-95.
Nelissen, R. L., C. L. Will, et al. (1994). "The association of the U1-specific 70K and C proteins with U1 snRNPs is mediated in part by common U snRNP proteins." EMBO J **13**(17): 4113-25.
Nesic, D., G. Tanackovic, et al. (2004). "A role for Cajal bodies in the final steps of U2 snRNP biogenesis." J Cell Sci **117**(Pt 19): 4423-33.
Neugebauer, K. M. (2002). "On the importance of being co-transcriptional." J Cell Sci **115**(Pt 20): 3865-71.
Nottrott, S., H. Urlaub, et al. (2002). "Hierarchical, clustered protein interactions with U4/U6 snRNA: a biochemical role for U4/U6 proteins." Embo J **21**(20): 5527-38.
O'Brien, K., A. J. Matlin, et al. (2008). "The biflavonoid isoginkgetin is a general inhibitor of Pre-mRNA splicing." J Biol Chem **283**(48): 33147-54.
Ohno, M. and Y. Shimura (1996). "A human RNA helicase-like protein, HRH1, facilitates nuclear export of spliced mRNA by releasing the RNA from the spliceosome." Genes Dev **10**(8): 997-1007.
Patterson, G. H. and J. Lippincott-Schwartz (2004). "Selective photolabeling of proteins using photoactivatable GFP." Methods **32**(4): 445-50.
Paushkin, S., A. K. Gubitz, et al. (2002). "The SMN complex, an assemblyosome of ribonucleoproteins." Curr Opin Cell Biol **14**(3): 305-12.
Paushkin, S., A. K. Gubitz, et al. (2002). "The SMN complex, an assemblyosome of ribonucleoproteins." Curr Opin Cell Biol **14**(3): 305-12.
Pena, V., A. Rozov, et al. (2008). "Structure and function of an RNase H domain at the heart of the spliceosome." EMBO J **27**(21): 2929-40.
Phair, R. D. and T. Misteli (2001). "Kinetic modelling approaches to in vivo imaging." Nat Rev Mol Cell Biol **2**(12): 898-907.
Poser, I., M. Sarov, et al. (2008). "BAC TransgeneOmics: a high-throughput method for exploration of protein function in mammals." Nat Methods **5**(5): 409-15.
Querido, E. and P. Chartrand (2008). "Using fluorescent proteins to study mRNA trafficking in living cells." Methods Cell Biol **85**: 273-92.
Rackham, O. and C. M. Brown (2004). "Visualization of RNA-protein interactions in living cells: FMRP and IMP1 interact on mRNAs." Embo J **23**(16): 3346-55.
Raghunathan, P. L. and C. Guthrie (1998). "A spliceosomal recycling factor that reanneals U4 and U6 small nuclear ribonucleoprotein particles." Science **279**(5352): 857-60.
Raker, V. A., G. Plessel, et al. (1996). "The snRNP core assembly pathway: identification of stable core protein heteromeric complexes and an snRNP subcore particle in vitro." Embo J **15**(9): 2256-69.
Reed, R. (2000). "Mechanisms of fidelity in pre-mRNA splicing." Curr Opin Cell Biol **12**(3): 340-5.
Rino, J. and M. Carmo-Fonseca (2009). "The spliceosome: a self-organized macromolecular machine in the nucleus?" Trends Cell Biol **19**(8): 375-84.
Rino, J., T. Carvalho, et al. (2007). "A stochastic view of spliceosome assembly and recycling in the nucleus." PLoS Comput Biol **3**(10): 2019-31.
Rino, J., J. M. Desterro, et al. (2008). "Splicing factors SF1 and U2AF associate in extraspliceosomal complexes." Mol Cell Biol **28**(9): 3045-57.
Rio Frio, T., N. M. Wade, et al. (2008). "Premature termination codons in PRPF31 cause retinitis pigmentosa via haploinsufficiency due to nonsense-mediated mRNA decay." J Clin Invest **118**(4): 1519-31.
Rivolta, C., T. L. McGee, et al. (2006). "Variation in retinitis pigmentosa-11 (PRPF31 or RP11) gene expression between symptomatic and asymptomatic patients with dominant RP11 mutations." Hum Mutat **27**(7): 644-53.
Rizzo, M. A., G. H. Springer, et al. (2004). "An improved cyan fluorescent protein variant useful for FRET." Nat Biotechnol **22**(4): 445-9.

Rodriguez, A. J., J. Condeelis, et al. (2007). "Imaging mRNA movement from transcription sites to translation sites." Semin Cell Dev Biol **18**(2): 202-8.
Rodriguez, A. J., S. M. Shenoy, et al. (2006). "Visualization of mRNA translation in living cells." J Cell Biol **175**(1): 67-76.
Sapra, A. K., M. L. Anko, et al. (2009). "SR protein family members display diverse activities in the formation of nascent and mature mRNPs in vivo." Mol Cell **34**(2): 179-90.
Shav-Tal, Y., X. Darzacq, et al. (2004). "Dynamics of single mRNPs in nuclei of living cells." Science **304**(5678): 1797-800.
Shav-Tal, Y., R. H. Singer, et al. (2004). "Imaging gene expression in single living cells." Nat Rev Mol Cell Biol **5**(10): 855-61.
Shin, C., Y. Feng, et al. (2004). "Dephosphorylated SRp38 acts as a splicing repressor in response to heat shock." Nature **427**(6974): 553-8.
Shpargel, K. B. and A. G. Matera (2005). "Gemin proteins are required for efficient assembly of Sm-class ribonucleoproteins." Proc Natl Acad Sci U S A **102**(48): 17372-7.
Shpargel, K. B., J. K. Ospina, et al. (2003). "Control of Cajal body number is mediated by the coilin C-terminus." J Cell Sci **116**(Pt 2): 303-12.
Schaffert, N., M. Hossbach, et al. (2004). "RNAi knockdown of hPrp31 leads to an accumulation of U4/U6 di-snRNPs in Cajal bodies." Embo J **23**(15): 3000-9.
Schaub, M. C., S. R. Lopez, et al. (2007). "Members of the heterogeneous nuclear ribonucleoprotein H family activate splicing of an HIV-1 splicing substrate by promoting formation of ATP-dependent spliceosomal complexes." J Biol Chem **282**(18): 13617-26.
Schmidt, U., K. B. Im, et al. (2009). "Assembly and mobility of exon-exon junction complexes in living cells." RNA **15**(5): 862-76.
Singh, J. and R. A. Padgett (2009). "Rates of in situ transcription and splicing in large human genes." Nat Struct Mol Biol **16**(11): 1128-33.
Sleeman, J. (2007). "A regulatory role for CRM1 in the multi-directional trafficking of splicing snRNPs in the mammalian nucleus." J Cell Sci **120**(Pt 9): 1540-50.
Sleeman, J. E., P. Ajuh, et al. (2001). "snRNP protein expression enhances the formation of Cajal bodies containing p80-coilin and SMN." J Cell Sci **114**(Pt 24): 4407-19.
Sleeman, J. E. and A. I. Lamond (1999). "Newly assembled snRNPs associate with coiled bodies before speckles, suggesting a nuclear snRNP maturation pathway." Curr Biol **9**(19): 1065-74.
Sperling, J., M. Azubel, et al. (2008). "Structure and function of the Pre-mRNA splicing machine." Structure **16**(11): 1605-15.
Sprague, B. L. and J. G. McNally (2005). "FRAP analysis of binding: proper and fitting." Trends Cell Biol **15**(2): 84-91.
Sprague, B. L., R. L. Pego, et al. (2004). "Analysis of binding reactions by fluorescence recovery after photobleaching." Biophys J **86**(6): 3473-95.
Staley, J. P. and C. Guthrie (1998). "Mechanical devices of the spliceosome: motors, clocks, springs, and things." Cell **92**(3): 315-26.
Stanek, D. and K. M. Neugebauer (2004). "Detection of snRNP assembly intermediates in Cajal bodies by fluorescence resonance energy transfer." J Cell Biol **166**(7): 1015-25.
Stanek, D. and K. M. Neugebauer (2006). "The Cajal body: a meeting place for spliceosomal snRNPs in the nuclear maze." Chromosoma **115**(5): 343-54.
Stanek, D., J. Pridalova-Hnilicova, et al. (2008). "Spliceosomal small nuclear ribonucleoprotein particles repeatedly cycle through Cajal bodies." Mol Biol Cell **19**(6): 2534-43.
Stanek, D., S. D. Rader, et al. (2003). "Targeting of U4/U6 small nuclear RNP assembly factor SART3/p110 to Cajal bodies." J Cell Biol **160**(4): 505-16.
Stevens, S. W., D. E. Ryan, et al. (2002). "Composition and functional characterization of the yeast spliceosomal penta-snRNP." Mol Cell **9**(1): 31-44.
Strzelecka, M., S. Trowitzsch, et al. "Coilin-dependent snRNP assembly is essential for zebrafish embryogenesis." Nat Struct Mol Biol **17**(4): 403-9.
Tanaka, N., A. Aronova, et al. (2007). "Ntr1 activates the Prp43 helicase to trigger release of lariat-intron from the spliceosome." Genes Dev **21**(18): 2312-25.

Tardiff, D. F., S. A. Lacadie, et al. (2006). "A genome-wide analysis indicates that yeast pre-mRNA splicing is predominantly posttranscriptional." Mol Cell **24**(6): 917-29.
Tardiff, D. F. and M. Rosbash (2006). "Arrested yeast splicing complexes indicate stepwise snRNP recruitment during in vivo spliceosome assembly." RNA **12**(6): 968-79.
Terns, M. P. and R. M. Terns (2001). "Macromolecular complexes: SMN--the master assembler." Curr Biol **11**(21): R862-4.
Terskikh, A., A. Fradkov, et al. (2000). ""Fluorescent timer": protein that changes color with time." Science **290**(5496): 1585-8.
Tsai, R. T., R. H. Fu, et al. (2005). "Spliceosome disassembly catalyzed by Prp43 and its associated components Ntr1 and Ntr2." Genes Dev **19**(24): 2991-3003.
Tsai, R. T., C. K. Tseng, et al. (2007). "Dynamic interactions of Ntr1-Ntr2 with Prp43 and with U5 govern the recruitment of Prp43 to mediate spliceosome disassembly." Mol Cell Biol **27**(23): 8027-37.
Turner, I. A., C. M. Norman, et al. (2004). "Roles of the U5 snRNP in spliceosome dynamics and catalysis." Biochem Soc Trans **32**(Pt 6): 928-31.
Tycowski, K. T., N. G. Kolev, et al. (2006). The ever-growing world of small nuclear ribonucleoproteins. The RNA world. R. F. Gesteland, T. R. Cech and J. F. Atkins. New York, Cold Spring Harbor Laboratory Press**:** 327-368.
Urlaub, H., V. A. Raker, et al. (2001). "Sm protein-Sm site RNA interactions within the inner ring of the spliceosomal snRNP core structure." EMBO J **20**(1-2): 187-96.
Verdone, L., S. Galardi, et al. (2004). "Lsm proteins promote regeneration of pre-mRNA splicing activity." Curr Biol **14**(16): 1487-91.
Vithana, E. N., L. Abu-Safieh, et al. (2001). "A human homolog of yeast pre-mRNA splicing gene, PRP31, underlies autosomal dominant retinitis pigmentosa on chromosome 19q13.4 (RP11)." Mol Cell **8**(2): 375-81.
Vithana, E. N., L. Abu-Safieh, et al. (2003). "Expression of PRPF31 mRNA in patients with autosomal dominant retinitis pigmentosa: a molecular clue for incomplete penetrance?" Invest Ophthalmol Vis Sci **44**(10): 4204-9.
Wahl, M., F. Koberling, et al. (2004). "Time-resolved confocal fluorescence imaging and spectrocopy system with single molecule sensitivity and sub-micrometer resolution." Curr Pharm Biotechnol **5**(3): 299-308.
Wahl, M. C., C. L. Will, et al. (2009). "The spliceosome: design principles of a dynamic RNP machine." Cell **136**(4): 701-18.
Wang, C. and U. T. Meier (2004). "Architecture and assembly of mammalian H/ACA small nucleolar and telomerase ribonucleoproteins." EMBO J **23**(8): 1857-67.
Wassarman, D. A. and J. A. Steitz (1992). "Interactions of small nuclear RNA's with precursor messenger RNA during in vitro splicing." Science **257**(5078): 1918-25.
Wen, X., Y. P. Lei, et al. (2005). "Structural organization and cellular localization of tuftelin-interacting protein 11 (TFIP11)." Cell Mol Life Sci **62**(9): 1038-46.
Wetterberg, I., G. Bauren, et al. (1996). "The intranuclear site of excision of each intron in Balbiani ring 3 pre-mRNA is influenced by the time remaining to transcription termination and different excision efficiencies for the various introns." RNA **2**(7): 641-51.
Wetterberg, I., J. Zhao, et al. (2001). "In situ transcription and splicing in the Balbiani ring 3 gene." EMBO J **20**(10): 2564-74.
Wilkie, S. E., K. J. Morris, et al. (2006). "A study of the nuclear trafficking of the splicing factor protein PRPF31 linked to autosomal dominant retinitis pigmentosa (ADRP)." Biochim Biophys Acta **1762**(3): 304-11.
Wilkie, S. E., V. Vaclavik, et al. (2008). "Disease mechanism for retinitis pigmentosa (RP11) caused by missense mutations in the splicing factor gene PRPF31." Mol Vis **14**: 683-90.
Will, C. L. and R. Luhrmann (2001). "Spliceosomal UsnRNP biogenesis, structure and function." Curr Opin Cell Biol **13**(3): 290-301.
Will, C. L. and R. Luhrmann (2006). Spliceosome structure and function. The RNA world. R. F. Gesteland, T. R. Cech and J. F. Atkins. New York, Cold Spring Harbor Laboratory Press**:** 369-400.

Wyatt, J. R., E. J. Sontheimer, et al. (1992). "Site-specific cross-linking of mammalian U5 snRNP to the 5' splice site before the first step of pre-mRNA splicing." Genes Dev **6**(12B): 2542-53.

Xing, Y., C. V. Johnson, et al. (1995). "Nonrandom gene organization: structural arrangements of specific pre-mRNA transcription and splicing with SC-35 domains." J Cell Biol **131**(6 Pt 2): 1635-47.

Yeo, G., S. Hoon, et al. (2004). "Variation in sequence and organization of splicing regulatory elements in vertebrate genes." Proc Natl Acad Sci U S A **101**(44): 15700-5.

Yu, Y. T., E. C. Sharl, et al. (1999). The growing world of small nuclear ribonucleoproteins. The RNA world. C. Gesteland and Atkins. New York, Cold Spring Hrabor Laboraory Press**:** 487-524.

Yuan, L., M. Kawada, et al. (2005). "Mutations in PRPF31 inhibit pre-mRNA splicing of rhodopsin gene and cause apoptosis of retinal cells." J Neurosci **25**(3): 748-57.

Zhang, Y., F. Buchholz, et al. (1998). "A new logic for DNA engineering using recombination in Escherichia coli." Nat Genet **20**(2): 123-8.

Zhang, Y., J. P. Muyrers, et al. (2000). "DNA cloning by homologous recombination in Escherichia coli." Nat Biotechnol **18**(12): 1314-7.

Zhao, C., D. L. Bellur, et al. (2009). "Autosomal-dominant retinitis pigmentosa caused by a mutation in SNRNP200, a gene required for unwinding of U4/U6 snRNAs." Am J Hum Genet **85**(5): 617-27.

Univerzita Karlova v Praze, 1. lékařská fakulta

Kateřinská 32, Praha 2

Prohlášení zájemce o nahlédnutí do závěrečné práce absolventa studijního programu uskutečňovaného na 1. lékařské fakultě Univerzity Karlovy v Praze

Jsem si vědom/a, že závěrečná práce je autorským dílem a že informace získané nahlédnutím do zpřístupněné závěrečné práce nemohou být použity k výdělečným účelům, ani nemohou být vydávány za studijní, vědeckou nebo jinou tvůrčí činnost jiné osoby než autora.

Byl/a jsem seznámen/a se skutečností, že si mohu pořizovat výpisy, opisy nebo kopie závěrečné práce, jsem však povinen/a s nimi nakládat jako s autorským dílem a zachovávat pravidla uvedená v předchozím odstavci.

Příjmení, jméno (hůlkové písmo)	**Číslo dokladu totožnosti vypůjčitele (OP, pas)**	**Signatura závěrečné práce**	**Datum**	**Podpis**